Changes in The Seasonality of Sea Ice and The Underlying Mechanisms Across Hudson Bay (HB) From 1979-2018

by

Ratiba Munir

A dissertation submitted to
The Faculty of Graduate Studies
In partial fulfillment of the requirements for the degree of
Master of Science

Graduate Program in Geography
York University
Toronto, Ontario

May, 2020

Abstract

Sea ice in Hudson Bay (HB) holds great importance ecologically, climatologically, economically, and for the Inuit culture. It has been widely established that sea ice seasons: Break-Up (BU), Ice-Free (IF), Freeze-Up (FU) and Ice-Covered (IC) have been shifting, but the underlying mechanisms remain unknown. To identify changes in sea ice coverage seasons and the underlying mechanisms, data consisting of daily albedo (α), along with components of the energy and radiation budget from 1979-2018 were downloaded from the North American Regional Reanalysis (NARR) model.

From 1979 to 2018, ice-coverage in the Bay has been decreasing. Among the 40 years, 1992 was the year of maximum ice-coverage due to the eruption of Mt. Pinatubo in Philippines. Conversely, 2010 was the year of minimum ice-coverage because the North Atlantic Oscillation (NAO) was in extreme negative mode which resulted in warmer weather conditions. The trends and patterns in ice-coverage show that albedo can be used as a proxy to understand changes in sea ice coverage across the Bay and the onset and duration of each ice-season.

This analysis has revealed that over the past 40 years, the onset of the IF season has not shifted, however the season has become longer, increasingly extending later into the fall. The IC season begins later and is becoming shorter. The changes to both the IF and IC seasons occur due to systematic changes in the BU and FU seasons. HB is transitioning towards earlier BU, but its duration is taking longer. Earlier onset of BU is partly in response to a trend towards thinner ice at the end of the IC season. BU season is shifting away from the summer solstice and towards the spring equinox when radiant energy gains are weaker.

In contrast, the FU season is beginning later, and its duration is becoming shorter. Despite this, there has been no trend in the net energy exchange from the ocean during this season over the

past forty years. This consistent loss of energy during the formation of complete ice cover on Hudson Bay, is accompanied by the Bay losing energy more intensely as the shortened FU season shifts closer to the winter solstice.

Overall, this research fills important gaps in understanding the duration and energetics of each ice season. It also addresses the limitations of NARR albedo data in studying sea ice.

"***Instincts under pressure crush the carbon of conformity and create diamonds. Each new season of life offers to train us for the next season if we pay attention and adapt." T. D. Jakes***

Acknowledgments

This thesis would have not been possible without the support and encouragement of many people. I would like to thank Richard Bello, my supervisor, for his guidance and feedback during this process. Most of all, thank you so much for putting up with my frustrating emails. I am very grateful for all the opportunities you have given me. I would also like to thank Kaz Higuchi, my co-supervisor for teaching me about timeseries analysis and forecasting. I am sure I will use it sometime in the future as no knowledge goes to waste.

Special thanks to Olalekan whose familiarity with programming was very helpful during the data extraction phase of this study. Without your help, working with NARR data files would have been close to impossible. Most of all, thank you for your kind words that truly helped me to work on this thesis when I was completely hopeless.

Finally, I would like to acknowledge my mother-Zahida. Thank you for your support and encouragement through times of stress, which made all these times of success possible. Most of all thank you, to an old friend Farid Tamkin for teaching me enormous life lessons; as well as, the importance of finding my passion and the importance of righteous people.

Table of Contents

List of Figures

List of Tables

List of Symbols

Symbol	Description	Units
Q^*	Net Radiation	Wm^{-2}
Q_H	Sensible Heat Flux	W/m^{-2}
Q_E	Latent Heat Flux	W/m^{-2}
Q_{ST}	Subsurface/ Ocean Heat Flux	W/m^{-2}
Q_A	Advection	W/m^{-2}
$K\uparrow$	Upward Shortwave Radiation	W/m^{-2}
$K\downarrow$	Downward Shortwave Radiation	W/m^{-2}
K^*	Net Shortwave Radiation	W/m^{-2}
$L\uparrow$	Upward Longwave Radiation	W/m^{-2}
$L\downarrow$	Downward Longwave Radiation	W/m^{-2}
α	Albedo	%
IG	Ice growth	mm
L_F	Latent Heat of Fusion	$0.334\ MJkg^{-1}$
ρ_{ice}	Density of Ice	$920\ kgm^{-3}$
T_0	Surface Temperature	^OC
T_A	Air Temperature	^OC
ε	Surface Emissivity	0.97 unitless
σ	Stefan-Boltzmann Constant	$5.67*10^{-8}\ Wm^{-}K^{-4}$
N	Sample Size	Dimensionless

Chapter 1:Introduction

1.1 Introduction

Hudson Bay (HB) is a closed sea (Gagnon & Gough, 2005; Hochheim & et al., 2011) that is surrounded by land with vast dimensions to support many aquatic and coastal ecozones. The survival of aquatic and coastal species is highly related to sea-ice cover which forms an integral part of the marine ecosystem of HB. The surface of sea ice provides habitat for sea birds and marine mammals that use sea-ice for mating, nursing their young, resting between trips underwater, expand feeding grounds and migration (i.e. seals and polar bears). Underwater, rich phytoplankton communities that drive the marine food web depend on nutrients from melting sea-ice and its thickness (i.e. light transmission). The ecosystem is affected directly by the changes in sea-ice habitats or indirectly through changes in the marine productivity processes. Moreover, sea ice itself and the supported wildlife is essential part of Inuit culture who have spent generations learning the distinctions and sensitivities of their local sea ice, and the seasonal ice covering to develop well-travelled routes (Aporta, 2010 & Laidler & et al 2009). This enabled Innuits to travel and obtain a portion of their food from wildlife harvested on sea ice (Laidler & et al., 2009 & Chan & et al., 2006).

The marine ecosystem of HB is becoming vulnerable to climate change. This can bring an end to the world's largest refugium. Regional temperature of HB has shown resistance to warming largely because of sea ice that provides a negative feedback on regional climate. The average temperature of HB is 6oC colder than the average for its latitude, its influence extends southwards making the Great Lakes 3OC cooler (Bello & Higuchi, 2018). However, in the mid-1990s HB crossed a climate tipping point with an increase in air temperature by 3OC (Chambellant & et al., 2012), triggering an ecological tipping point with visible shifts in algae communities (Rühland & et al., 2013). The

transition is caused by shifting ice seasons of HB. In the recent decades, ice seasons across the Bay have shifted to an earlier break-up date , and later freeze-up date allowing ice-free season to be longer season with great spatiotemporal variations (Gagnon & Gough, 2005; Andrews,2018; Kowal, 2017) . The formation, persistence and melting of sea ice is not a simple process- being influenced by atmospheric temperature and wind (i.e. thermodynamic and dynamic forcings) (Barber & Hochheim, 2014; Ogi & et al., 2016) and external forcings (e.g. volcanic eruption) (Gagnon & Gough, 2005). These forcings have an immediate impact on the ice-albedo feedback loop that results in an energy imbalance which strengthens over-time bringing further changes to thermodynamic forces; in turn, affecting dynamic forces. Therefore, it is important to identify thermodynamic based mechanisms that are changing sea ice seasons on HB; especially, the great shift in mid-1990s.

Changes in sea ice seasons can result in ecological consequences that can outweigh the economic benefits. Currently, town of Churchill is connected to the Canadian railway system (Gagnon & Gough,2005) but the shipping season is limited by the ice conditions. This has spurred efforts to develop models that can stimulate sea ice for the region (Saucier & et al., 2004). However, to develop accurate models, better understanding of the thermodynamic components of HB should be established. This is essential to improve models that can predict future ice conditions across HB so that mitigation efforts can be placed to conserve biodiversity of the marine ecosystem. Also, shipping routes can be planned accordingly; and food security for Inuit population can be sustained. Therefore, it is important to be mindful of changing sea ice seasons and predicting sea ice by knowing the underlying mechanism.

1.2 Key Objectives

The purpose of this study is to utilize the data from the North American Regional Reanalysis (NARR) model to understand changes in sea ice coverage across HB over the past 40 years. Specific objectives of the study are:

1. Can albedo be used as a proxy to determine changes in sea ice coverage.
2. How have the ice seasons changed over the past 40 years across HB?
    a. Identify the shifting dates of each ice-season.
    b. Identify the duration of each ice-season.
3. Identify the underlying mechanisms of change based on thermodynamic forces.
    a. Examine Water Heat Flux (Q_{ST}) of the Energy Budget in each ice-season.
    b. Examine sea ice thickness computed from Q_{ST} term.
    c. Examine surface temperature (T_O).

Chapter 2: Literature Review

This literature review is intended to provide scientific context upon which this research is based. Most of the literature examines the entire Hudson Bay Complex (HBC); few papers examined HB by itself. Some papers include both HB and JB as one study area. However, for the purposes of this study, publications that looked at James Bay separately were used, but only findings on HB are discussed. Section 2.1 considers seasonal patterns of sea ice across HB throughout the year. Section 2.2 examines the interannual variability in sea ice; in particular, shifting dates of each ice season. Section 2.3 aims to explain the forces (underlying mechanisms) behind the changing ice-cover. Finally, section 2.5 highlights research gaps.

2.1 Seasonal Patterns of Sea Ice in HB

The "typical" timing of each sea ice season.

2.1.1 Freeze-up and Ice-Covered

HB is seasonally ice-covered for most of the year. Ice reformation begins in October with intrusions of ice originating from northwest HB along the coast of Southampton Island. Predominant northwest winds move the ice packs to the south east, removing ice from northwest which promotes new ice growth (Ehn & et al., 2006). This allows formation of ice to gradually expand towards the south along the west coast of HB. By the end of October, continuous ice sheet forms extending south to Churchill but only a short distance offshore (Danielson, 1971). As weather grows progressively cold by early November, costal ice begins to form in other parts of the Bay but most of the Bay remains ice-free. Ice grows rapidly in northwestern HB; especially, along most of the coastline creating land fast ice that extends further offshore from protected or shallow coastline than from exposed or cliff and headland coast. The extent and ice thickness increases rapidly from November-December reaching 90% sea-ice concentration (Saucier & et al., 2004). However, freeze-up is

completed by the end of December; and remains ice-covered from early January to April or early May (Danielson, 1971; Gough & Allakhverdova, 1999, Hochheim & et al., 2010). Ice-cover in central HB during midwinter is not exactly 100% but slightly less due to occasional leads. Once, the Bay is ice-covered, mobile ice floes are pushed onshore by wind and tidal mixing (Danielson, 1971) that allow breaking up and piling of ice-floes against the coast or boundary of landfast ice (Ehn & et al., 2006) . Polynyas are common near islands along the southeast coast; while, largest recurring polynyas occur along northwestern HB (Saucier & et al., 2004).

After the Bay is ice-covered, pack ice begins to grow in thickness. Saucier & et al. (2004) observed that growth of ice in late December is at maximum reaching 2.4cm/day and decreases to mean monthly values between 1and 2 cm/day between January and March. Nonetheless, significant open-water ice growth occurs in March-April. The average ice thickness simulated using course resolution ocean general circulation model across the HB is 1.2m (Gough & Allakhverdova, 1999) but spatial variation in ice thickness is present not only from south to north; as well as from west to east. Maximum ice thickness occurs towards the end of ice-covered season. It ranges from 1m in southern HB; to 2m in northwestern HB. Local maximum ice thickness is greatest along the east coast of HB with 1.75m (Gough & Allakhverdova, 1999). However, moving ice can be piled up in one area which produces sea-ice ridges of various heights. In southern and northern HB Markham (1986) observed 4-10 ridges/km with an average of 6 ridges per km; 6% of them were over 1.5m, 26% over 1m; and less than 1% exceeded 2m; in particular, maximum height was 3.0-3.5m. Prinsenberg (1988) suggested that as the ridges form, some ice-free areas are left behind which are thought to refreeze but these do not exceed thickness of the undisturbed ice or the ridges. This gives an impression of the HB surface as undulating ice-covered land in winter.

2.1.2 Ice Break-Up and Ice-Free

The seasonal shift in ice cover to open water is rapid across HB. Typically, ice retreat begins between late May and early June (Gough & et al., 1999; Stewart & et al., 2010). First, land-fast ice detaches itself from the coast becoming part of mobile pack of ice. This leads to widening of the shore leads up to 65.9km on the west coast and 46.7 km on the east coast (Danielson, 1971). Sea ice concentration reduces to 70% in early June (Saucier & et al., 2004). However, a clear direction to ice retreat exists just as for ice formation; north vs. south and east vs. west. The first area to lose ice appears along the Southampton Island. Meanwhile, the southwestern region of HB is the last to be ice-free in summer (Etkin, 1991). By July, the Bay is relatively ice-free (ice concentration <10%); by the second week of August to late September it remains completely ice-free (Saucier & et al., 2004; Hochheim & et al., 2011). There is no multi-year ice in HB; hence, it is classified as seasonal ice region.

2.2 Recent Trends in Sea Ice Extent (SIE) in HB

The development of a multichannel satellite passive-microwave data record began with the deployment of the Scanning Multichannel Microwave Radiometer (SMMR) following its launch on NASA's Nimbus 7 satellite in October, 1978 (***Cavalieri*** & Parkinson, 2008). Numerous studies have used passive microwave data to examine long-term changes in sea ice concentration (SIC). or sea ice extent (SIE). SIC is the percentage of sea ice compared to some reference area; whereas, SIE measures the area of water body where there is at least some seas ice. This is defined based on a minimum SIC threshold~15%.Previous research has revealed that the extent of the marine Arctic ice cover has been decreasing over the last few decades (e.g., Maslanik et al., 1996, Johannessen et al., 1999; Parkinson et al., 1999; Vinnikov et al., 1999) but spatial variation exists across the marine water bodies- Greenland Sea, Barents Sea, Canadian Archipelago, Hudson Bay, Arctic Ocean.

Parkinson & et al. (1999) used passive microwave observations to show that during 1979-1996 (18-yr timeseries) there was a very slight insignificant negative trend in annual ice cover, SIC with -1.8%/ decade. SIE over HB decreased at a rate of 1.4×10^3 km^2 y^{-1}, with negative trends in all seasons; except, in winter. Interannual variability in SIE was minimum in winter due to the physical constraints of the Bay. Nonetheless, passive microwave observations tend to underestimate SIC during break-up (melt season) due to the extensive puddles that form on the ice-cover (Etkin and Ramseier, 1993).

Parkinson & et al. (1999) published the same study as in 2008 but with extended time-series from 1979-2006 (28-yr timeseries). The extended time-series showed cyclical behaviour with a negative insignificant trend in fall and showed the SIC had dropped by −5.3 ± 1.1%/decade. Most importantly, prior to mid-1990s SIE had a positive trend but dramatic reductions occurred in 1996 (Calaveri & et al., 2008). The decrease in sea ice has accelerated in the 21st century (e.g., Meier et al., 2007; Cavalieri and Parkinson, 2012; Stroeve et al., 2012) especially; since, the mid-1990s with continuing interannual variability (e.g., Screen et al., 2011).This existed due to the heavy ice conditions in 1983-1984; in response, to the strong El Niño of 1982–1983, which was also tied to deepened Icelandic Low and negative anomalies in the sea surface temperatures of Baffin Bay/Labrador Sea (Mysak & et al., 1996). Heavy ice-coverage in the early 1990s was related to the lesser 1991–1992 El Niño and North Atlantic Oscillation (NAO). As well as, eruption of Mt. Pinotubuo in Phillippines in 1991 that resulted in a significant cooling of the global climate during 1991 and 1992 (Gagnon & Gough, 2005). Another, strong El Niño occurred in 1997-1998 but this was not followed by heavy ice-coverage. Parkinson & Calveri (2012) extended their study from 1979-2010 (32-yr timeseries) to further emphasize changes in sea ice. The addition of 4 years showed that sea ice concentration (SIC) have declined in HB by −5.1 ± 0.9 % decade−1.

Tivy & et al. (2011) used ice charts from the Canadian Ice Service to examine changes in average summer SIE in Canadian Arctic between 1968 and 2008. A significant drop in ice ; 10.4% 3.1% decade^{-1} for HB and James Bays (July–October) were found. The authors further reported that within Hudson Bay, trends in summer SIE were strongest in the northwest, followed by the central Bay and then the northeast, with no significant trends along the east coast (Tivy et al., 2011). Finally, Tivy & et al. (2011) reported greatest reduction in the ice-cover of HB among the circumpolar Arctic. The continued decline in sea ice led to the strengthening of the positive ice-albedo feedback that influenced regional, seasonal and interannual variabilities. Therefore, many studies have been conducted to understand the shifts in each phase of the cryogenic cycle. Great volume of research indicates that the typical timing of sea-ice break-up, freeze-up, and ice-free dates have been changing over the recent decades correlated with warming temperature driven by climate change.

2.1.3 Recent Shifting Dates of Sea Ice Seasons on Hudson Bay

Several recent articles have examined the timing and duration of ice and seasonal changes in SIE; specifically, in HB. Research mainly focuses on freeze-up, ice-free and break-up dates; whereas, ice-covered holds least importance.

Gagnon & Gough (2005b) identified secular trends in the ice seasons by identifying the variability in the timing of sea-ice formation and retreat during the period of 1971-2003. The dates of ice freeze-up and break-up at 36 location across HB were recorded for each year from weekly ice charts provided by the Canadian Ice Service. Break-up was defined as the earliest date when the ice concentration was 5/10 or less; while, freeze-up occurred when ice concentrations reached 5/10 or more during October-December. Strong interannual variability in the timing of freeze-up and break-up existed over HB. Moreover, break-up date had the highest variability at points located closest to

the western shore of HB. Statistical significant negative trend towards earlier break-up ranged from: -4.9 to -12.5 days decade^{-1} in western HB, along southern coast of HB were detected. In addition, significant later freeze-up dates in fall were confined to the northwestern portion of HB with freeze-up ranging from: -3.2–5.5 days decade^{-1}.

Galbraith & Larouche (2011) used ice charts from Canadian Ice Service to understand the timing of ice break-up defined by SIC < 50% from 1971-2009 across the entire HB complex. The data resolution was 1/4° of latitude and longitude, roughly equivalent to 28 km north/south and 10–17 km east/west. The author reported significant trend of -3.2 days in break-up dates from 1971-2009 but from 1971-1991 no significant trend in break-up dates was detected. It was noted, that on a more local scale significant trend in HB occurred on the western side of HB. Stroeve & et al. (2014) aimed to magnify freeze-up and break-up season. The authors used passive microwave with spatial resolution of 25 × 25 km in a polar stereographic grid and an algorithm that aimed to understand changes in break-up season and sea ice loss. Two indicators for break-up and freeze-up were used to provide indicators for seasonal transition periods between 1979-2013. For break-up: first day of melt (EMO) and the period of continuous melt onset (MO). For freeze-up: start of continuous freeze (FO) and early freeze onset or the very last day of melt (EFO). Early ice break-up and late freeze-up was reported; in particular, significant EMO (-3.3 days/decade) and MO (-3.1 days/decade), EFO (3.4days/decade) and insignificant FO (2.3days/decade) occurred.

Hochheim & Barber (2014) examined the timing of break-up and freeze-up between 1980-2010 using a 2011 version of the Comiso (2000) passive microwave-based sea ice concentration dataset, which was overlaid on a 25 km × 25 km pixel grid. Thresholds for open-water was defined as 50% of the pixels in an area having SIC below 60% was identified as break-up. The authors

compared the ice-free season of 1980-1995 and 1996-2010. It was found that difference in SIEs between 1980–1995 vs. 1996–2010 is 30.5% (±6.6%). An average growth of 3.1 weeks for HB with break-up 1.5 weeks earlier and freeze-up 1.6 weeks later was reported. The results of Barber & Hochheim suggested that ice-free season has been lengthening especially in eastern HB.

Kowal & et al (2017) examined sea ice timing in break-up and freeze-up between 1971-2011. This research was built upon work by Gagnon and Gough (2005). Three matrices were examined: dates of break-up, freeze-up and ice-free season. The author found earlier significant trend towards earlier break-up (-0.49 days/ year), late freeze-up (0.46 days/year). Most importantly, 31 of 36 points had a significant trend towards a longer ice-free season and the average trend across all points was 0.91 days $year^{-1}$. At spatial scale, break-up trend was least significant in eastern HB; while, freeze-up trends were uniform. Overall, the author's results indicated strengthened magnitude and significance for a trend in 1971-2011 compared to 1971-2003; especially during freeze-up.

In summary, HB has been undergoing shifting ice seasons; since, the mid-1990s. Interannual variability is present in the changing SIE patterns across HB. Most importantly, break-up occurs earlier contributing to longer ice-free season followed by late-freeze-up. However, ice-covered season is given less importance due to physical constraints. Once, the Bay is ice-covered dramatic changes in sea ice are not expected.

2.3 Underlying Processes of Change

The interannual trends in SIE, dates and durations of each phase in the sea ice seasons are a product of thermodynamic and dynamic forcing. This contributes to spatial heterogeneity in sea ice across the Bay.

2.3.1 Sea Ice Dynamics

Sea ice dynamics describes changes in sea ice caused by wind and currents. HB receives freshwater >750km^3/yr. (*Déry & et al., 2011*) from two main sources- sea ice melt and river discharge. Main source of freshwater in HB is river discharge but on time scales less than a year, sea ice melt/growth plays an essential role in the freshwater budget; as opposed to, river discharge (Prinsenberg, 1988). Freshwater from river discharge is found along the coast; while, freshwater from sea ice melt is distributed more equally around the Bay (Granskog et al., 2007, Granskog et al., 2011). Both contribute to water circulation by diluting salt water and creating density driven currents that influence freeze-up. The formation of ice in late fall sequesters freshwater and rejects salt; while, in spring it releases layers of freshwater at the surface. Low salt concentrations are presents in seasons with freshwater inputs (Saucier & et al., 2004) which coincides with the summer solstice.

By using chemical tracers the distribution and pathways of riverine water in the Bay can be identified. Granskog et al. (2011) found that high fraction of river discharge (>5%) was present in the interior surface water and along the coast. The exchange of freshwater between the interior and outer boundary region occurs through Ekmann transport in summer, while during fall, the interior releases freshwater to the boundary (St-Laurent et al.,2011). Gyres are driven by wind, density and salinity differences and the deep wind-driven flow is expected to be onshore carrying lighter water beneath the dense water. This will result in unstable gravity configuration leading to vertical mixing; hence, ice formation in winter will occur later along the shore. At the larger spatial scale, eastern and

southern HB have higher concentrations of riverine water compared to western (Prinsenberg, 1984) and northern HB, yet freeze-up occurs late. This results due to water circulation and wind patterns; resulting in northern transport of warm water which delays freeze-up in eastern HB.

Wind is the primary dynamic force responsible for current flow and ice motion. Barber & Hochheim (2014) used CANGRID data to examine the role of dynamic and thermodynamic forcing in SIE. During the break-up season, 25% of interannual variation in sea ice cover is explained by wind. Currents within HB are dominantly wind-driven and cyclonic at all depths (Ingram & Larouche, 1987; Prinsenberg, 1988; Saucier & et al., 2004). Wang & et al. (1994c) modelled summer ocean circulation for HB using Blumberg- Mellor Model it was found that stable cyclonic circulation exists in August. Wang et al. (1994) modelled ice velocity fields for the spring (mid-April) and summer (mid-July) and found that in the absence of wind forcing, a "large amount" of ice is exported out of northeastern Hudson Bay via local currents, especially during the April period when ocean current forcing is strong, versus mid-July when it is much weaker

Ridenour & et al., (2019a) used a 3-dimensional (3D) ocean and sea ice coupled model to investigate HB circulation in spring, summer and fall. It was found that circulation is not cyclonic year-round. During summer, small cyclonic cell exists in southwestern HB; while, anticyclonic cell exists in eastern HB (Pinsenberg, 1986b; Saucier et al., 2004). The surface eddy activity is the strongest during ice-free periods; associated with synoptic wind forcing. Circulation is characterized by the coastal current intensifying from southwestern HB towards James Bay, then north along the eastern shore of HB, and finally through southern Hudson Strait HS (Saucier et al., 2004). This contributes to early melting along the Southampton Island; despite, low air temperature in the north. The persistence of north winds move ice from the north southwards to melt. During break-up and ice-free season sea ice coverage decreases faster in the west due to the strong northward current

running along the east coast that carries ice out of the Bay in to Hudson Strait. Moreover, westerly winds produce leads along the east coast during the break-up period which generally loosens the ice pack producing ice floes which hastens both melting and export allowing eastern HB to be ice-free earlier than western HB.

The circulation at all depths in HB is cyclonic and strongest during fall, reaching a maximum in November when the winds are strongest. This results in large convective losses of heat allowing ice formation. The occurrence of ice in all seasons along the east coast of Southampton Island is controlled by discharge of Foxe Basin ice, which thaws, loosens and begins to move south relatively late in the season (Danielson, 1971). Around mid-November, the surface salt flux is controlled by brine rejection from the growing ice cover that reaches 90% at the end of December (with a broad maximum in December–January when the sea-ice grows rapidly, and with sustained production through mid to late April (Saucier & et al., 2004). Spatial variation in sea-ice formation are controlled by thermodynamic processes. However, dynamic processes of advection and ridging are dominant factors contributing to ice thickness in the southern and eastern parts of HB (Saucier & et al., 2004; Gagnon & Gough, 2006).

2.3.2 Sea Ice Thermodynamics

"Sea ice thermodynamics" can be defined as the growth of sea ice as a result of heat loss from water and sea ice. It plays less of a direct role in placing ice under pressure to form ice ridges. However, sea ice thermodynamics remains important in determining ice-thickness and coverage, formation and break-up of ice; as well as, persistent convective losses of latent and sensible heat, Q_E and Q_H from polynyas that impact ocean surface albedo, α. This plays an important role in energetics across marine HB.

Water of HB is stratified by salinity rather than temperature. The presence of salt in water causes freezing point of sea water to be typically -1.8^{o}C. In fall, surface air temperature (SAT) drops, causing surface layer to cool, and water becomes more dense and sinks. However, it is prevented from sinking completely by the density (salinity) stratification. Rather than mixing, the top layer cools and ice can form; thus, ice can form well before the entire water column is cooled; in doing so, a lot more ice is formed quickly. After water cools down, it passes through various stages that produce ice-covered HB. As described in Serreze and Barry (2005), sea ice formation begins with a slush of needle-like ice crystals on the surface of water called frazil ice. On calm days, ice crystals form thin flexible sheets called nilas ice that does not deform into rafts or ridges. Hence, it continues to grow by a bottom-freezing process known as congelation. However in fall, aggressive wind and wave action tend to be more common. Therefore, ice forms under rough wave conditions that push crystals of ice together into semi-consolidated circular discs of slush called pancake ice that cements together and consolidate into a coherent ice sheet with a rough bottom surface.

Once, sea ice forms into a solid ice sheet it continues to grow downwards through the winter. The growth is dependent on conductive heat loss through the ice which is a function of the temperature gradient between the surface and water. Snow cover on the ice is a poor conductor (i.e. strong insulator) and decreases the conductive flux and slows ice growth. Sensible heat must be lost from the insulating layer of ice itself before the basal ice temperature can decrease to the freezing point and new ice can be formed. As ice thickens, it also freshens as brine (salt water) is rejected downwards through the ice increasing water salinity and density. This describes the components of thermodynamic forces- air and water temperature, salinity and energy budget that interplay during freeze-up and ice-covered seasons of HB. Many studies have investigated changes in air temperature, sea surface temperature, and salinity as causes of changing sea ice seasons.

Caya & et al. (2011) outline how ice break-up begins as increased solar radiation reaches the water column- reaching a peak in July of 185 Wm^{-2} (Figure 2). Caya & et al. (2011) showed that with an increase in $5^{O}C$ along the southern shore; $3^{O}C$ in central HB and a slight increase in sea surface temperature, SST northwards produces variability in ice break-up that starts from east and progresses into the west. This occurred as a decline in snow and ice across the Bay results in lower α; which allows more energy to be absorbed. In doing so, this slows the formation of ice across the Bay in winter; thus, interannual variability exists in SIE due to prolonged open water in spring and summer because the energy fluxes are altered. In the spring the convective transfer of energy from atmosphere to water is dependent on the inversion temperature gradient during the melt season which contributes to stability of the atmosphere and weakens convective transfer of energy downwards. During the open water season, convective energy exchange between the ocean surface and atmosphere could be in either direction as inversion conditions will transform to lapse conditions, and return to inversion conditions depending on the lag between the warming rates of the atmosphere and ocean. During the fall, strong lapse temperature gradients lead to instability in the atmosphere which enhances the convective losses of energy to the atmosphere as sensible and latent heat.

Air temperature (T_A) and SST are correlated. It was found that a correlation of 0.8 exists between T_A and SST, a correlation of 0.8 between open water percentage and SST; and a correlation of 0.59 between break-up dates and SST. Close to shore, air masses sometimes carry a characteristic signal from land (e.g. warmer and less humid than ocean surface in summer) while farther from shore, in most of the ocean, characteristics of the surface boundary layer are adjusted to the underlying marine system and carry a characteristic temperature and humidity originating from the ocean surface.

Barber & Hochheim (2014) used CANGRID data to examine the role of dynamic and thermodynamic forcing in SIE. In particular, the role of T_A and windspeeds was linked to SIE across HB during break-up, freeze-up and ice-free season. It was noted that since mid-1990s negative anomalies in SIE were largely attributed to positive anomalies in air temperature, which could be a cause or effect. It was noted that combined effect of later freeze-up dates and earlier break-up dates contributed to longer ice-free season, the changes in these seasons are related to T_A. During the break-up period, both spring and fall SAT proportionally (75%) account for interannual variation in HB with the remaining variability explained by wind. Lastly, it was noted that for every $1^{O}C$ increase in T_A, freeze-up was delayed by 0.7 weeks in HB.

Salinity and energetic in HB are critical components in understanding sea ice thermodynamics. Saucier & et al. (2004) used an ocean model- z-level, hydrostatic, shallow water, incompressible formulation from Backhaus to explain circulation, sea ice thickness, and factors such as salinity. It was found that formation of ice in late fall sequesters freshwater and rejects salt; while, in the melting period it releases layers of freshwater at the surface. A cyclic pattern in salinity content is present in the Bay that corresponds to the heat content of the Bay; a decline in heat energy results in salt content which is related to solubility of salts in water at higher temperatures. Low salt concentrations are presents in seasons with larger freshwater inputs. Also, salt flux is dominated by ice formation and melt during late fall to spring, and precipitation minus evaporation during summer and early fall. In addition, diurnal oscillations in the salinity flux are associated with daytime melting during spring. Since saltwater is more dense than freshwater it sinks; with this, salt concentration increases with depth. Seasonal changes in salinity affects the subsurface temperatures that come into play through diffusive exchange of heat with the surface. Below 50 m depth there should be little seasonal change in these distributions seasonally or from year to year (Stewart & et al., 2005) with

the maximum depth of pycnoline being 25m (Prinsenberg, 1984). Most of the literature examines underlying factors resulting in declined sea ice but the unknown thermodynamic energy components remain unknown.

A recent paper by Bello & Higuchi (2019) is one of the recently published and the only study that examines monthly surface radiation and energy budgets by comparing a recent two decade period (1997-2016) with the climate normal period (1981-2010) using NARR. There were many notable changes observed in the radiation balance (Figure 2.1a). K↓ follows the astronomical pattern with a maximum around 300 Wm-2 in June and begins to decrease towards the equinoxes. K↑ follows the sea ice melting pattern (using albedo as a proxy). From July onwards increases L↓ are observed with maxima occurring in August. The changes in L↑ reflect the ocean surface temperature and exceed L↓ for all months. The anomalies in the radiation balance show greater K↓ from January to June, large reductions in K↓ during July-August due to increased cloud cover anomalies (– 5.0 to -4.0 tenths) but K↓ recovers in fall. K↑ has declined in the last 20 years due to the reduction in ice in summer and spring months. Meanwhile, fall and winter months show small reductions despite large changes in albedo due to small K↓. L↑ shows positive anomalies; except, from January-August but L↑ exceeds L↓ from September to December contributing to enhanced radiative cooling at the surface. From May to July absorption of K↓ dominates allowing Q* to be maximum but as December approaches, enhanced losses of L↑ which exceed K↓ bringing small increases in Q*. Overall during the summer, radiative fluxes are the dominant agent of energy; throughout, early spring to mid-summer Q* heats up water or melts ice but the exact portioning of energy is not known.

Some of the most notables anomalies were: Q* was dominant term during summer and spring melt months (94% of ocean gains from radiation and only 6% from convective transfer), Q_H and Q_E

heat-up water during summer due to weak atmospheric temperature inversion, but towards the end of summer Q_H and Q_E reverse sign with large losses occurring in fall depleting Q_{ST} as the winter solstice is approached. Q_{ST} reaches maximum in July (~200Wm^{-2}); and declines following July as energy starts to go into fuelling convective losses. Q_H (~55Wm^{-2}) and Q_E (~52 Wm^{-2}) reach maximum in November; while, greatest decline occurs in Q_{ST}. As polar night approaches, temperatures cool and winds increase the Bay starts re-freezing. During mid-winter, although HB is completely ice-covered, polynyas form that allow Q_E to be lost; primarily Q_E losses occur because for effective Q_H loss, lapse temperature conditions are required. These are largely absent although lapse vapour pressure gradients can occur under inversion conditions.

The anomalies (Figure 2.1b) showed QST did not vary greatly from January to April when radiation fluxes and turbulent exchange with the atmosphere is weak. From May to July, Q* is going into the ocean; hence, large positive anomalies in the subsurface heat flux. From August onwards, large increases in latent and sensible heat transfer to the atmosphere. On the annual basis, it was concluded that the change in climate has generated an increase in the radiant flux inputs. However, large increases in the losses of turbulent fluxes to the atmosphere have contributed to a decline in the rate of oceanic gains. It was concluded that air temperature has increased; absorbed Q* is primarily responsible for ice to melt faster. Warming air temperatures are a result of turbulent fluxes being released from the ocean in fall. Therefore, diminishing sea ice itself is contributing to Arctic amplification of air temperatures over the Bay despite the original perturbation possibly being of atmospheric origin.

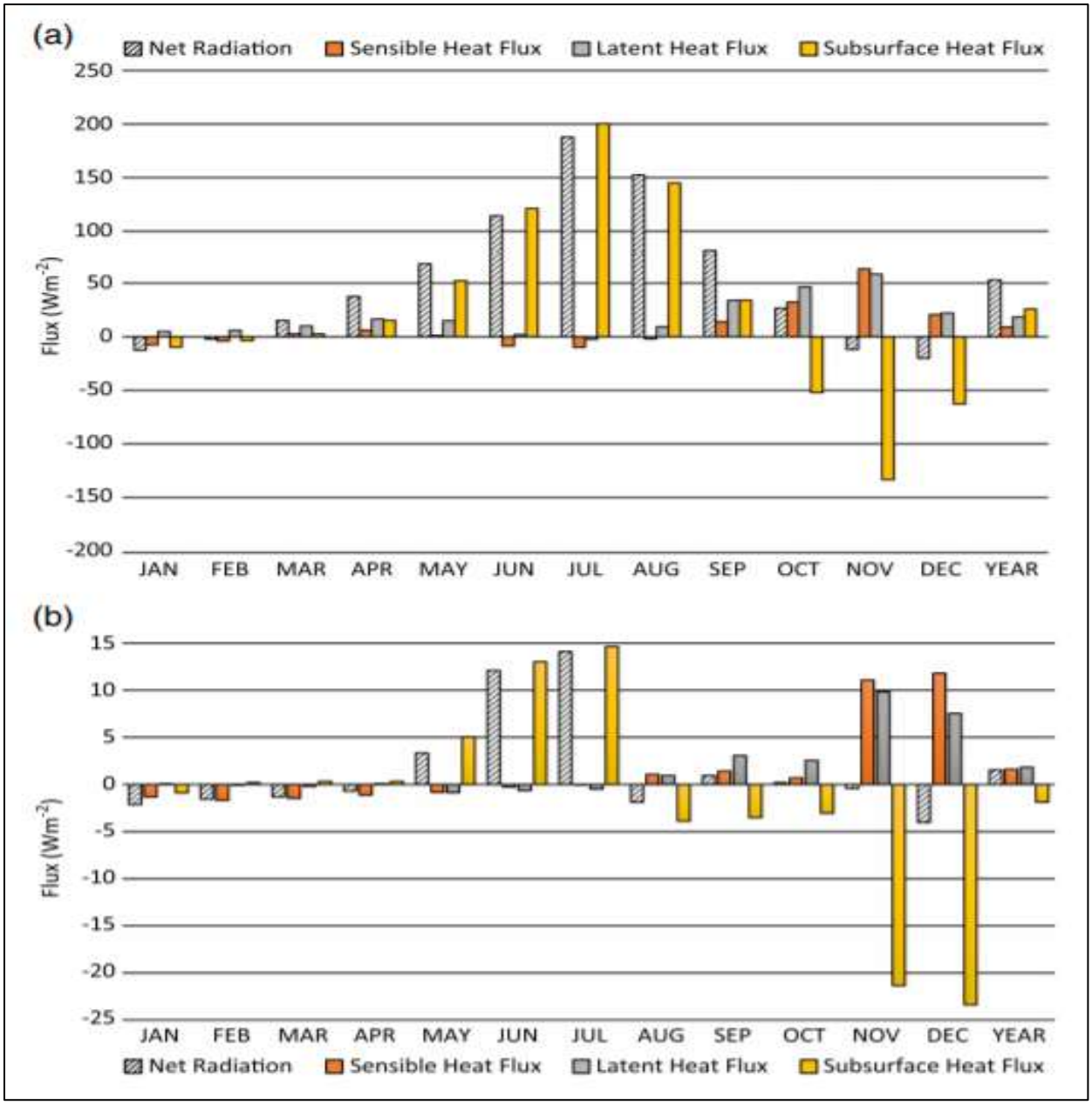

Figure 2.1: Hudson Bay monthly average energy budget components (W m^{-2}) from (a) the recent period (1997–2016) and (b) corresponding anomalies from the climate normal period (Bello and Higuchi, 2019).

I. Albedo

Sea ice studies across HB often consider albedo. Standard knowledge of sea ice albedo that is known about HB is well described in Oke, (2002). The role of surface albedo is one of the most important factors affecting radiation balance of HB. Snow and ice have the highest albedo of all surface types; given this, most of the solar radiation on the surface of snow/ice is reflected back into the atmosphere. This exists due to grain structure and colour of snow/ice. The albedo of snow/ice ranges from 50% to 90%; in particular, fresh snow albedo reaches 90% (Oke, 2002). However, melting snow/ice accelerates ice retreat, as dark bare ice is exposed leading to formation of melt ponds that further reduce albedo. Consequently, increase absorption of solar radiation leads to open-water with albedo varying from 5% to 20% (Oke, 2002) due to changes in zenith angle, cloudiness and surface roughness. With cloudless skies and sun at least 30^{O} (Oke, 2002) above the horizon water is most effective at absorbing radiation. Meanwhile, around sunrise and sunset zenith angle is close to the horizon causing the reflection to be mirror-like. In addition, wind causes wave formation making the surface of water to be rougher; in turn, allowing more K↓ to be reflected back into the atmosphere. Since, albedo of open-water is very small; with extended ice-free season "polar amplification" can be associated with ice albedo feedbacks. The role of albedo has been emphasized in climate studies across the Arctic Ocean (Curry & et al., 1995; Perovich & et al., 2002) or the different regions of Arctic with HB and James Bay considered as the entire HB.

Recent study by Bello & Higuchi (2019) found that normally, winter albedo is high (~60%), begins to decrease in May and eventually reaches a minimum in September (~8-10%). Over the last 20 years, albedo has been decreasing with small changes in winter and large changes in summer and fall. Spatial variations were present in monthly albedo anomalies. To begin with, from April to May albedo declined 0.5%, in June and July albedo declined by 5% for 35% of the Bay; while,

smaller proportions showed declines of 15%. In August 10% of the Bay showed an increase in 0.5%. In October, half of the Bay experienced negative anomalies in albedo but some parts of the Bay have not changed. From November- December, 80% of the Bay experienced large decline in albedo with most areas having albedo drop by 5%; with a few locations showing anomalies as large as ~20%. In addition, spatial variation existed in the annual albedo anomalies; especially at the mouth of rivers with a 17% decline in albedo. Ice degradation in HB (using declining albedo as a proxy) plays an important role in limiting the transfer of Q_H from the ocean, especially during the freeze up season . This raised the possibility that net warming of HB could reach an asymptote (i.e. reach a new equilibrium) if the decline in warming rates were to continue in HB.

2.4 Research Gaps and Limitations

Research has showed that ice seasons of HB have shifted. Earlier break-up and longer ice-free season have been augmented by late freeze-up. However, studies mainly examine break-up dates and freeze-up dates; from which, the ice-free season is estimated; while, ice-covered season is often ignored. Dates of sea ice seasons are widely studied but physical processes at work that are triggering and translating the albedo feedback remain unknown. This indicates the importance of times-series observations to understanding the seasonal development of sea-ice cover and underlying thermodynamic processes.

Declining SIE is a well-known fact in HB. The underlying cause of changes in sea ice is widely believed to be of atmospheric origin- air temperature via increases in GHG concentrations. Bello & Higuchi (2019) suggest that recent warming across HB in the last two decades is primarily caused by loss of sea ice and increased radiation gains rather than air temperature. In the past, many studies did not examine how strengthened positive albedo feedback can perturbed the HB system further. This indicates the importance of energetics in the HB system. Also, monthly changes in

albedo and energetics highlighted the importance of understanding the ice-seasons; in terms of length and duration, variations in the energetic in each ice season is unkown. Most importantly, a key question that remains unknown is how much of the variation in sea ice retreat and reduction can be explained by heat losses through open-water vs. ice-covered parts of HB. This is a major research question that has to date been given very little to no attention in models and recent energetic studies on HB.

Coupled models (dynamic + thermodynamic – mainly air temperature) are used to understand mechanisms causing change. Research has clearly demonstrated that energy surplus during extended ice-free and early break-up has contributed to late freeze-up; yet; most research tends to focus mainly on dynamic forces; even, in studies that use coupled models. Nonetheless, vertical growth and decay of ice occurs; in response, to energy fluxes at the upper and lower part of the water column. Vertical diffusion process acts within ice which changes the internal heating due to penetrating solar radiation and heat storage. Dynamic processes can influence sea ice cover by setting ice into motion creating leads. Therefore, formation and break-up of ice is largely controlled by thermodynamic processes; later sea ice changes are in response, to dynamic forces. This highlights the importance of understanding the underlying energetics responsible for declined sea ice across HB in the last 40 years. Lastly, time-series observation are crucial to understand the seasonal changes in ice. These form the focus of the chapters which follow.

Chapter 3: Research design and Methods

3.1 Study Area

Hudson Bay (HB), James Bay (JB), Hudson Strait (HS), and Foxe Basin (FB) are grouped together in the academic and grey literature (Andrews, 2018) as the Hudson Bay Complex, HBC. There is a good reason for this grouping: a large inland sea characterized by the mixing of Arctic marine seawater coming in from the north and vast amounts of freshwater runoff flowing in from terrestrial river systems and flowing out through Hudson Strait. For this study, Hudson Bay (Figure 3.1) is the main study area.

Among the four inland seas and globally HB is the largest with surface area of 8.03×10^5 km^2 (*Cornwall & et al., 2004*). It borders on three Provinces (Manitoba, Ontario, Quebec) and one Territory (Nunavut). The surrounding landmasses and exchanges of water are limited by narrow channels in northern part of HB (Gagnon & Gough, 2005). HB is located in between FB, JB, and HS allowing water from FB and JB to mix and flow into HS. In fall, cold, saline Arctic water from FB enters northwestern HB and it continues to flow eastward along the southern coast of HB where some of the water enters JB, remainder is deflected northward into HS from where it exits (Ridenour et al., 2019 b). This has resulted in HB to be a shallow (150m), large estuarine system connected to the Labrador Sea through HS that also receive freshwater inputs from rivers (Saucier & et al., 2004). Each year, river discharge contributes >750km^3yr^{-1} (Déry & et al., 2011) that is mainly dependent on the timing and pattern of snow melt and river ice break-up. The residence time of water; as well as, the energy exchanges in HB are likely to change more rapidly compared to lakes situated at the same latitude (i.e. Great Slave Lake). The location and large size of frozen HB poses challenges to

accessing the Northwest Passage or a route to European trade markets from the Port of Churchill resulting in HB to being of heightened importance among the other HBC seas.

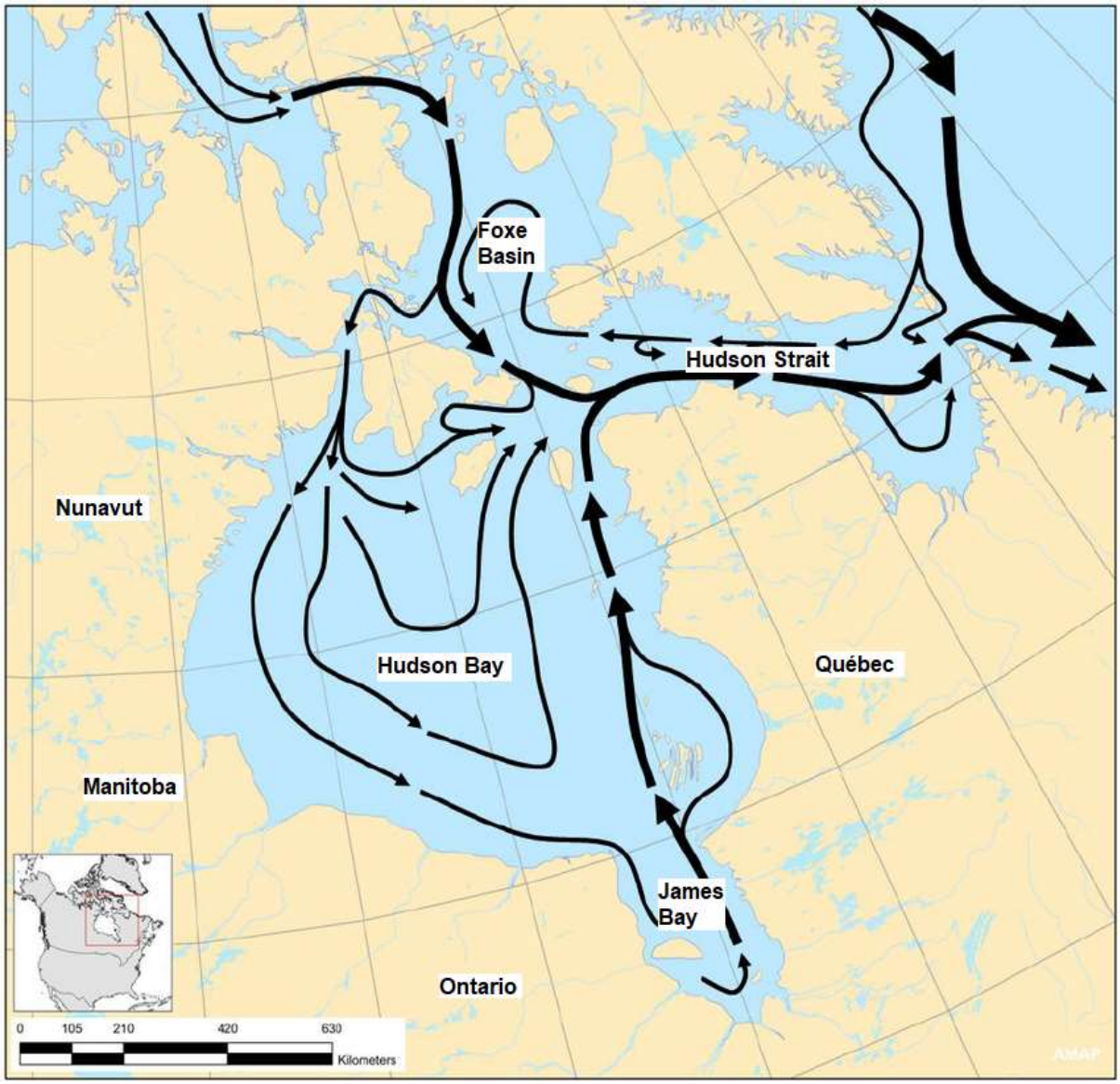

Figure 3.1: Describes water circulation in HB (Stewart & Howland, 2009).

3.2 Data Collection

3.2.1 Model Selection

North American Regional Reanalysis (NARR) is a reanalysis model that uses a systematic approach to produce data sets for weather forecasting and long-term climate monitoring and research. The National Centre of Environmental Predictions (NCEP, NOAA) created NARR as an improvement of NCEP-DOE (R2) with the aim of providing higher temporal and spatial resolution (32km x 29 pressure levels, 3-hours) for land-hydrology and land-atmosphere interaction data-sets. Its spatial domain covers entire North American continent and parts contiguous Pacific and Atlantic Oceans. The model obtains atmosphere's and earth's surface data from satellites to generate forecasts every 3hours. Then, a weighted factor- *3D var* analysis is applied to the difference between forecasted and observation data; to determine how much of a correction should be made to the forecast based on the new information from the observations. This generates a new forecast for atmospheric, land surface hydrology variables from 1979-present that are updated by the model 3 times daily from 45 vertical levels (Kennedy & et al., 2011). The data is archived at: https://www.esrl.noaa.gov/psd/data/gridded/data.narr.monolevel.html.

NARR provides estimates of various physical processes such as radiative fluxes, temperature, humidity, pressure and wind to calculate cloud formation, precipitation, and convective fluxes that are required to understand the processes by which weather and climate evolve. It is fully established that NARR is best suited for diagnosis of synoptic and mesoscale conditions over the Atmospheric Radiation Measurement (ARM) Southern Great Plains (SGP) (Kennedy & et al., 2011); with great accuracy in precipitation data (Beckers & et al, 2009). It has shown strong correlations with ground-based meteorological measurements and plot-scale in-situ observations for snow and

soil thermodynamic and passive microwave radiometric modelling (e.g. Langlois et al., 2009; Kohn and Royer, 2010).

For the purpose of this study, the suitability of NARR data was determined by looking at the time coverage, accessibility for the study area. Current global reanalysis data are most reliable in Northern Hemisphere mid-latitudes, in the middle to upper troposphere (about 4 to 20 km above Earth's surface), and for regional and larger areas (Schubert & et al., 2008). This exists because there are more measurements (more weather stations) to validate reanalyses results. However, reanalysis models have been extensively used to study Arctic climate (Serreze & et al., 2001; Tilinina & et al., 2014); since, they provide continuous, temporal, and spatial coverage; as well as variables that can be difficult, if not impossible to directly measure. A limitation to all reanalyses models is the impact of clouds; since, clouds decrease K↓ and increases L↓; thereby, modifying surface melting by trapping thermal radiation or cooling it by K↑. Most importantly, surface albedo generates shortwave radiative feedbacks to the Arctic climate system and amplifies the Arctic warming rate. Therefore, evaluation of reanalysis of surface albedo and radiative fluxes is essential. Many studies have shown that all reanalyses exhibit biases in surface radiation and albedo (Cao & et al., 2016; Kennedy & et al., 2011) mainly . However, greater accuracy and resolution makes the reanalyses model very reliable and convenient to study energy and radiation budget changes. Nonetheless, Arctic Research Office (ARO) has recommended the use of NARR data in Arctic research community and users of Arctic climate information with access to climate variability as it provides insights into Arctic Climatology.

3.2.2 Data Extraction

I. Latitude and Longitude:

2011 Census- Boundary Files provide the framework for mapping to support Geographic Information System (GIS) application used for land-use and demographic studies, or social, economic, and market research (Stats Canada, 2015). It provides shape files for provinces/ territories, census divisions, population centres, but most importantly hydrographic references available for: coasts, rivers and lakes. For the purpose of this study, Canadian Coast Water (Polygon) file was selected. This file was created by National Geographic Database (NGD) which is jointly affiliated with Statistics Canada-Elections Canada that takes the role of developing and maintaining a spatial database which serves the needs of both organizations. The file was created by selecting a subset of hydrographic features which represent the coastal water bodies adjoining Canada with a suite of cartographic boundaries. The files can be accessed from:

https://www12.statcan.gc.ca/census-recensement/2011/geo/bound-limit/bound-limit-2011-eng.cfm.

The shape file for Canadian Coastal Water (Polygon) was downloaded and opened into ArcMap 10.7.1. After, the attribute table consisting of FID, SHAPE, HYDROUID, NAME, RANK, and PRUID was opened. The polygons corresponding to HB were selected (Figure 3.2a). The data for the selected area was exported as the study site area (Figure 3.2b). Then, an arbitrary surface sensible heat flux, Q_H NETCDF file was downloaded into ARCGIS and converted into a NETCDF Raster Layer for variable name LAT (latitude) and was selected using *multidimensional tools* in the ARCGIS toolbox. Afterwards, the projection of the file was changed to Lambert_Conformal_Conic by altering the coordinate system in *properties.* It was done so that study site shape file could be used as a mask over the Q_H raster file (Figure 3.2c.); and help locate the points at which NARR

collected the data at every 32 km across HB. Then, the masked raster was converted to point ; which resulted in 753 point IDs on the shape file (Figure 3.2d), corresponding to latitude for each point. The attribute table containing point IDS, and latitude was copied into an excel worksheet. The same steps were repeated to retrieve data for LON (longitude). An Excel .csv file was created that contained both latitude and longitude along with the corresponding point IDs to be used for further data extraction.

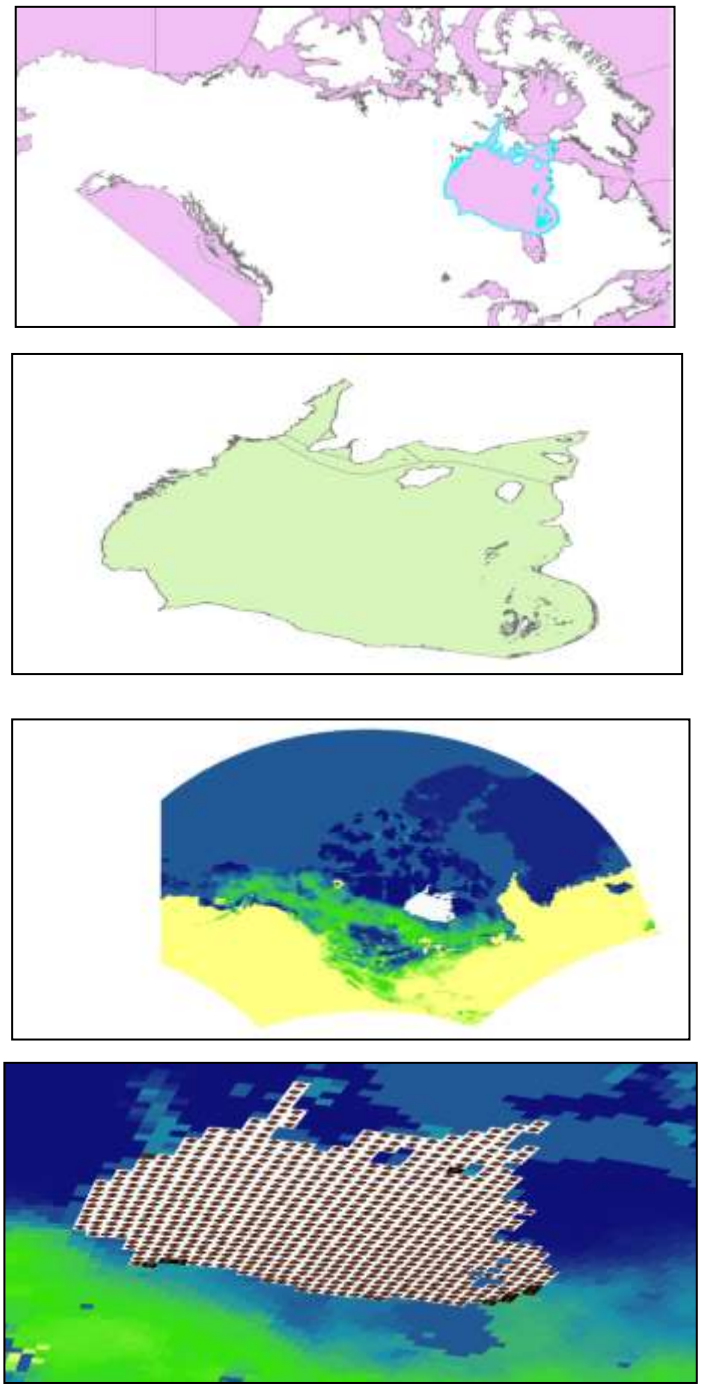

Figure 3.2: The four maps depicts the four steps used to extract NARR data using ArcMap 10.7.1. A) Coastal water boundaries in Canadian Census are shown in pink and turquoise colour outlines the polygons that correspond to HB in the shape file. B) Selected polygon was extracted as the study site. C) Study site region masked over NARR NETCDF file depicted as raster for variable LAT. Masked area shown in white. D) The raster data is converted into point ID that correspond to latitude from which NARR collects and generates data.

II. Energy and Radiation Budget Components and Albedo:

The surface radiation balance describes the net radiation on a two-dimensional plane of zero thickness at the surface accounted by the incoming and outgoing fluxes of radiation (Wm^{-2}). It is described as:

$$Q^* = (K\downarrow - K\uparrow) + (L\downarrow - L\uparrow) \quad (1)$$

$$K^* = K\downarrow(1-\alpha) \quad (2)$$

where Q*- net all-wave radiation, K↓-incoming shortwave radiation, K↑- reflected shortwave radiation, L↓- incoming longwave radiation, L↑- outgoing longwave radiation, K* is the net shortwave radiation and α is the surface albedo.

The surface energy budget accounts for the partitioning of the surface net radiation into three vertical fluxes (Wm^{-2}) and one horizontal flux (Wm^{-2}) and can be expressed as:

$$Q^* = Q_H + Q_E + Q_{ST} + Q_A \quad (3)$$

where Q_H-sensible heat flux, Q_E- latent heat flux, Q_A- advection flux, Q_{ST}- subsurface or ocean heat flux. Q_H, Q_E, are positive when directed away from the surface into the atmosphere; while, Q_{ST} is positive when directed away from the surface while HB is gaining heat. Q_A - advection flux is considered negligible due to small horizontal divergence between the grid points. Because surface short- and long-wave radiation fluxes and the surface sensible and latent heat fluxes are directly available from the NARR archive, the subsurface or ocean heat flux can be calculated by residual by rearranging (3) as,

$$Q_{ST} = Q^* - Q_H - Q_E \quad (4)$$

Q_{ST} considered the energy gains and losses from water of Hudson Bay.

NARR archives daily data at *monolevel* for forty years from 1979-2018 for the four radiation budget components; except, Q*. These data files were downloaded from the archived data page:

https://www.esrl.noaa.gov/psd/data/gridded/data.narr.monolevel.html. A code was written in Rstudio Version 1.2.1335 to extract data points corresponding to the latitude and longitude of HB study area. Next, a map showing each point ID was examined and some point IDs were located close to, or on coastlines. These point ID's were flagged for removal from further analysis. Also, when daily albedo was plotted versus time a pattern emerged that appeared in all years. Those point IDs close to coast-lines had albedos within the range of 12% to 80% or from 10% to 55% between summer to winter; while, point IDs over water had a binary albedo of either 6% or 65% from summer to winter (Figure 3.3). This further validated that removing point IDS close to coastlines would ensure that only marine HB was part of the study. These include:1,3, 9-10, 15,23, 34,36, 47, 57, 73-74, 87-88, 92, 108, 139-140, 163, 216, 300, 328, 387-388, 420-421, 454, 487, 521-522, 55-556, 615, 618, 648, 677, 680-681, 705-708, 728-730, 745, 749-751(Figure 3.4). These points ids were removed from the 752 grid points for every variable resulting in 702 point ids that covered only marine part of HB.

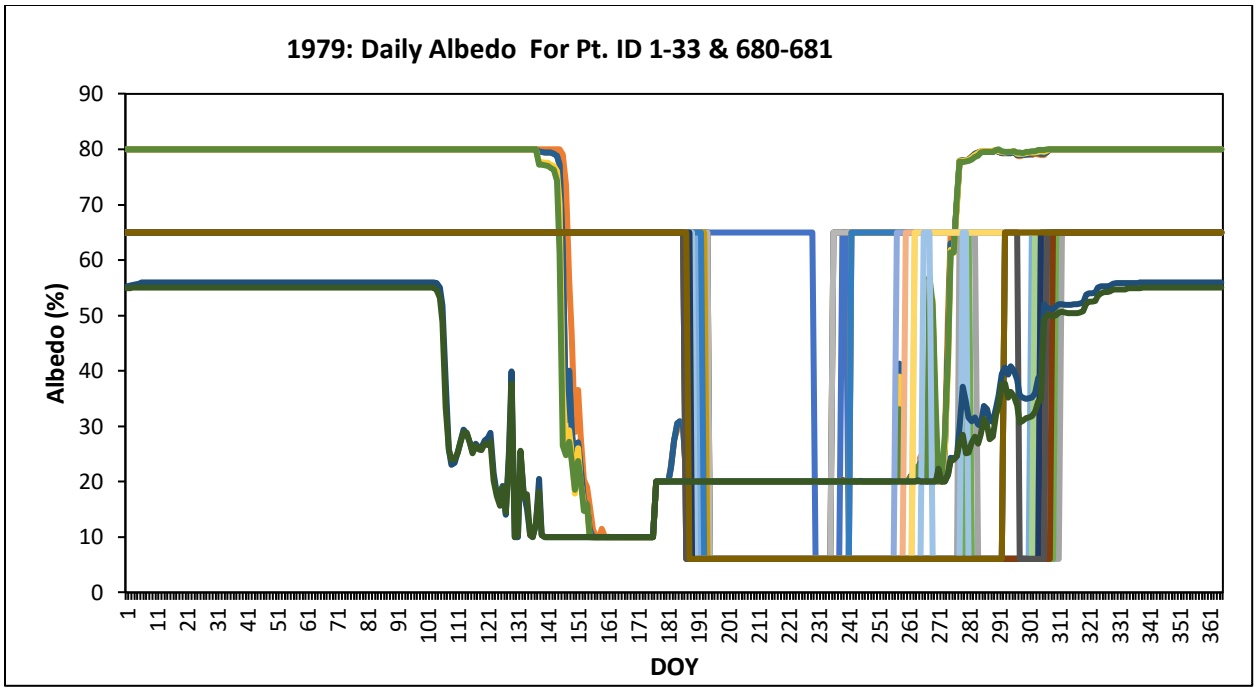

Figure 3.3: Describes general variation in albedo values coded by NARR.

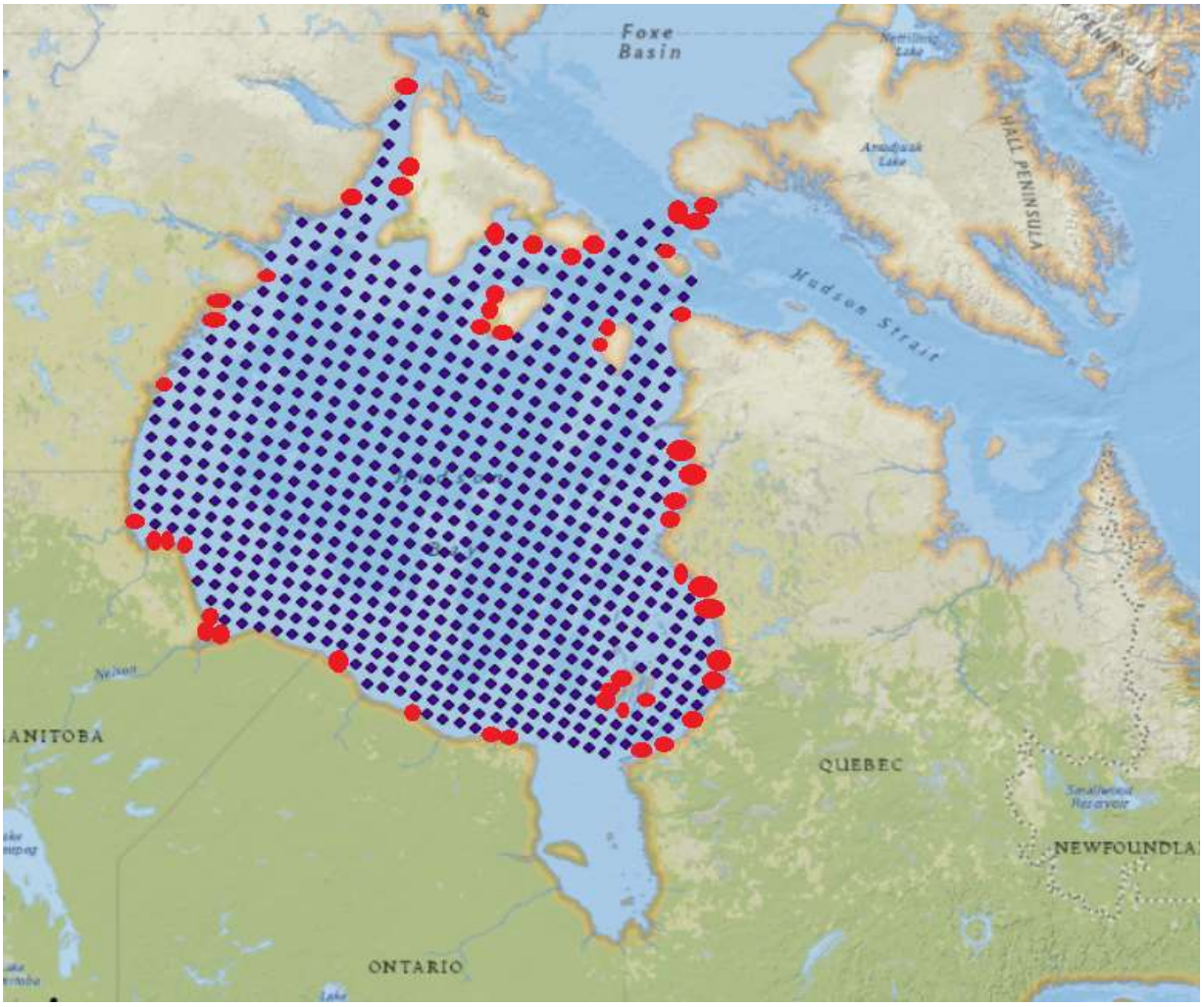

Figure 3.4: Describes each point from where NARR measured the data from at 32 km resolution. Red points indicate the points ids that are not included in analysis.

3.3 Data Analysis

3.3.1 The First Day of Each Season and Its Duration

I. Defining Proportional Ice Coverage

Sea ice concentration (SIC) or sea ice extent (SIE) data is used to determine changes in the cryogenic cycle. Note: the term SIE is not used to describe sea ice coverage because in literature SIE is measured in km^2; while SIC is measured in % relative to other pixels. Since, NARR albedo responds to the absence and presence of ice across the entire Bay in percentage terms "sea ice coverage" is used. Studies on Arctic Ocean have examined the relationship between SIC, SIE and albedo. Perovich & et al (2002) identified five distinct phases in the evolution of albedo: dry snow, melting snow, pond formation, pond evolution, and autumn freeze-up. In April the surface albedo was high (0.8–0.9) and spatially uniform. By the end of July the average albedo was 0.4, and there was significant spatial variability, with values ranging from 0.1 for deep, dark ponds to 0.65 for bare, white ice. These changes were reflected in SIC and SIE data-set. However, similar studies have not been conducted on HB. Nonetheless, to identify seasons in albedo of HB, the monthly albedo data was plotted for each year. Figure 3.5 provides a sample plot for the year 1979.

In HB, four stages of average albedo for the entire Bay could be identified. First, albedo >64% from Dec-May, 63.9%>α>10% from Jun-Jul, <7% from Aug-Sept, and 63.95<α<10% in Oct-Nov (Figure 3.5). This illustrates the evolution in albedo due to seasonal transitions in sea ice cover as described in the literature. SIE and albedo have a positive relationship over the Arctic Ocean, and NARR data clearly indicates presence and absence of ice as 65% and 6%, respectively. The albedo for a specific grid location can be used as a proxy to establish the presence or absence of ice at a given location while the albedo for a region or the entire HB can be used as a proxy for sea ice coverage and to understand changes in sea ice seasons. Since, NARR albedo responds to the absence and presence of ice across the entire Bay in percentage terms "sea ice coverage" is used. To calculate

sea ice coverage, HB was divided into ice-covered and open-water grid locations and these were calculated daily and expressed as a proportion of the total number of grid locations. For ice-covered, number of Pt. Ids with a>7.01% were counted; while, for open-water number of point Ids with a<7.00% were calculated. 7% was selected as threshold for changes in coverage to include the point ids that had albedo ranging from 6.01% to 6.99. As expected, the seasonal changes in albedo closely follow the seasonal changes in ice-coverage and the coverage of ice and open-water change, over the seasons, in a reciprocal manner (Figure 3.6a and 3.6b).

$$\text{Proportion of Open-Water: } \frac{\#\ of\ pt\ ids\ with\ albedo \leqq 7.0\%}{Total\ \#\ of\ grid\ points} \tag{4}$$

$$\text{Proportion of Ice-Covered: } \frac{\#\ of\ pt\ ids\ with\ albedo \geqq 7.01\%}{Total\ \#\ of\ grid\ points} \tag{5}$$

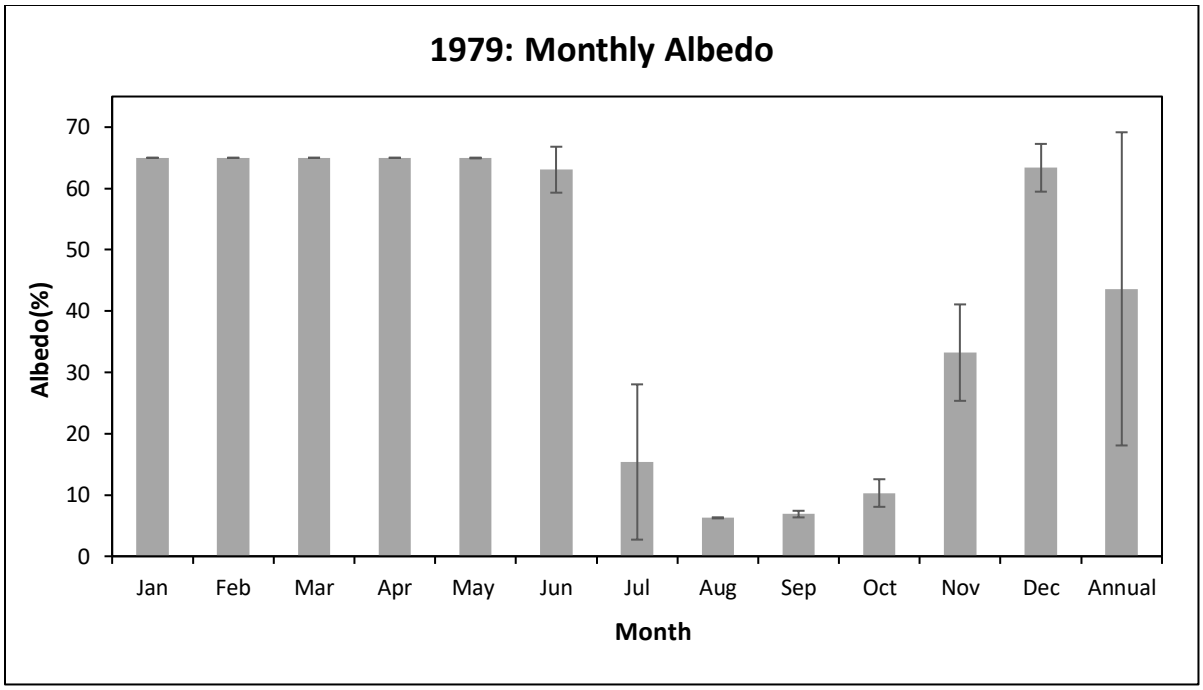

Figure 3.5: Monthly changes in HB average albedo during 1979. Bars indicate standard deviations.

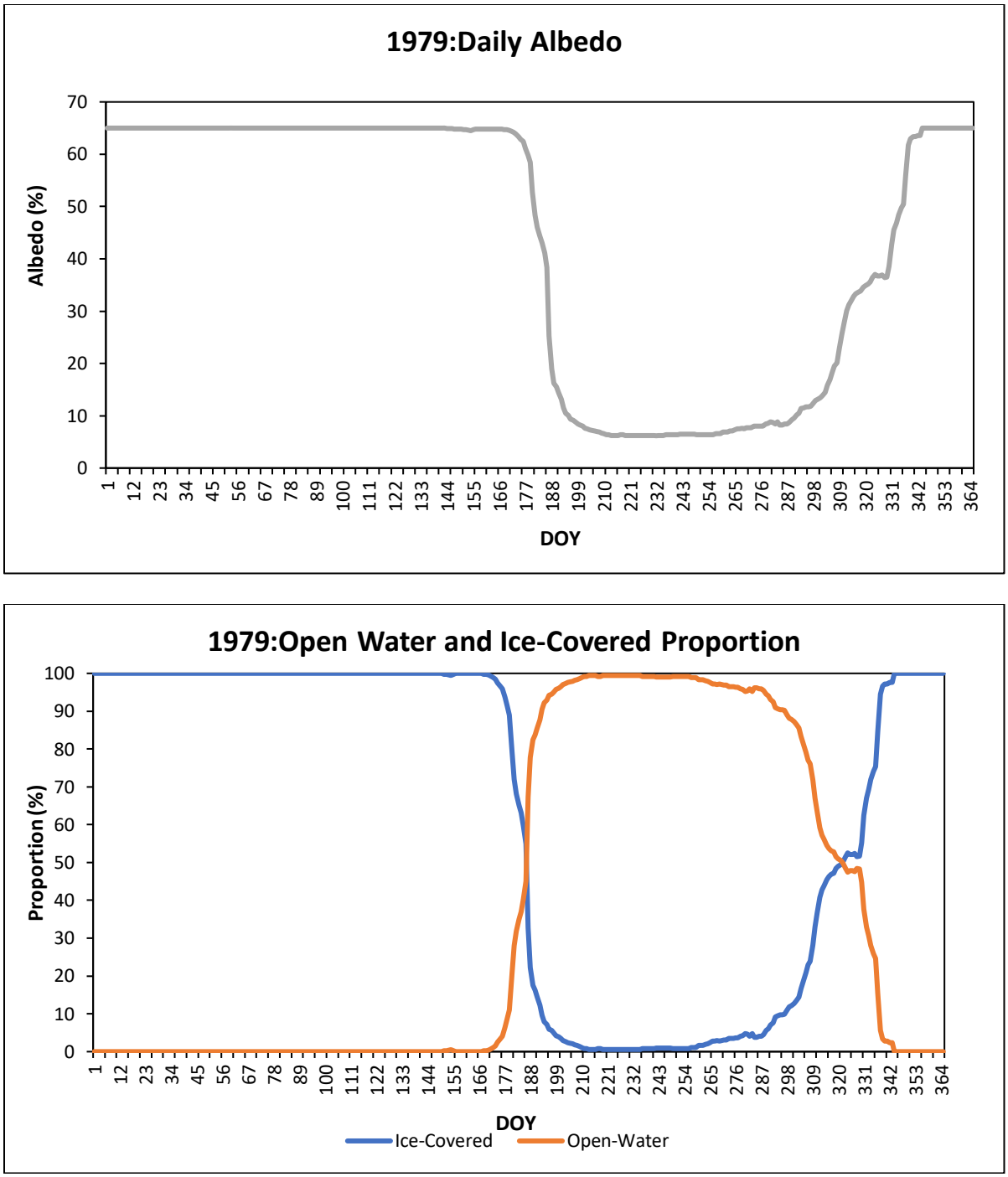

Figure 3.6: A time series from 1979 showing a) the seasonal evolution of HB average daily surface albedo, and b) reciprocal ice-covered and open-water coverage (%) of HB. Note the more abrupt decline in ice coverage during the 1979 break-up season compared to the more gradual recovery of ice-coverage during the 1979 freeze up season.

II. Definition of Annual Dates and Durations of Sea Ice Seasons

Four seasons in the annual ice regime were identified from the proportion of ice-coverage. Rather than define seasons based on the calendar, this study adopts four seasons based on these seasons. First, Ice-Free (IF) which occurs when HB only has water at the surface and no snow or ice exists. In some years, ice-coverage did not reach 0% as it fluctuated around 1-2%; hence, ice-coverage <2% was selected as the starting threshold for IF.

Second, Ice-Covered (IC) season in which HB completely lacks open-water while the ice may grow thicker. However, HB typically does not freeze-up everywhere completely as leads and polynyas emerge and disappear intermittently and are numerous. Also, in a few years HB had ice persisting through August and September which is normally ice-free and therefore never reached 0% ice coverage. To account for these, a threshold of >95% was chosen for the onset of the IC season. The full IC season extends beyond the end of the calendar year into the first few months of the ensuing year.

Third, freeze-up (FU) season occurred when surface temperature falls below the freezing point and further ocean heat loss triggers ice formation. Ice-coverage is expected to increase during this time. The ice-coverage threshold that defines this season begins at >2% and ends at 95%. Variable proportions of the Bay are covered with ice and water during this season.

Lastly, in break-up (BU) season, ice has thinned to the point that it loosens and breaks off from the main ice pack separated by open water. During this season sea ice-coverage is expected to decline and open water coverage increases. Thresholds of <95% and >2% in ice coverage were used to define this season. The beginning and ending dates and duration of each ice season were computed to understand the changes in thermodynamics of HB over the last 40 years. Date is defined as the first day of the year (DOY) when ice-coverage was above or below the threshold. To determine the

date of each season, daily average ice-coverage was calculated for each year and these were put into a master sheet consisting of all 40 years.

A time-series graph was created for each year- daily average albedo on y-axis and DOY on x-axis. This resulted in 40 graphs and notable patterns were noted down. It was expected that ice-coverage would fluctuate across the defined thresholds of different seasons over a night or 4-5 days but that didn't occur. Daily ice-coverage fluctuations were not dramatic as they tended to increase or decrease steadily within each season. Figure 3.6a shows that once the ice-coverage crossed a threshold it remained there. Moreover, seasonal changes on HB were not consistent with the standard calendar seasons; for example, in some years HB remained ice-free until mid-November. Therefore, ice-coverage thresholds; in combination, with monthly thresholds were assigned to each season after examining the variation in all ice seasons over the 40 years.

Four monthly thresholds were created for each ice season. Break-up of ice is caused by dynamic and thermodynamic forces that can be very active in winter; while, some years can be very cold which extend the beginning of the BU period into spring. To take this into consideration monthly thresholds from January1st to August 31st were selected. IF period was proposed to occur from March 21st to Nov 30th within the same calendar year. March 21st corresponds to spring equinox; which marks the beginning of daylength equalling the duration of night-time and generally marks the beginning of radiative surpluses. However, during this time, ice is expected to break and have mixture of open water and ice-covered areas across HB but averaging the daily average albedo across 702 grid point removes that spatial heterogeneity and gives an overall average for HB.

Typically, HB begins to freeze-up in October but as the 2000s approached HB remained ice-free until the end of November. Freeze-up season months do not always occur within the same calendar year, as in some years it extended into January of the following year. While in some years,

FU occurred as early as September 1st. Based on this, a freeze-up months were defined from September 1st to January 31st of the following year. This means that freeze-up period roughly consisted of 5 months. It must be noted that FU start dates and BU end dates and the corresponding durations cannot be calculated for exceptional years when HB was not ice-free. These years were: 1992 and 1999. Lastly, ice-covered season in HB does not occur in one calendar year; instead, it proceeds onto the next year. However, it was observed that some years HB became ice-covered as early as November; while, in extremely cold years it stayed frozen until July based on the ice-coverage. However, to simplify the threshold dates August 31st was chosen as the cut—off for ice-covered season to consider years such as 1993 that had very short IF season. Therefore, monthly threshold for ice-covered period extended from Nov of previous year to August 31st of next year; which consisted of 10 months. It must be noted that data-set lacked September 1st to December31st, 1978; January 1st to August 31st which, means freeze-up and ice-covered duration and dates could not be calculated for the year 1979, and 2018. Figure 3 provides a schema for dates and duration for the year 1980.

The combination of monthly and ice-cover thresholds were used to calculate the duration and date of each season from 1979-2018 in Excel 365. This was done as a command cannot be written in excel to allow it to pick the time-frame when the ice-coverage is increasing or decreasing. To calculate the duration, the number of days in each of the BU, IF, FU and IC seasons were counted using the "COUNTIF" command in Excel. The daily average ice-coverage graphs were created for each year these were examined to identify the days corresponding to each season manually. In addition, date identification was automated using excel as described by the formulas in Table 2. It must be noted that in years 2001 and 2010 HB became ice-covered in January of next year the

manual date was used rather than automated date. Later, both manual and automated dates were compared these were found to be identical; ensuring that the formula is working correctly.

Table 3.1 Defines the four ice seasons.

Season	Definition	Ice-Coverage Threshold (%)	Monthly Threshold
Break-Up	Loosening of ice. Combination of both water and ice.	95 <Ice-Coverage< 2.01	Calendar Year January 1st - August 31st.
Ice-Free	Absence of ice.	<2.0	Calendar Year March 21st to November 30th
Freeze-up	Ice starts to form, combination of both water and ice.	2.01<Ice-Cover<95	Winter September 1st to January 31st.
Ice-Covered	Fully covered in ice.	>95.01	Winter November 1st to August 31st.

.

Table 3.2 Formula used to compute the Juliann Date for each year in Excel 365

Season	Excel Formula	Formula Meaning
Break-Up	If ice-coverage values are present then from January to August count the number of days when the ice-coverage was greater than 95.01%.	=IF(D6>0,COUNTIFS(D6:IL6,">"&NL1),"")
Ice-Free	If ice-coverage values are present then from January to August count the number of values that are less than 2.0% and subtract this from 244. *244 for leap years. * 243 for normal years.	=IF(D6="","",IF(COUNTIFS(D6:IL6,"<"&NM1)=0,0,244-COUNTIFS(D6:IL6,"<"& NM1)))
Freeze-up	If ice-coverage values are present count the number of values that are less than 7.0% from September 1st to December 31st then add 244. *244 for leap years. * 243 for normal years.	=(IF(COUNTIFS(JR6:OI6,"<"&OQ1)=0,0,COUNTIFS(JR6:OI6,"<"&OQ1)+244))
Ice-Covered	If ice-coverage values are present Subtract the number of days from 366 when the albedo was greater than 61% from September 1st to December 31st . *366 leap year * 365 normal year	=NB1-COUNTIFS(IK4:OI4,">"&OR1)

III. Statistical Tests for Dates and Durations:

The dates and durations were plotted as time-series: dates and duration on the y-axis and year on x-axis. In particular, for ice-covered DOY for the years HB became ice-covered in January 30 days were added to 365 days. This means number of days above 365 indicates that it occurred in the next year. For example, in 2011 HB was ice-covered on January 14, 2012; to represent this on the DOY graph 365+14= 379 was plotted on the graph.

Time-series consist of three components: trend assumed to be linear; serial correlation at lag 1 (r1) and white noise. Serial correlation is also known as autocorrelation and does not affect consistency of ordinary least square (OLS) estimators but it does affect their efficiency. With positive serial correlation, the OLS estimates of the standard errors are smaller than true standard errors and the opposite occurs with negative serial correlation (Williams, 2015). . This can result in false conclusion that there is a relationship when there really isn't. There will be a tendency to reject the null hypothesis (H_O) when it should not be rejected. Nonetheless, the presence of serial correlation can indicate interannual variability in each season which is important to understand thermal memory that influences ice growth and break-up from one year to another. AR_1 coefficient was determined by correlating the time-series with subsequent observation using Excel. To determine whether it lies within the upper and lower limits of autocorrelation, the confidence intervals was calculated using the following equation:

$$\frac{-1-1.96\sqrt{N-2}}{N-l} \leq r_1 \leq \frac{-1+1.96\sqrt{N-2}}{N-1} \quad (6)$$

where r_1= lag 1 autocorrelation coefficient and N= # of years (Salas & et al., 1980). If r_1 falls within the above interval, the timeseries is composed of independent observations. Otherwise, the data is serially correlated at the 95% confidence interval; positive r_1= positive serial correlated while negative r1= negative serial correlation. It was important to identify positive and negative AR_1; since,

it can indicate whether dates and durations in one year depend on the previous. Meanwhile, negative AR_1 would reveal oscillation in dates and durations with above average values immediately followed by below average values.

Yue & et al. (2002) proposed a 4 step method before assessing the statistical significance of trends in presence of serial correlation. The method consists of four steps. First, the slope of the data is estimated using Theil-Sen Approach (TSA) which is ideal for non-parametric tests and provides a better slope estimate than least square method because outliers and extreme values in the timeseries affect it less (Gagnon & Gough 2004). The slope of the TSA trend line for season's duration and dates was calculated using Rstudio by downloading the package 'modofiedm' and command 'bcpw' which generates the TSA slope. Afterwards, TSA trend line was calculated using the following expression:

$$Y=mx+b \tag{7}$$

$$b= -Y+mx \tag{8}$$

where b= intercept , Y= median of variable tested for, m= TSA slope, x= median of time only including the years for which the data is present for. TSA trend was removed from the time-series. Secondly, Autoregression at lag 1 (AR_1) was extracted from the detrended time-series. AR_1 component was calculated by shifting the y-values forward by 1 year and conducting regression analysis between the original and shifted time-series on Excel. This determines the AR_1 component that was extracted from the detrended time series. Third, the residual and linear trend time-series were combined. Fourth, the Mann-Kandall (MK) test, also known as Kendall's tau, where x-axis is time, was applied to determine whether the trend is significant or not at statistical level of 0.05 which corresponds to 95% confidence interval. The non-parametric test indicated whether y-values increase or decrease with time and was only valid in the absence of serial correlation. However, MK

test does not provide an estimate of the trend magnitude; hence, TSA slope was used. In the absence of serial correlation, only the first and fourth steps were performed. Nonetheless, to understand whether parametric and non-parametric approaches affect the slope and significance least square regression was performed for duration of each season vs. years.

To further understand, whether duration of one season affects the length of another season; in other words, climate memory scatter plots were created- ice-covered vs. break-up, ice-free vs. freeze-up, ice-covered vs. freeze-up and break-up vs. ice-free. Linear regression at 95% confidence interval was conduced to determine significance.

3.3.2 Energy Budget

One dimensional energy budget components were examined. Net radiation, Q* was computed using expression 1. The energy fluxes were plotted for the entire time-series to identify any cycles, maximum and minimum. However, it was observed that Q_H and Q_E sign convention was opposite of what is described in literature- positive in fall and winter months. It was found that NARR codes these variable due to the ETA model. Therefore, these fluxes were multiplied with the correcting factor of -1. Then, Q_{ST} was calculated using expression 4 for each point id for each year's daily average data. Q_{ST} was calculated for each point id then averages were calculated for seasons and regions including the whole of HB. This ensured that horizontal divergence that existed due to positive and negative advection at each grid location, cancels (Bello & Higuchi, 2019) provided HB behaves as a closed system. This is only approximately true as ocean currents carry water flowing in and out of the Bay from river runoff through two straits.. Also, because Q_{ST} was calculated as a residual, it combines systematic errors in any of the independent terms (Bello and Higuchi, 2019) in expression 1 and 4. Daily averages for the whole Bay and ice and water cover locations were calculated and plotted versus time to examine the variability in Q_{ST} throughout each ice season over the past 40 years.

T_o calculate, a portion of energy fluxes for total, open-water, and ice-covered areas of HB two techniques were used: weighted Q_{ST} flux and non-weighted Q_{ST} flux. The same techniques were applied to all the other component fluxes. The unweighted fluxes portray the average energy regime of a given cover type (i.e ice or water), regardless of its dominance. Weighted fluxes take into consideration the proportional coverage of ice and open water. The sum of the weighted fluxes would represent the energy regime of the Bay as a whole.

NARR fluxes are archived in units of Wm^{-2} and were downloaded as daily averages. The conversion to $MJm^{-2}d^{-1}$ is straightforward requiring the number of seconds in a day. (86400 x 1E-06). The less intuitive step involves converting fluxes from their daily equivalent to their seasonal equivalent. Normally this is straight forward and involves a multiplier which considers the number of days in a particular season, which is fixed for calendar seasons (except February every four years). But for the ice seasons considered here, the seasonal average flux includes both the influences of changes in flux intensity from year to year and the duration of the seasons from year to year. Therefore, the behaviour of a seasonal flux average and seasonal flux total may vary from one another over time depending on which factor is responsible for the change in magnitude. The intensity and magnitude of energy loss/gain from the Bay during different seasons are both important.

3.3.3 Ice Thickness

The day the snow or ice disappears each year depends on both the amount of snow or ice that has accumulated and the cumulative amount of energy available for melt. The property of ice that controls the amount of time it takes for ice to break-up is ice-mass per unit area and assuming a uniform density is directly convertible to ice-thickness. During the FU and IC seasons subsurface flux energy (Q_{ST} in MJ/m^2) lost or gained from the ice-covered parts of the Bay was used to calculate ice-growth, IG (mm) using the following relationship as a first approximation.

$$IG = -Q_{ST}/L_F/\rho_{ice} \quad (9)$$

where Q_{ST}- is the subsurface heat flux (MJ/m^2),L_F- latent heat of fusion (0.334 MJ/kg), ρ_{ice}- density of ice (920 kg/m3). This value was used as ice thickness on Day0 of each season, and ice growth was calculated by accumulating growth (+/-) for each day of the season This approximation ignores variations in ice density that may exist through the ice pack, variations in Lf that may arise due to the effects of salinity and divergence of energy across the top and bottom of the ice pack, as only the surface flux is available. It does however make the same assumptions for all seasons and for all years, and hence may provide an estimate of the variability of ice growth from year to year. Ice thickness, computed this way, was plotted throughout the IC season for all years and showed that ice had, not only thinned but disappeared completely towards the end of the ice-covered season. Therefore, only maximum ice thickness during ice-covered season was considered. It is noted that ice thickness was not calculated for 1992 and 1999 (absence of IF Season); and 1988 (no growth of ice). Maximum ice thickness during IC season and ice thickness at the end of the Freeze-Up season were plotted against time to identify whether thickening or thinning trends are present

.

3.3.4 Surface Temperature

Surface temperature (T_0) was identified to be one of the variables of interest as the surface freezing point should signify the onset of freezing or melting. Temperature profiles of the entire water column are not available. It was calculated from the longwave fluxes as a daily average for each location on HB using:

$$T_0 = \left(\frac{L\uparrow - L\downarrow(1-\varepsilon)}{\varepsilon\sigma}\right)^{0.25} \quad (9)$$

where ε=surface emissivity- 0.97 and σ= Stefan-Boltzmann constant-$5.67*10^{-8}$. T_0 was subtracted from 273.15 to convert K into ^oC. and was calculated for both open-water and ice-covered areas. T_0 was plotted as a timeseries to identify any trends; as well, linear regression was performed against Q_{ST} to identify whether the two are related. This was only done for BU and FU seasons as these seasons are responsible for 75% variation in SIE (Barber & Hochheim, 2014).

Chapter 4: Results

4.1 Trends in Ice Coverage

In general, sea ice undergoes a complete cycle each year. HB is completely ice-covered and remains frozen longer as shown by the flattened peaks; whereas, ice-free troughs are not flattened indicating that the IF season does not last as long as the IC season (Figure 4.1). Variations exist in sea ice-coverage throughout the timeseries at both annual and monthly time-scales. The region begins to freeze-up in November and is completely ice-covered by January. Break-up begins in May and by August it is completely ice-free and remains ice-free throughout September-October (Figure 4.4). Notably, a steep drop occurs in ice-coverage from June to July; while, a steep incline occurs from November-December (Figure 4.4). Nonetheless, monthly sea ice-coverage behaves similarly in some months allowing it to be divided into 4 groups: January-May, July and November, June and December, August-October (Figure 4.5). The greatest variation was present in both November and July, followed by June and December ; while, from January-April sea ice-coverage has not changed dramatically except for May (Figure 4.5a). The major shifts in the month of greatest variability began in the mid-1990s (Figure 4.5; Figure 4.2; Figure 4.3) with sea ice-coverage declining in all months; except for ice-free months (Figure 4.4).

In the last 40 years, annual sea ice-coverage had positive serial correlation ($r= 0.64$, $df=39$, $p<0.05$); and MK test unveils trends strong ($tau=0.47$) statistically significant at 95% confidence interval that ice-coverage has been decreasing each year by -0.22% (Figure 4.3). At magnified scale, the annual ice-coverage trend can be split into two group: 1979-1995 when ice-coverage is increasing; and 1996-2018 when ice coverage decreases (Figure 4.3). The distribution of ice-coverage in each year reveals that starting 1996 ice-coverage began to shift towards first quartile; indicating, ice—coverage is declining. Overall, HB did not reach minimum of 0% instead average

is 0.28% in Ice-Free season and maximum of 99.08% in Ice-Covered Season (4.6a). Maximum (100%) and minimum ice-cover (0%-0.28%) were approximately the same each year. In the 40 years, annual maximum ice-coverage was 79.02% which occurred in 1992. 1992 had minimum sea ice coverage-18.02% in September which is higher than other years (Figure4.6b); Sea ice-coverage remained constant(100%) for most the year with fluctuation from day 195 (July 14th) to until it reached 100% towards the end of the year. On the other hand, 2010 was the year of minimum sea ice-coverage with annual sea ice-coverage of 52.24%. At the beginning of the year, sea ice-coverage was 100% but began to decline starting day 75 (March 16th) reaching a minimum of 0.28% throughout the year and did not reach maximum ice-coverage at the end of the year (Figure 4.6c). In other years, bay reached 0% ice-coverage during the IF season.

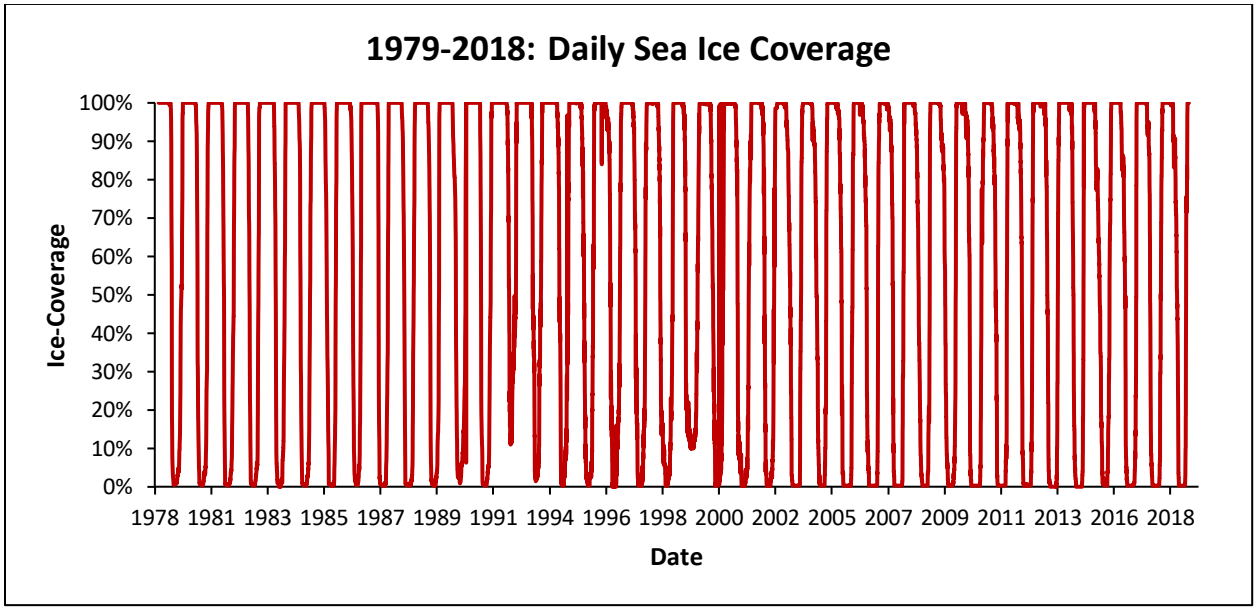

Figure 4.1: Time series of daily ice-coverage for HB from 1979 2018. (n= 40 x 365(6)).

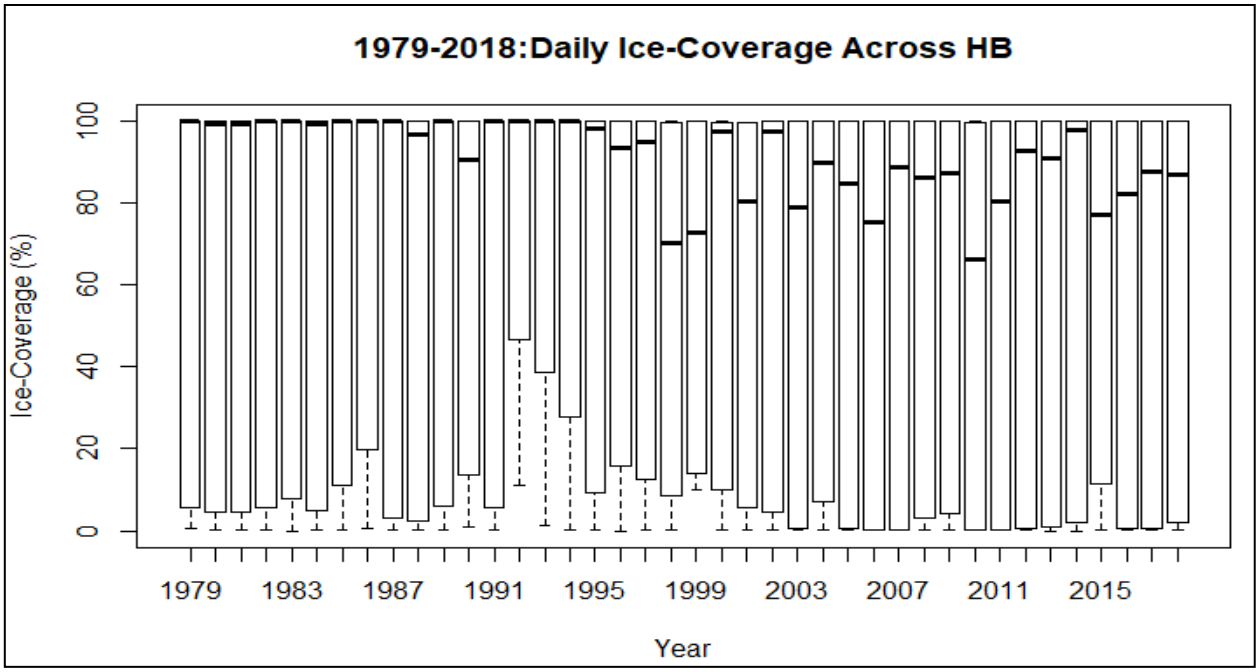

Figure 4.2:Box and whisker plot of daily ice-coverage by year for HB from 1979 to 2018.

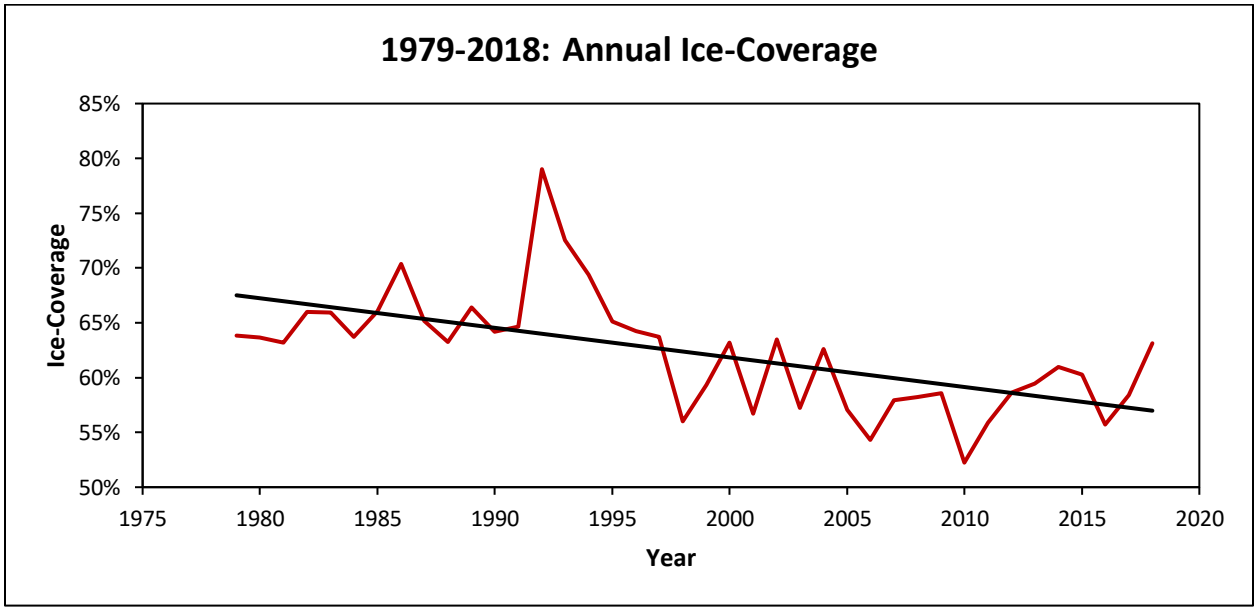

Figure 4.3: Trend in annual mean sea ice coverage from 1979-2018 with m=-0.22, tau=-0.47, p<0.05.

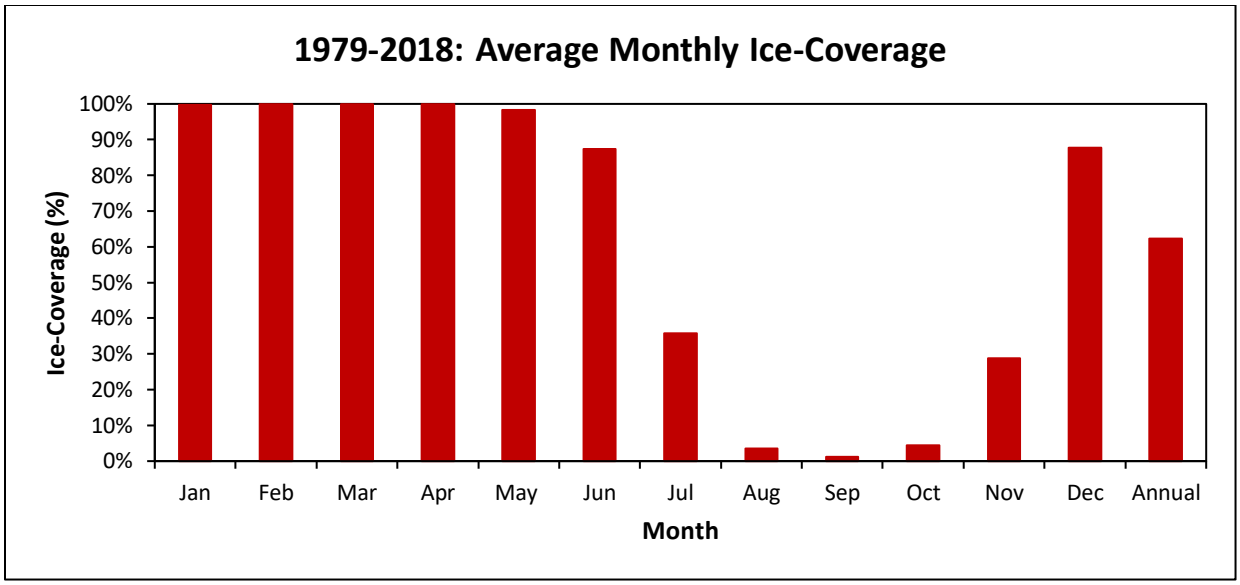

Figure 4.4: Forty-year (1979-2018) mean monthly ice-coverage.

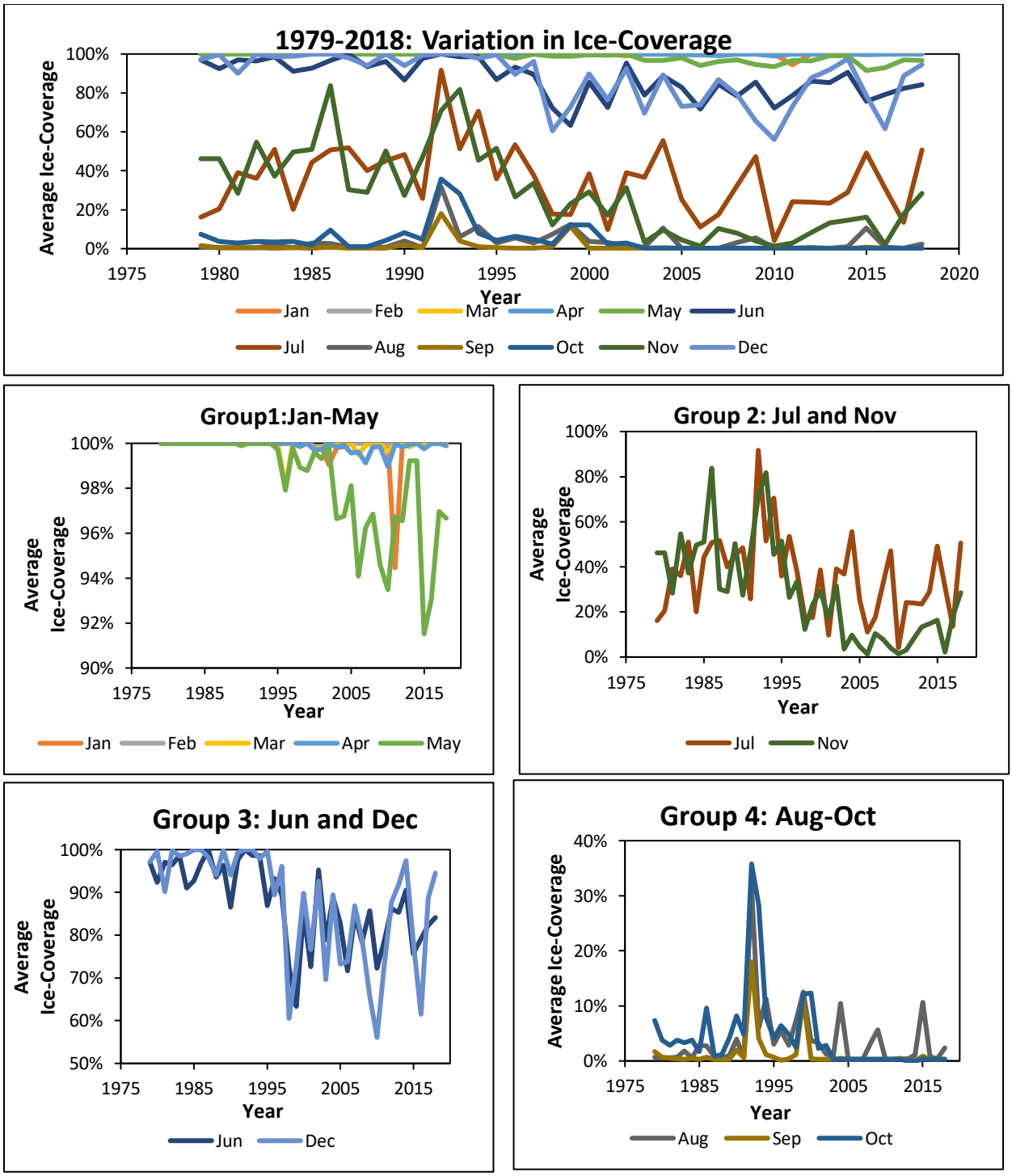

Figure 4.5:Forty year times series of mean HB ice-coverage by month. a) for all months, b) January through May, c) July and November, d) June and December, e) August through October.

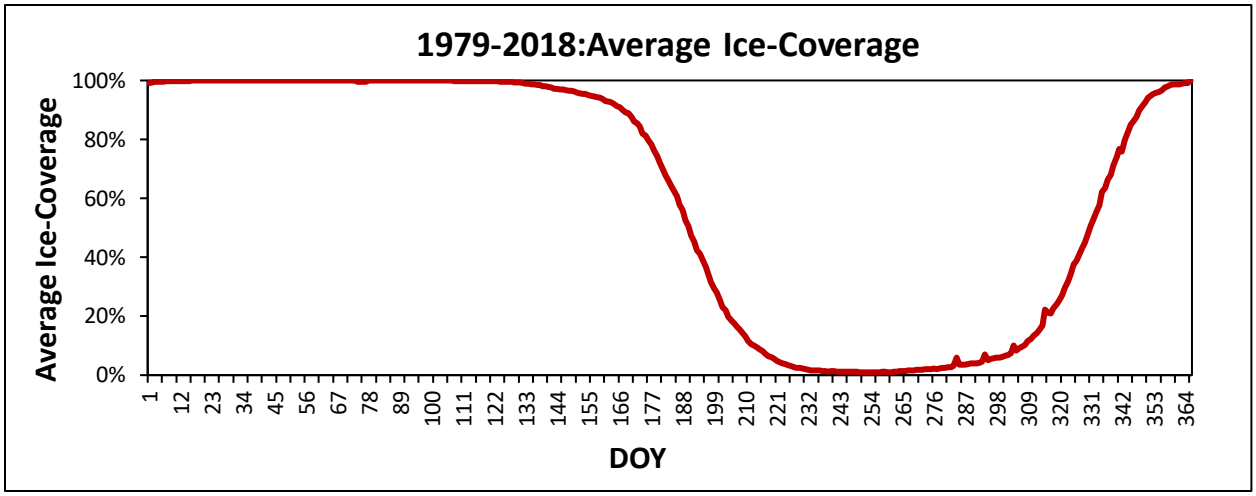

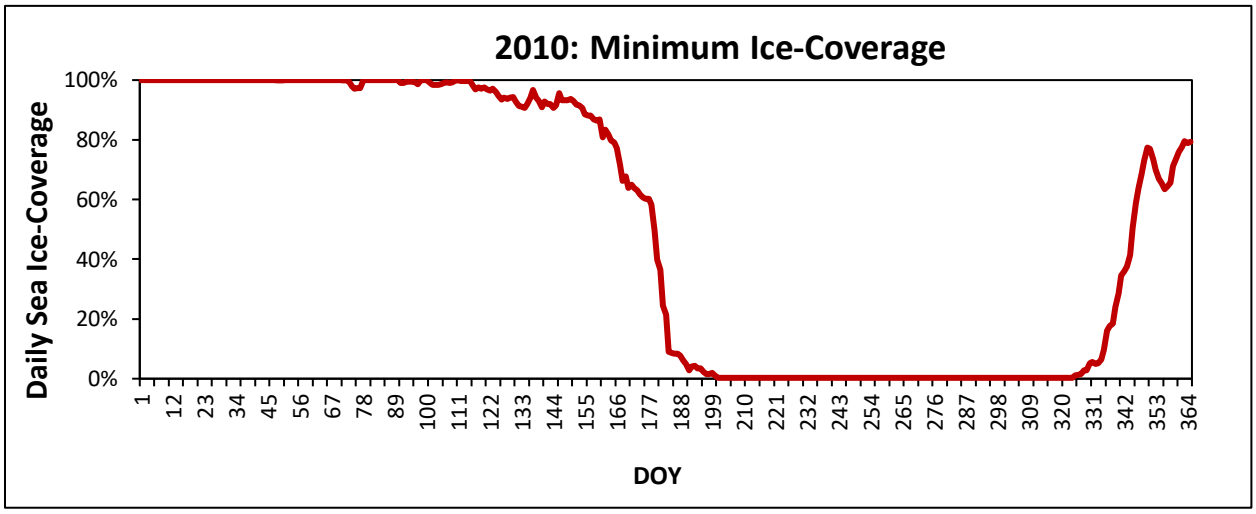

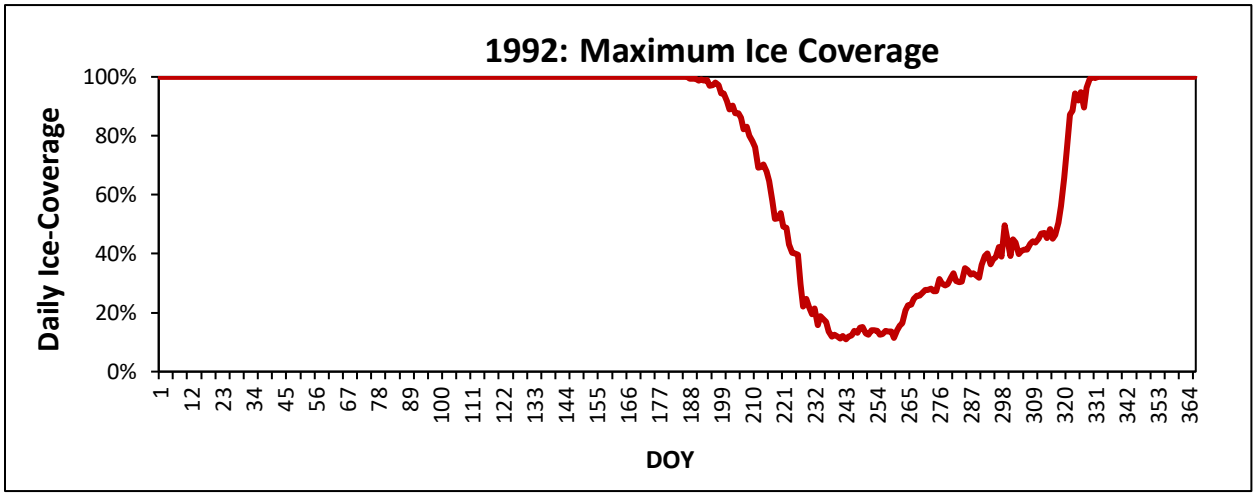

Figure 4.6.: Daily HB ice-coverage a) averaged for the years 1979-2018, b) for 2010 the year of minimum ice coverage, and c) for 1992 the year of maximum ice-coverage.

4.2 Trends in The Dates and Duration of Each Season Introduction

HB has been undergoing changes in ice coverage in all four ice seasons.

4.2.1 Dates and Durations of Each Ice Season

I. General Trends and Patterns in Dates and Durations

In general, break-up, BU season begins on day 158 (June7th). Throughout the last 40 years, ice broke earliest on DOY 125 (May 25th) in 2010; whereas, ice broke latest on DOY 188 (July 7th) in 1987 (Figure 4.7). Ice has been breaking earlier by 1.07 days per year with relatively strong Kendall's tau of 0.56 at 95% confidence interval. In addition, the average duration of the BU season is approximately 61 days. Variation exists among the years with a maximum duration of 94 days in 1998 and a minimum duration of 26 days in 1987 (Figure 4.9). However, ice is taking longer to break-up by 1.17 days later ($p<0.05$) over the last 40 years. The BU season is followed by the ice-free, IF season. On average, HB is completely ice-free by DOY 219 (August 6th). HB became ice-free latest in 1990 on DOY 250 (September 5th) and became ice-free earliest in 2010 on DOY 197 (July 16th). Ice-free dates over the past 40 years have no trend (Figure 4.7; Figure 4.8). However, the duration of IF season has been extended over the past 40 years. On average, HB remains ice-free for 73 days (Table 4.2) with no true ice-free season in 1992 and 1999; while the longest IF season occurred in 2010 and lasted for 131 days (Figure 4.9). IF seasons have been extended by 1.33 days per year (Figure 4.9).

Ice-free seasons are followed by freeze-up (FU) season. Typically, HB begins FU on DOY 296 (October 23rd) but over the years the onset of FU has been fluctuating with slightly later freeze-up dates before 1990, earlier onsets of freeze-up from 1989-2002 and steep delays in freeze-up from 2003-2018 . Overall, a delay in the onset of FU of 1.29 days per year has been occurring over the past 40 years (Figure 4.7). Nonetheless, dramatic changes were observed in the duration of the FU season. HB freezes up earlier by 0.68day per year (Figure 4.7) with the shortest FU season (23 days)

in 2014 and the longest FU season (83 days) in 2001 (Figure 4.9). Lastly, HB typically becomes ice-covered on DOY 345 (December 11th) but variation exists in the first day of complete ice cover from year to year. The earliest HB became ice-covered was in 1987 on DOY 316 (November 11th) and the latest was in 2011 on DOY 380* (* 365+15, January 15th). Overall, HB is becoming ice-covered later by 0.61days per year (tau=0.42, $p<0.05$) (Figure 4.7). In addition, the IC season has become shorter by -1.77days per year (tau=-0.61, $p<0.05$) (Figure 4.9). Lastly, parametric and non-parametric statistics were performed for durations of each season. Both showed very similar results; in terms of significance; while trends differed slightly. (Table 4.3)

Table 4.1: Average onset DOY and coefficient of variation and AR_1 components of each ice season from 1979-2018.

Season	ONSET DOY	Coefficient of Variation	Ar_1 Coefficient	Ar_1 Significance
Break-Up	158 (Jun 6th)	0.10	0.64	p<0.05
Ice-Free	219 (Aug 7th)	0.05	0.29	p>0.05
Freeze-Up	296 (Oct 23rd)	0.08	0.74	P<0.05
Ice-Covered	345 (Dec 10th)	0.04	0.42	p<0.05

Table 4.2: Average duration and coefficient of variation of each ice season from 1979-2018.

Season	Average Duration (days)	Coefficient of Variation	Ar_1 Coefficient	Ar_1 Significance
Break-up	61.26	0.32	0.35	p<0.05
Ice-Free	73.30	0.45	0.62	p<0.05
Freeze-up	48.16	0.36	0.59	p<0.05
Ice-Covered	178.69	0.15	0.76	p<0.05

Table 4.3: Comparison of non-parametric and parametric statistics for duration of each season from 1979-2018

Season	Least Square Regression Slope (Parametric)	Least Square p-Values	Theisen's Slope (Non-Parametric)	Theisen's Slope p-value
Break-Up	1.06	p<0.05	1.17	p<0.05
Ice-Free	1.42	p<0.05	1.33	p<0.05
Ice-Covered	-1.76	p<0.05	-1.77	p<0.05
Freeze-Up	-0.70	P<0.05	-0.68	p<0.05

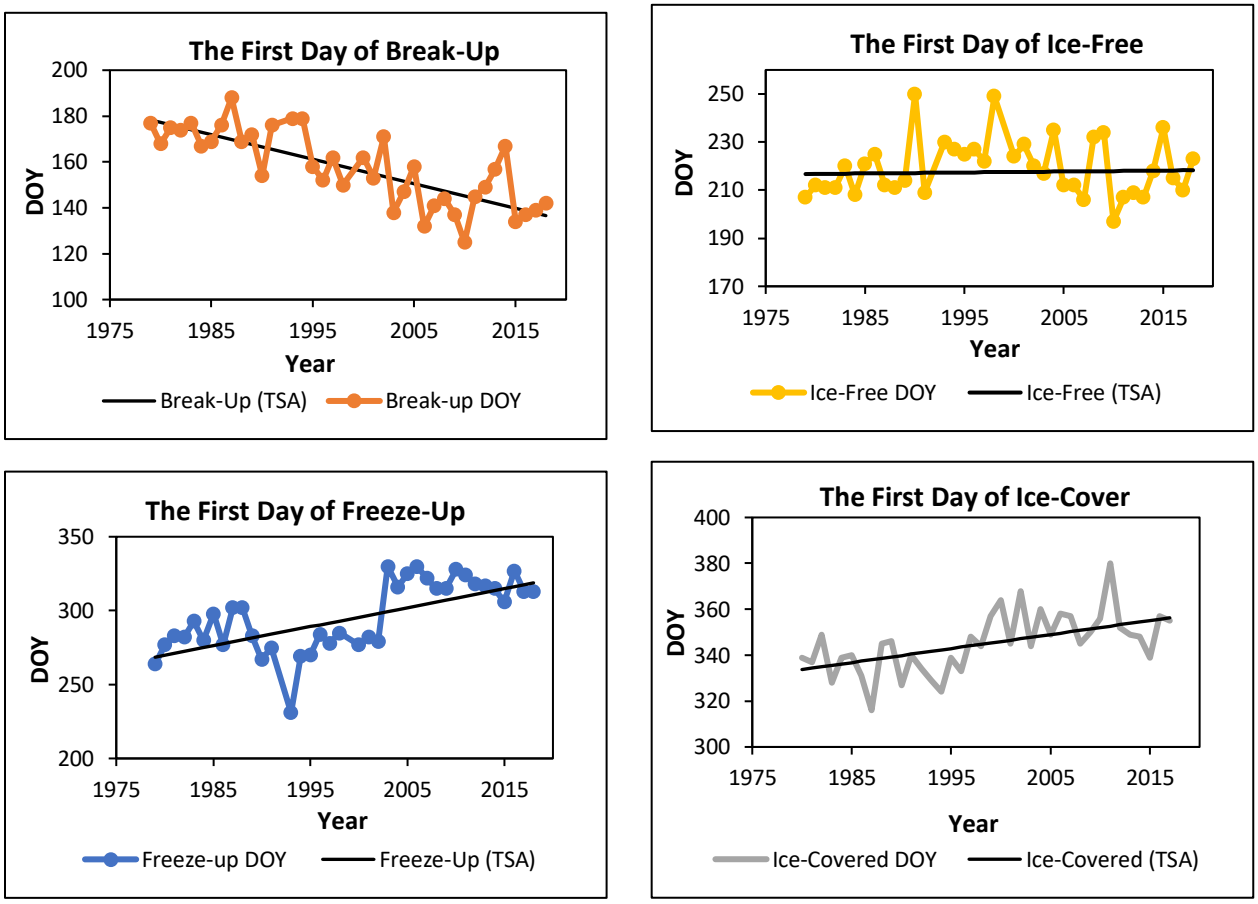

Figure 4.7.: First day of each ice season a) BU season m=-1.07, tau=-0.52, p<0.05, B) IF season m= 0.04, tau= -0.15, p>0.05, c) FU season m= 1.29, tau=0.31, p<0.05, d) IC season m=0.61, tau=0.42, p<0.05 .Note: red on the ice-covered graph marks that ice-covered occurred in the January of the next calendar year.

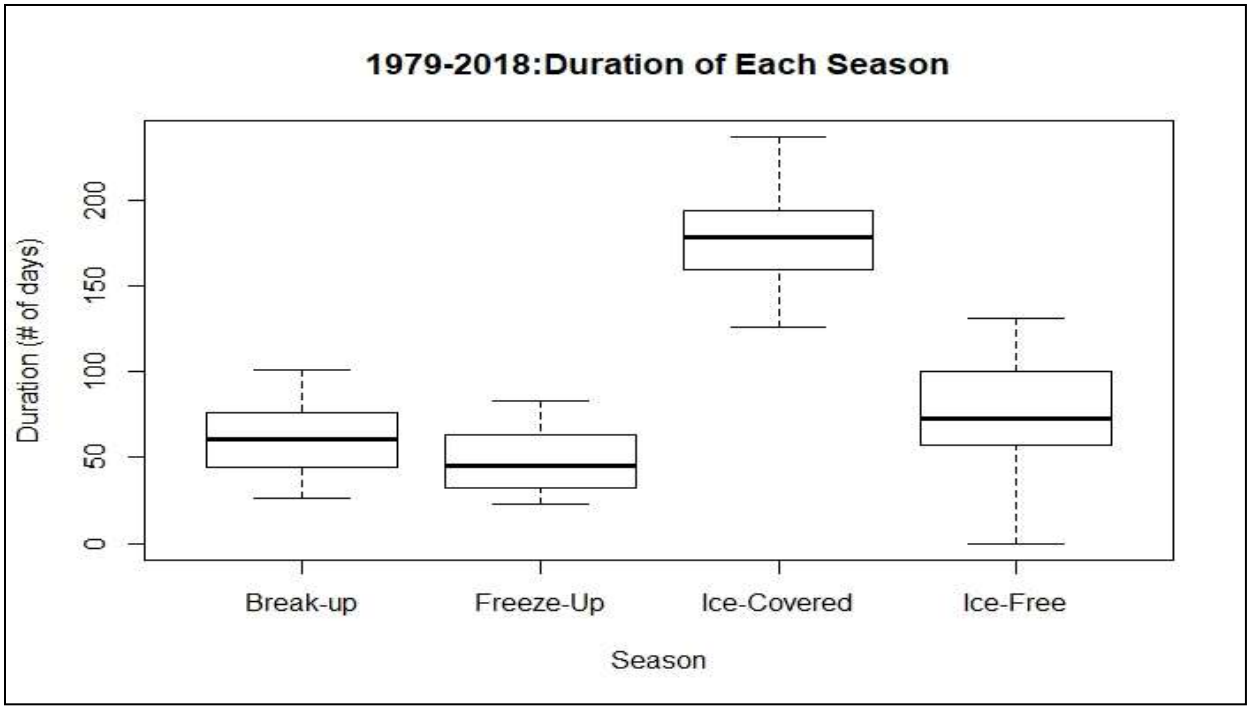

Figure 4.8: Comparison of distributions of duration (number of days) of each ice-season for the years 1979 to 2018.

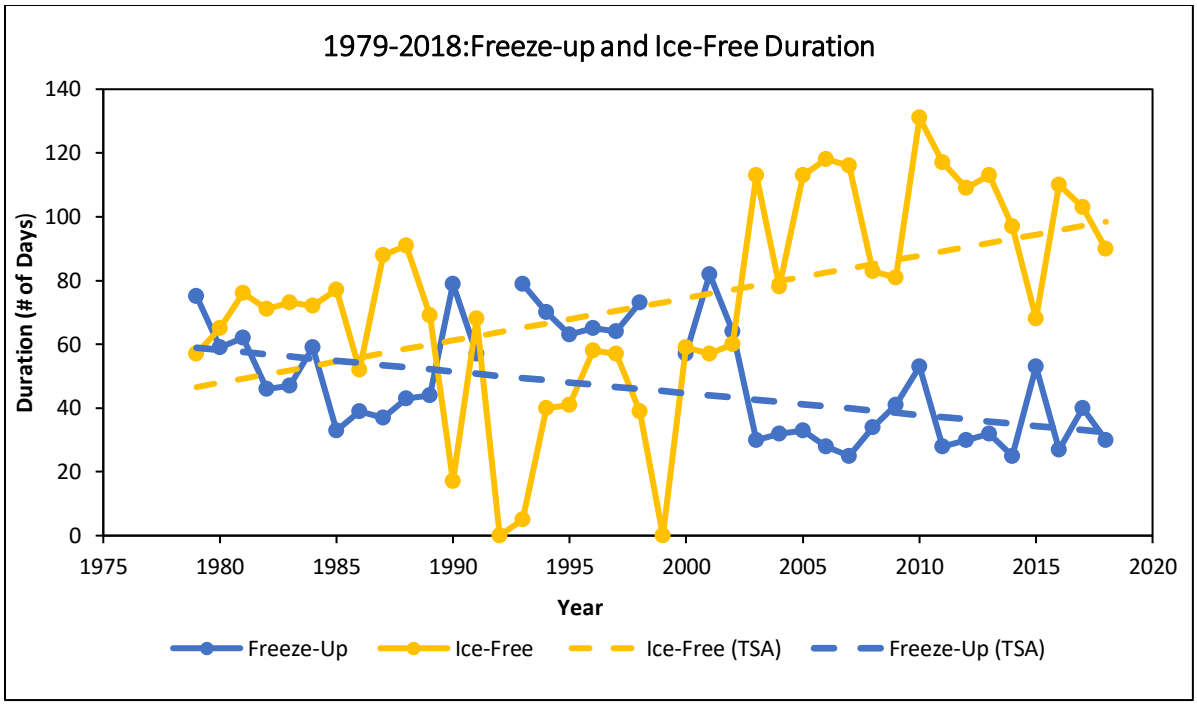

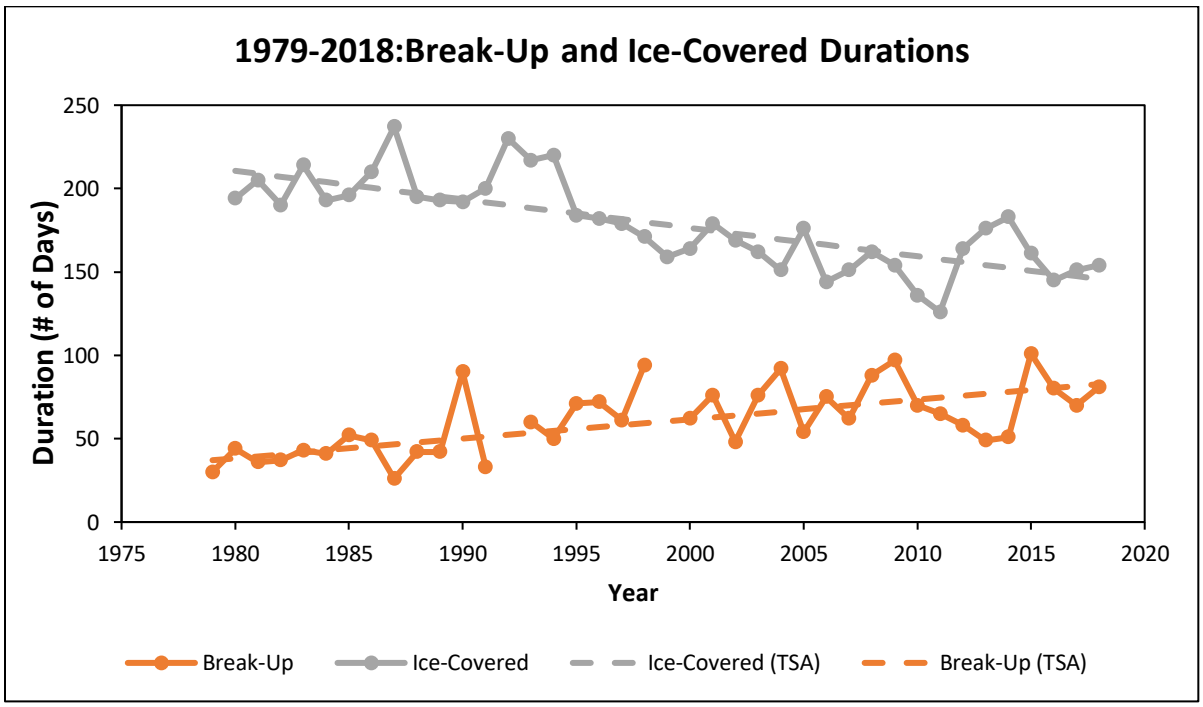

Figure 4.9: Time series of ice season durations and trends 1979-2018 for a) IF season , m=1.33, tau=0.38, p<0.05; FU season, m= -0.68, tau= -0.24, p<0.05 b) BU season , =1.17, tau=0.42, p<0.05; IC season , m= -1.77, tau=-0.61, p<0.05.

II. Relationships between ice season durations

For the first day and duration of each ice season, significant positive serial correlation was present, except for ice-free onset dates. Table 4.1 and Table 4.2 describe the serial correlation coefficients and their significance. The greatest variation, as indicated by coefficient of variation in DOY of each season can be ranked as: BU>FU>IF>IC (Table 4.1). Likewise, the greatest variation in the duration of each season is ranked IF>FU>BU>IC. Box-plots comparing the duration of each season provide further insight into the variability (Figure 4.8). BU is symmetric which means the length of the BU season is frequently closer to the mean (61.26 days). Also, the length of BU and FU seasons are similar. However, FU is skewed to the right indicating that it is becoming shorter. IC seasons tend to be the longest and the distribution is symmetric as well. The greatest variation exists in the IF season with right skew indicating that in the last 40 years IF durations are shorter. Also, open-water and ice-covered proportions change in each season across the Bay. During the FU season, the growth of ice cover follows an exponential growth; while, open-water decreases exponentially. During the IC season, the proportion of open-water remains fixed at 0%; while, the ice-covered proportion remains close to 100% with the opposite being true during the IF season (Figure 4.10).

The seasonal cycle of HB follows this order: Break-Up, Ice-Free, Freeze-Up and Ice-Covered. Figure 4.11 describes the trends in the relationships between the length of contiguous seasons. First, the BU season has a weanegative relationship with the preceding of IC season (R^2=0.40, $p<0.05$). An extended IC season is followed by a shorter BU season. Second, the length of IF season is unrelated to the length of the preceding BU season (R^2= 0.001, $p>0.05$). Third, the length of the IC season has a weak positive relationship with the preceding FU period (R^2=0.13, $p<0.05$). Last, the FU season is negatively related to the preceding IF season (R^2=0.65, $p<0.05$).

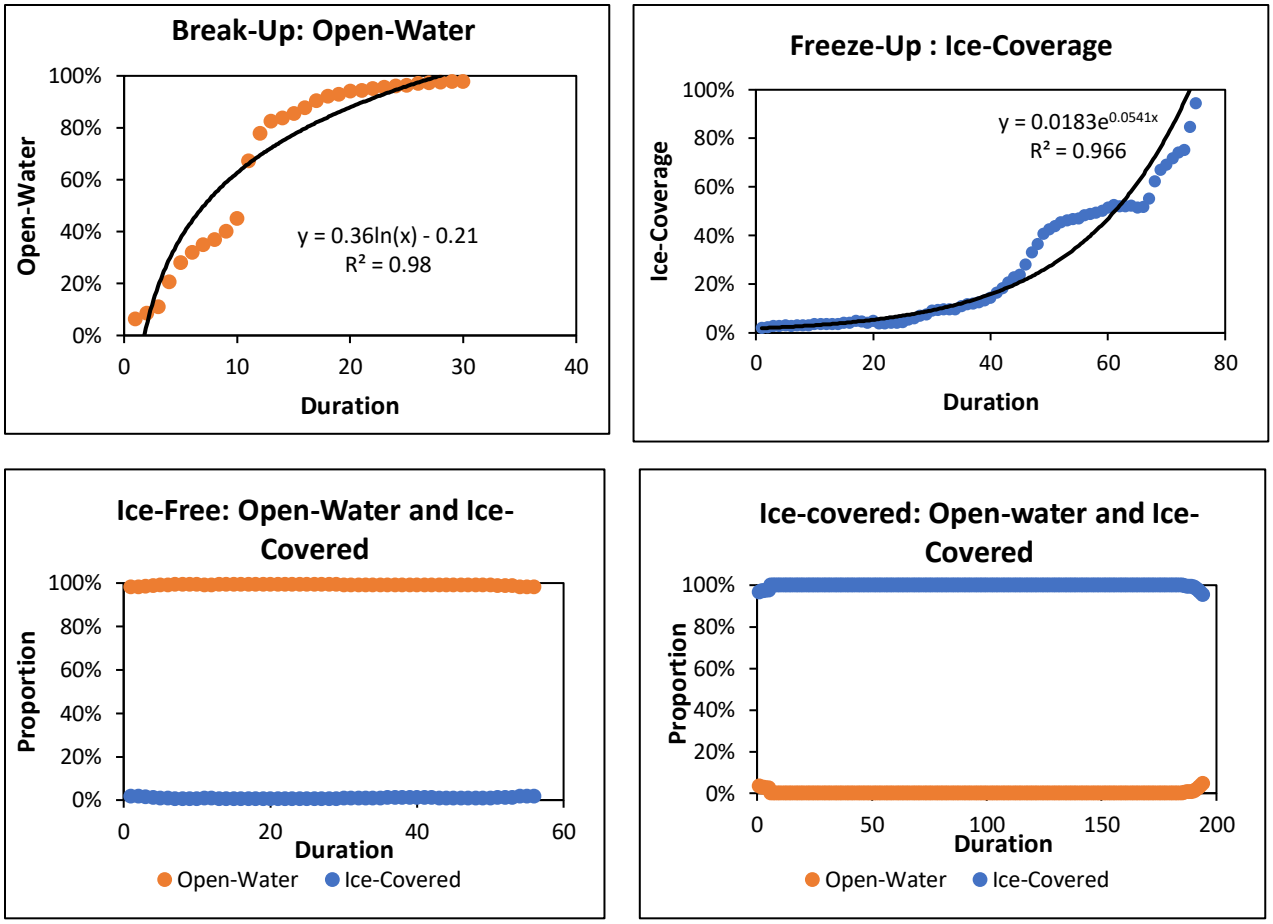

Figure 4.10: Characteristic changes in the proportion of ice-covered and open water in each season BU (a) FU (b) IF (c) IC (d) during 1979.

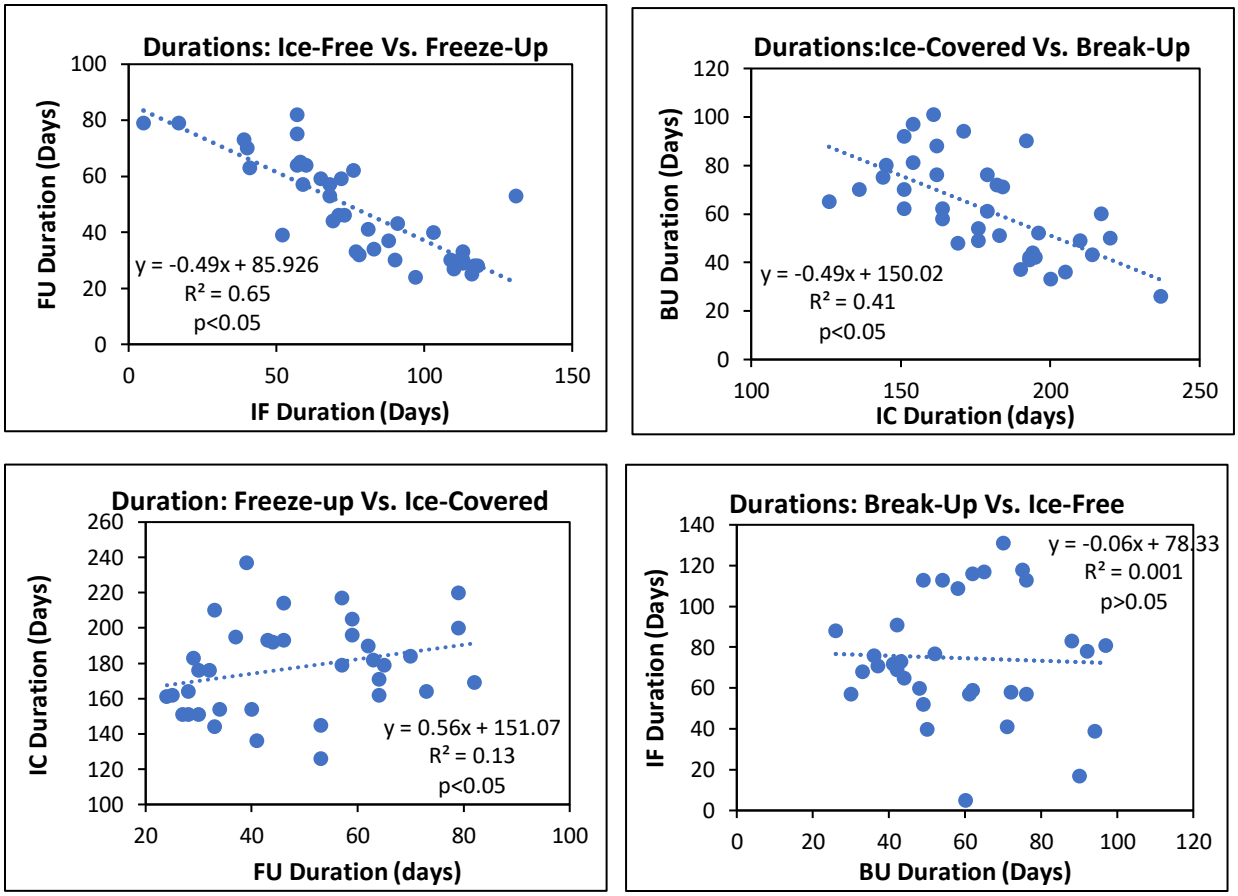

Figure 4.11: Relationships between the durations of contiguous ice seasons a) IF vs. FU, b) IC vs. BU c) FU vs. IC, d) BU vs. IF for the years 1979 to 2018.

III. Relationships between ice season onset and end dates

Despite the finding that the *duration* of the BU season does not affect the *duration* of the FU season (4.12a), a significant relationship at the 95% confidence interval (R^2=0.39) is indicated between the FU date of a given year and the BU date of the following year (Figure 4.12b). It shows that a delay of 1 day in the onset of the FU period results in a 0.42 day advance in the following BU season. However it was also found that a one-day delay in the BU season resulted in the FU season starting 1 day earlier (Figure 4.12c) (R^2=0.48 and $p<0.05$).

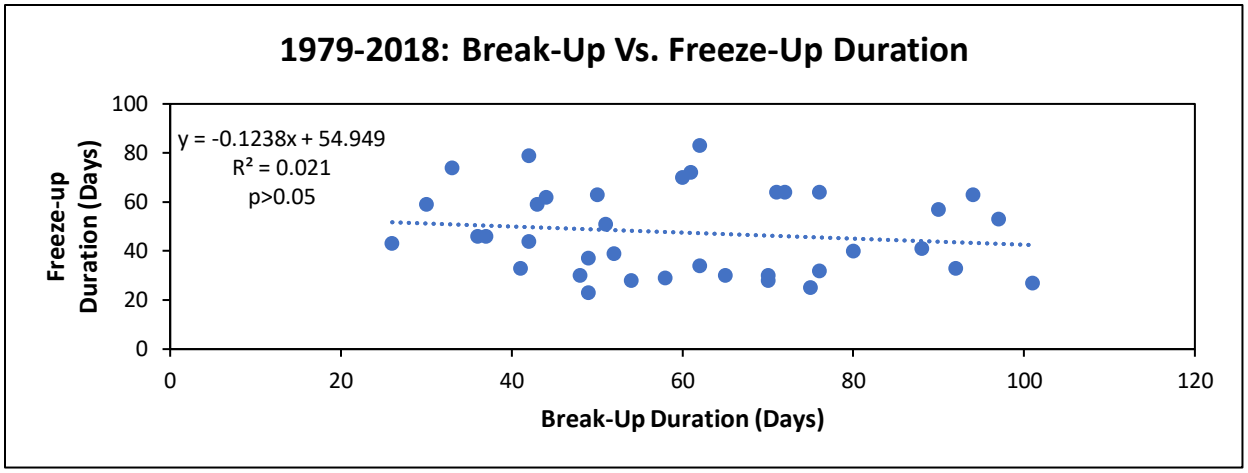

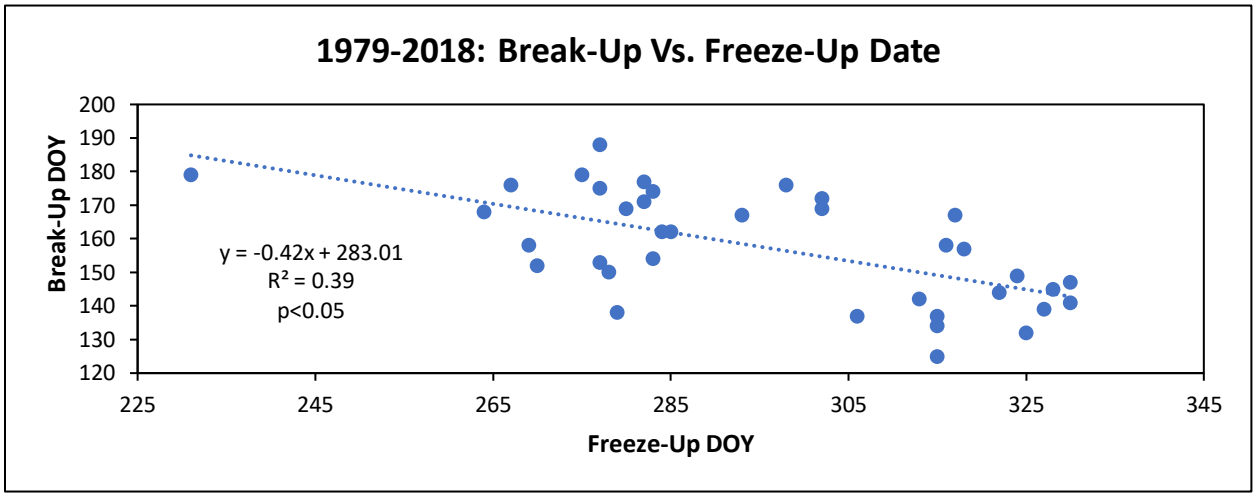

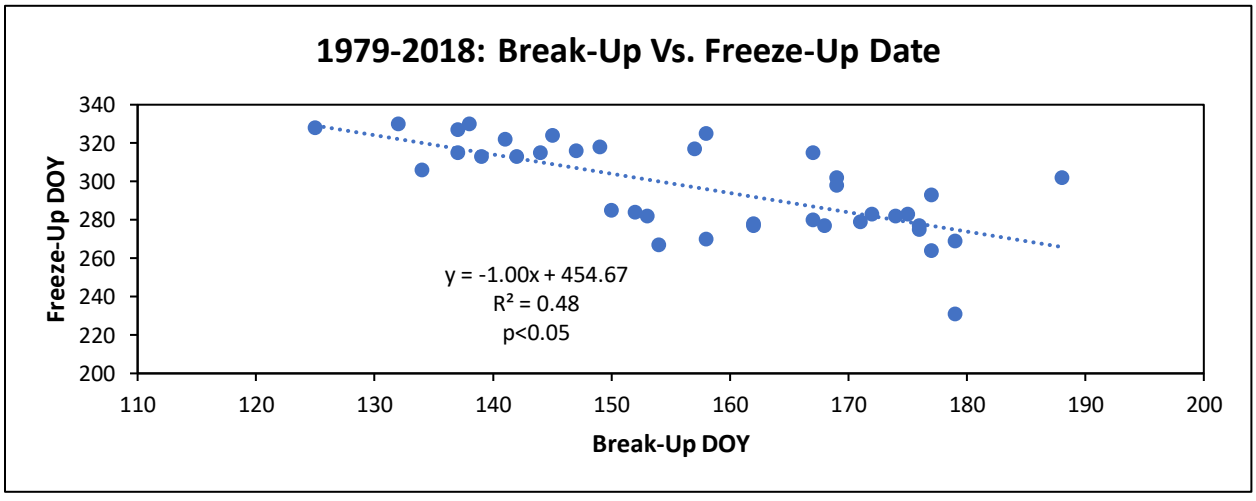

Figure 4.12: The relationship between a) FU and BU duration b) FU and BU onset DOY *of the following year* C) BU and FU DOY for the period 1979-2018.

4.3 Energy Budget Components and Ice Seasons

4.3.1 Temporal Variation in The Energy Budget Components Throughout Calendar Year

Figure 4.13 shows how energy budget components fluctuate over 1979; as indicated by peaks and troughs from day to day throughout the year. Prior to DOY 80 (Mar 21st) energy fluxes are negative. Afterwards, Q* begins to increase; Q_{ST} follows the same increase in magnitude. Meanwhile, Q_H remains lower than Q_E but on DOY 132 (May 12th) convective fluxes are negative reaching a minimum (Q_E = -10.43Wm^{-2} ; Q_H = -22.57 Wm^{-2}) on DOY 150 (May 30th). Q* and Q_{ST} begin to increase reaching maxima (Q*= 239.85 Wm^{-2} , Q_{ST}= 266.34 Wm^{-2}) on DOY 189 (Jul 7th). Q_{ST} drops dramatically on DOY 258 (Sep 15th) but maximum convective losses are observed (Q_E= 141.47 Wm^{-2}, Q_H= 99.17 Wm^{-2}). After this, Q_{ST} is largely negative; while, convective fluxes became positive. Q* continues to decline reaching negative values on DOY 295 (Oct 22nd). Toward the end of the year, Q_E losses are small but positive; whereas, Q_H is negative. Overall, at the beginning and toward the end of the year, nearer the winter solstice, Q_{ST} is sensitive to Q_H and Q_E; but in the middle of year it is largely influenced by Q*. Therefore, large magnitude losses and gains of energy via Q*, Q_E and Q_H are well reflected by the magnitude of Q_{ST}. This implies that features of Q*, or Q_H and Q_E can be anticipated from seasonal Q_{ST} patterns.

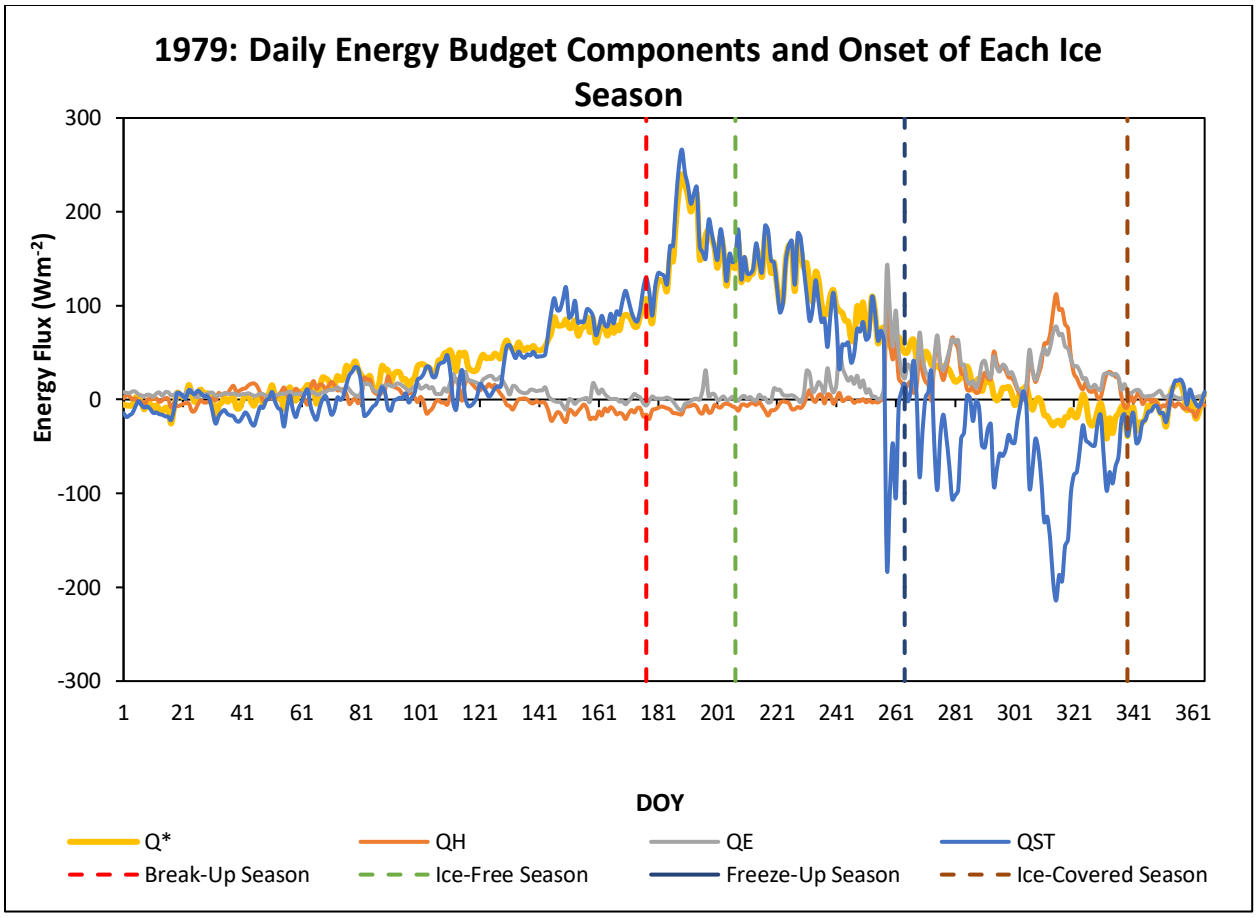

Figure 4.13: Diurnal variation in HB surface energy budget components throughout the year of 1979.The dashed line indicates the onset of each ice-season of 1979; as well as, onset of IC season of 1979/80.

4.3.2 Q_{ST} During Each Ice Season

I. Break-Up Season

Energy budget fluxes (equation 2), in Wm^{-2} , describe the daily average intensity of energy gains and losses during the BU season. Figure 4.14a describes daily changes in the intensity of each component flux during the 1979 BU season beginning on DOY 177 (June 26th) and ending on DOY 206 (July 25th). First, convective fluxes (Q_H and Q_E) remained extremely small throughout the season; but a peak exists on DOY 197 (July 16th). Second, Q* continues to increase throughout the season but Q_{ST} was slightly greater in magnitude. Maximum Q* and Q_{ST} were reached on DOY 190 (July 9th). During, BU season, Q* and convective fluxes (both towards the surface) contribute to Q_{ST}. The total amount of energy gained by the ocean during BU would both melt ice and warm water and therefore was partitioned for both open-water and ice-covered parts of the Bay (Figure 4.15 a). Open-water locations gain energy rapidly compare to ice-covered parts of HB; hence, open-water contributes greatly to energy gains. By the end of the Break-Up season Q_{ST} reached maximum.

In the past 40 years, total Q_{ST} gained by open-water was higher compare to ice-covered parts of HB. The boxplot shows that variability was small in the intensity (Figure 4.18a) but total energy gained has greater variability (Figure 4.18b). Notable peaks exist in Q_{ST} intensity during 1982, 1989, 2001 and 2014; and minima existed 1994, and 2004 (Figure 4.20a).Moreover, beginning in 2002, the intensity of energy gained decreases (4.20a). The BU season shows a slight increase starting in 2002 and it continues to fluctuate (Figure 4.20a). Peaks existed in total energy gained by the Bay during 1991, 1998, 2009, and 2015; and minima existed in 1981, 1987, 2007, 2013 (Figure 4.20a). No autocorrelation was detected in the intensity and total energy gains during the FU seasons. It was found that over the past 40 years, HB is gaining more energy $10.4 MJm^{-2}\ y^{-1}$ at a lower intensity of $0.73\ Wm^{-2}y^{-1}$ (Figure 4.16a; Figure 4.17a). Overall, the ice-covered portions of the Bay gained 267

MJm^{-2} at an intensity of 51 MJm^{-2} while, open-water gained 508 MJm^{-2} at an intensity of 102 Wm^{-2} (Table 4.4b) . Coefficients of variation were close to one another for both intensity and total energy for both ice-covered and open-water parts of the Bay (Table 4.4b).

During the BU season, intensity and total energy gained is related to the duration of the BU season. It was found that for a one day increase in BU season; the intensity of energy decreased by -0.60Wm^{-2} ($p<0.05$, $R^2=0.27$) (Figure 4.20a). Total energy gained increases by 9.46MJm^{-2} ($p<0.05$, $R^2= 0.85$) for a one day increase in the duration of BU season (Figure 4.21b). Lastly, HB gained 775 MJm^{-2} at an intensity of 153 Wm^{-2} (Table 4.4a). This was highest among all the other seasons.

II. Ice-Free Season

Figure 4.14b describes daily changes in the intensity of each energy flux during the IF season of 1979 that began on DOY 208 (July 26th) and ended on DOY 262 (September 19th). First, convective fluxes (Q_H and Q_E) remained extremely small throughout the season; but began to increase dramatically on DOY 258 (September 15th). Likewise, Q_{ST} became negative as convective losses increased upwards towards the end of the season. However, at beginning of the season, Q* and Q_{ST} remained about the same magnitude but started to decline as the season progressed. By the end of the season, Q_{ST} became largely negative, while the magnitude of Q* declined but was positive. Likewise, a similar trend can be seen from the total energy gained during the entire season (Figure 4.15b). Total Q_{ST} continued to increase; but on day 258 (September 15th) it continues to decline. Moreover, variability in the intensity of Q_{ST} throughout the IF season is near the mean (Figure 4.18a) but the IF season is becoming shorter (Figure 4.18b). In particular, during the IF season HB gained energy of 148MJm^{-2} with a coefficient of variation of 1.38, while the intensity was 29Wm^{-2} with a coefficient of variation of 0.82 (Table 4.4a). Lastly, the intensity (0.61Wm^{-2}) and total energy (1.62 MJm^{-2}) decreases significantly at the 95% confidence interval as the IF season gets longer (Figure 4.22a; Figure 4.22b).

III. Freeze-Up Season

Figure 4.14c describes daily changes in the intensity of each energy flux during the FU season of 1979 that began on DOY 264 (June 26th) and ended on DOY 338 (December 4th). First, convective fluxes (Q_H and Q_E) were positive throughout the season; but a peak exists on DOY 315 (November 4th). Secondly, Q* continues to decrease throughout the season; eventually, becoming negative towards the end of the season. Similarly, Q_{ST} declines in magnitude much more than Q* and day-to-day fluctuations were much higher than for Q*. It reached a minimum on DOY 315 (November 4th). During, the FU season, convective fluxes contributed greatly to declining Q_{ST}; producing open-water and ice-covered parts of the Bay. Open-water parts of the Bay continued to lose energy; whereas, ice-covered parts remained close to zero (4.15c).

Over the past 40 years, total Q_{ST} losses from ice-covered parts were higher compare to open-water areas of HB (Table 4.4b) . The boxplot shows that variability exists in the intensity of energy loss (Figure 4.18a) compared to total energy losses (Figure 4.18b). No autocorrelation was detected in the intensity and total ocean energy losses during the FU season. It was found that during the past 40 years, HB is losing the same amount of energy- 1.28MJm^{-2}y^{-1} while its intensity is increasing in magnitude by 1.44Wm^{-2}y^{-1}. Moreover, total energy loss during 1998-2001 is very small but its intensity is much higher comparing years prior to 1998 and after 2001 (Figure 4.16c; Figure 4.17c). In terms of ice-covered and open-water areas, peaks existed in the intensity of Q_{ST} during 1988, 1997 and 2015; and minima existed 1987 (Figure 4.18d). Likewise, peaks existed in total energy lost by the Bay during 1988, 1997, 2003, and 2016; and minima existed in 1998, 2001, 1990 (Figure 4.19d). Overall, the ice-covered portions of the Bay lost -4 MJm^{-2} at an intensity of -14 Wm^{-2}; while, open-water lost -377 MJm^{-2} at intensity of -103 Wm^{-2} (Table 4.4b) . The coefficient of variation for ice-covered portions was higher for both intensity and total energy losses, in comparison to open-water parts (Table 4.4b). Throughout the FU season, it was found that a one day

increase in the season led to a decrease in intensity of energy by 1.52 Wm^{-2} ($p<0.05$, $R^2=0.46$) (Figure 4.21a). Total ocean energy gained decreased by 2.44 MJm^{-2} ($p<0.05$, $R^2= 0.13$) with a one day increase in the duration of the FU season. Lastly, HB lost -391 MJm-2 at an intensity of -107 Wm^{-2} (Table 4.4a). This was lowest among all the other seasons.

IV. Ice-Covered Season

Figure 4.14d describes daily changes in the intensity of each energy flux during the IC season of 1979/80 that began on DOY 339 (December 5th) and ended on DOY 532* (*365+167, June 15th, 1980). First, convective fluxes (Q_H and Q_E) remain extremely small throughout the season; in particular, QE is positive (sublimation); while, QH is slightly negative (downwards). Q_{ST} is very small and continues to fluctuate the most compared to other fluxes. However, at beginning of the season, Q* was negative after DOY 434 (365+69, March 10th, 1980) after which it continued to increase. Likewise, Q_{ST} fluctuated between positive and negative fluxes but beginning on ice-covered day 493* (*365+128, May 8th, 1980) it continues to increase positively. By the end of the season, Q_{ST} follows the pattern of Q* but remains smaller in magnitude as Q_E and Q_H increase. declined but was positive. Most importantly, variability in the intensity was weak; and total energy lost was close to the mean (Figure 4.16a; Figure 4.1bb). In the past 40 years, during the IC season HB gained energy of 173 MJm^{-2} with coefficient of variation of 1.18; while, the intensity was 11Wm^{-2} with a coefficient of variation of 2.26 (Table 4.4a). Lastly, the intensity (0.12$Wm^{-2,}$ $R^2= 0.23$) and total energy (2.98MJm^{-2}, $R^2=0.48$) increases significantly at 95% confidence interval as the IF season gets longer (Figure 4.24a; Figure 4.24b).

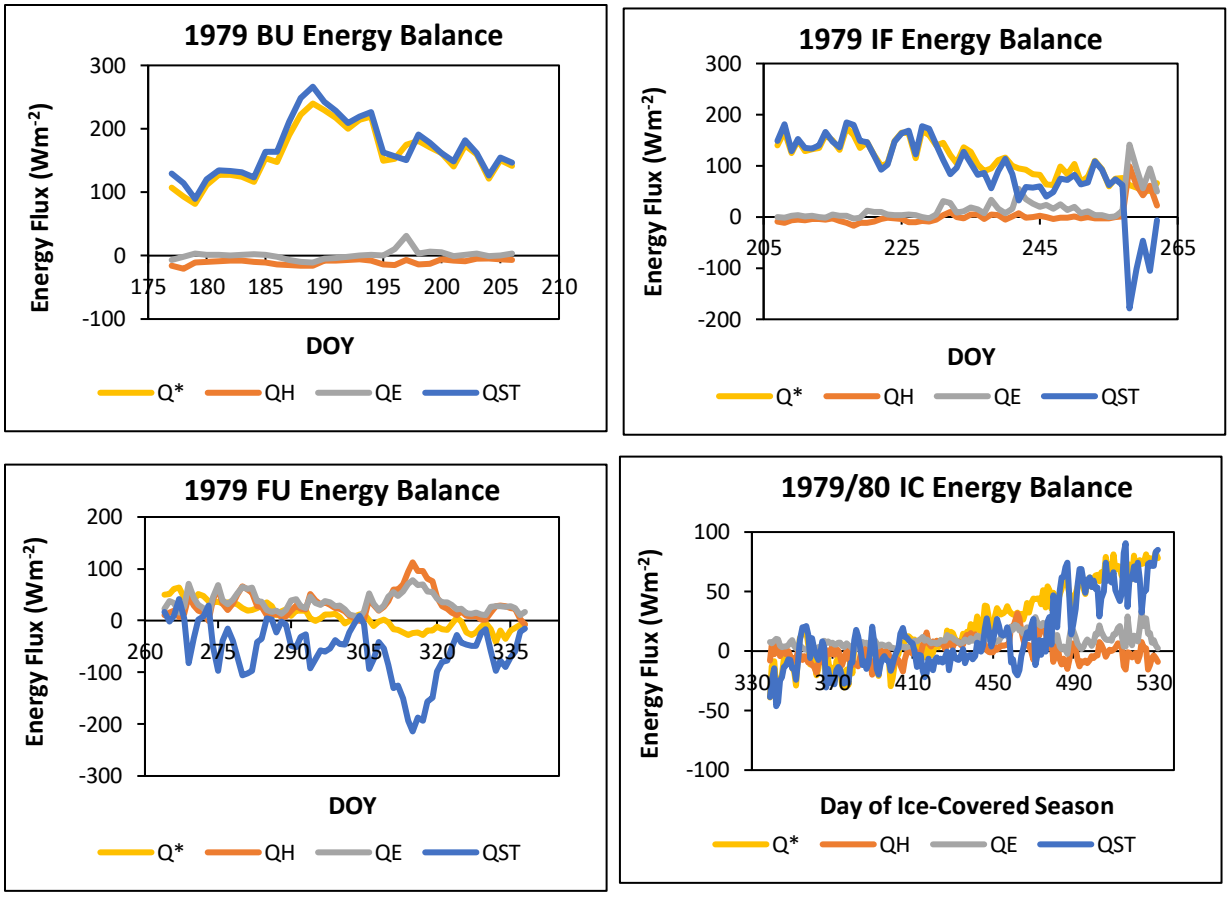

Figure 4.14: Characteristic energy balance components for each ice-season in 1979.

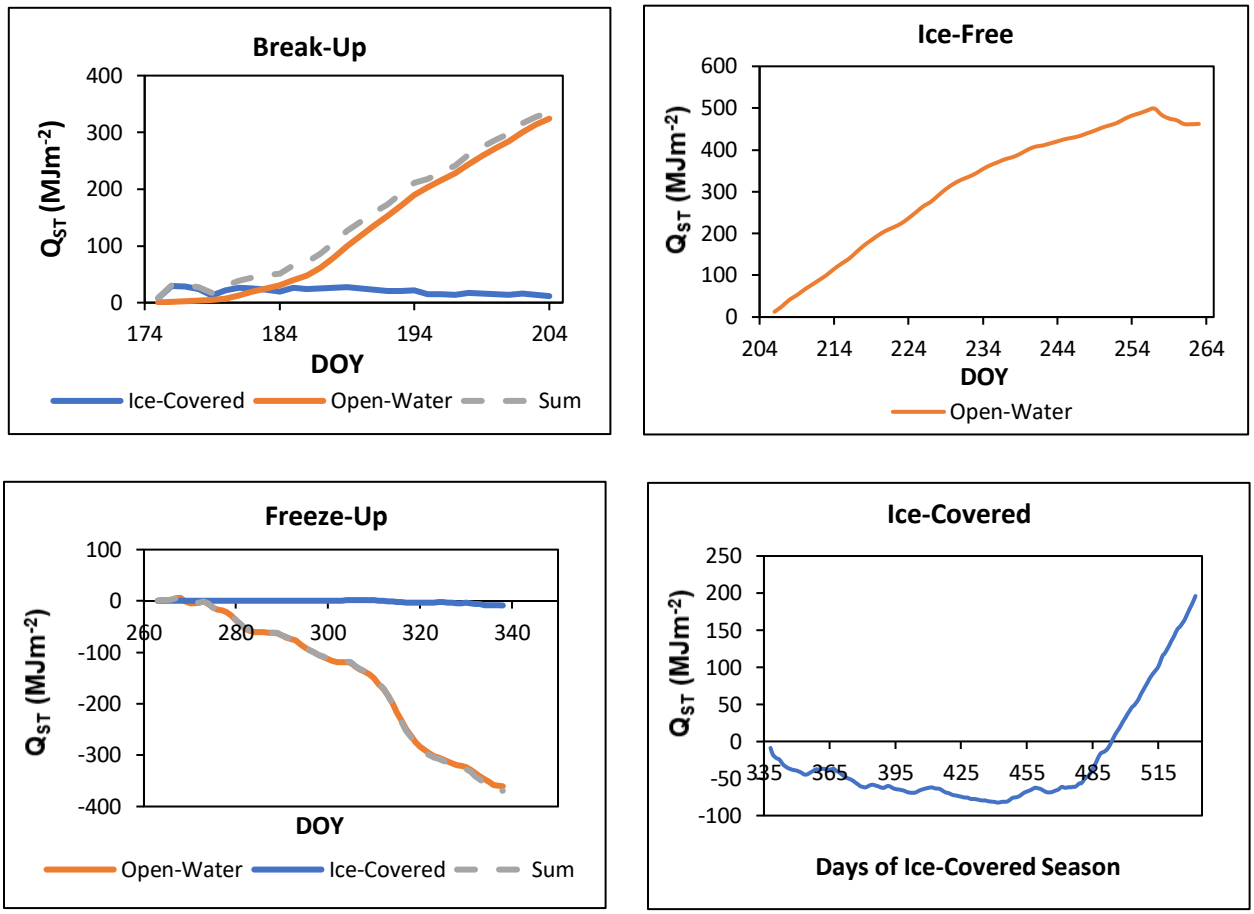

Figure 4.15: Patterns of seasonal cumulative Q_{ST} for a) BU , b) IF, d) FU , d) IC seasons during 1979.

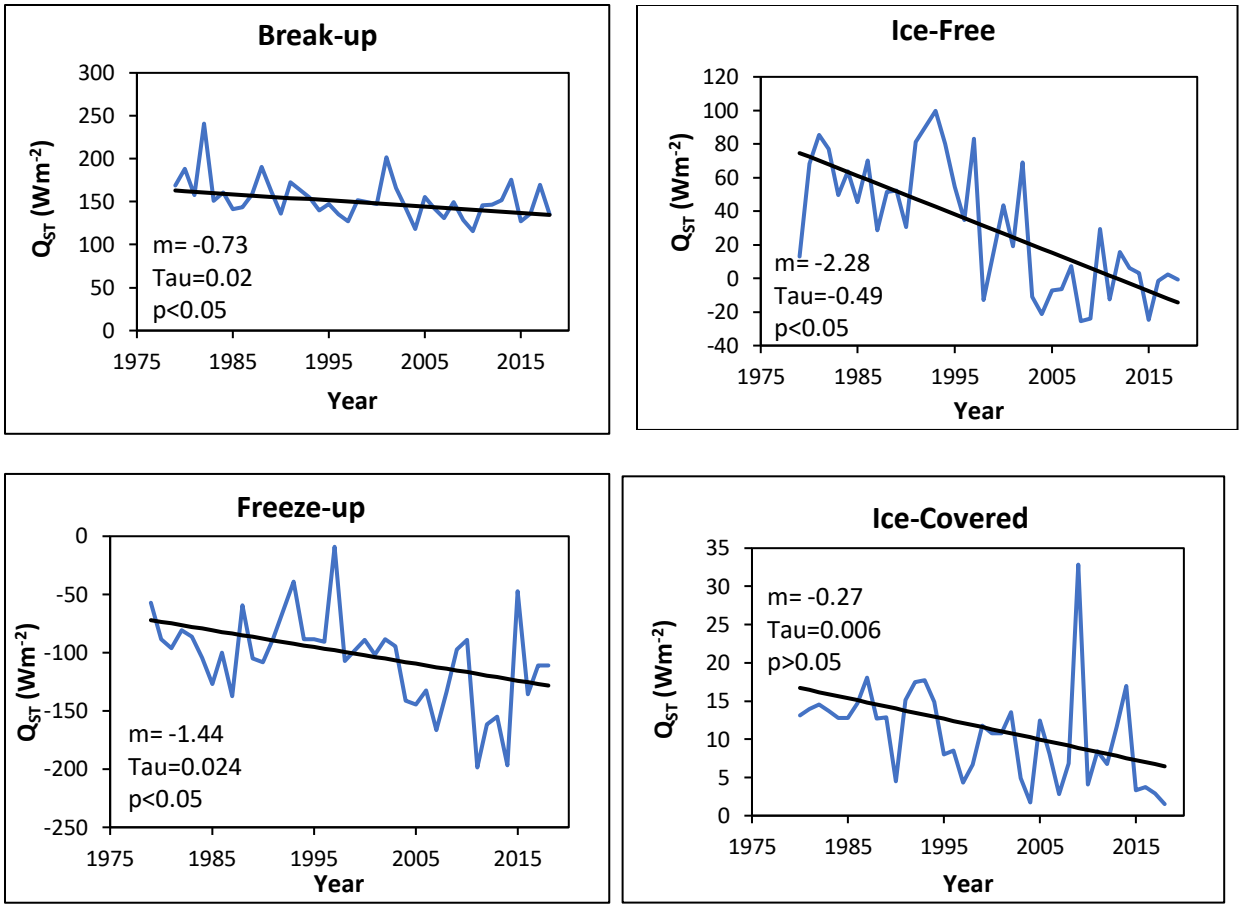

Figure 4.16: Time series of seasonal average Q_{ST} for a) BU, b) IF, c) FU, and d) IC seasons from 1979-2018.

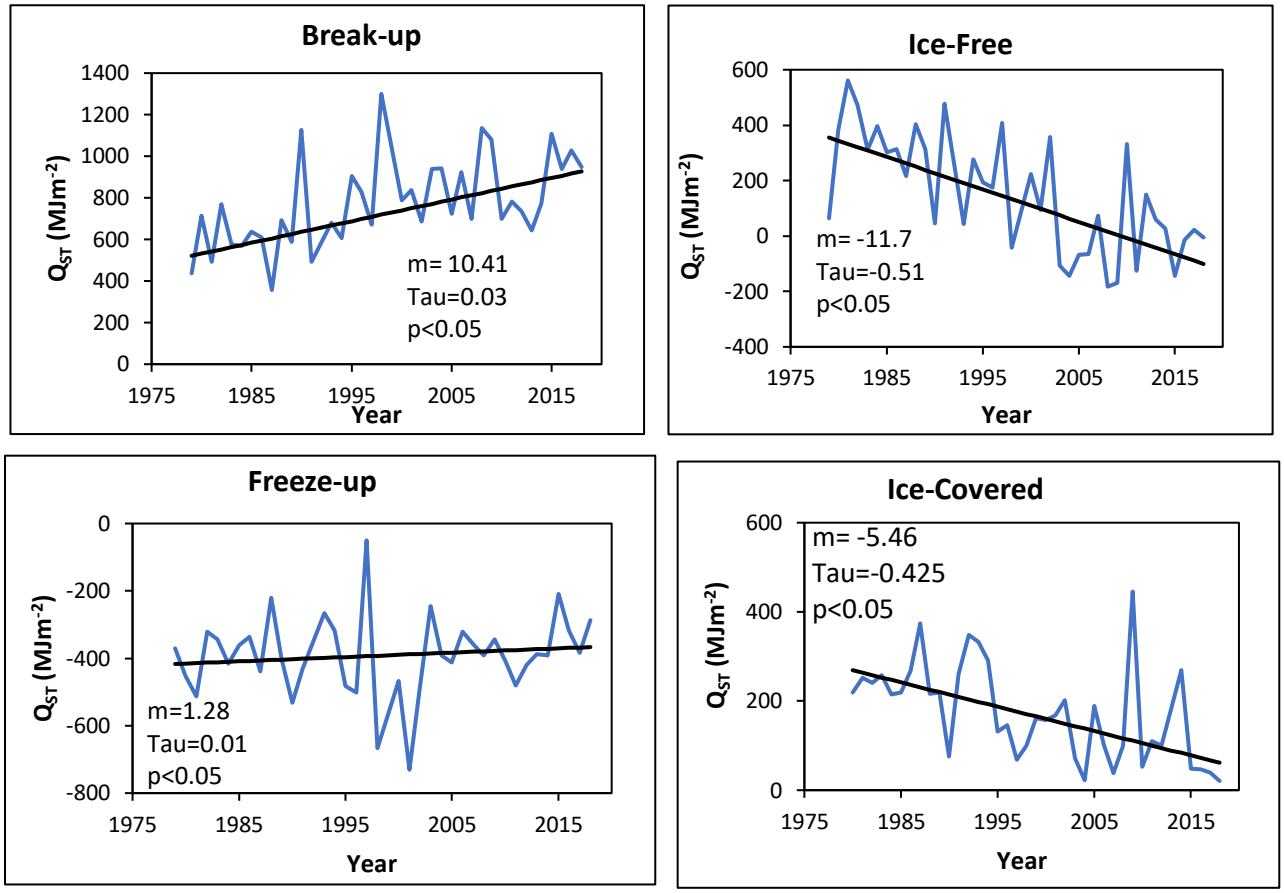

Figure 4.17: Time series of seasonal total Q_{ST} for a) BU, b) IF, c) FU, d) IC seasons from 1979-2018.

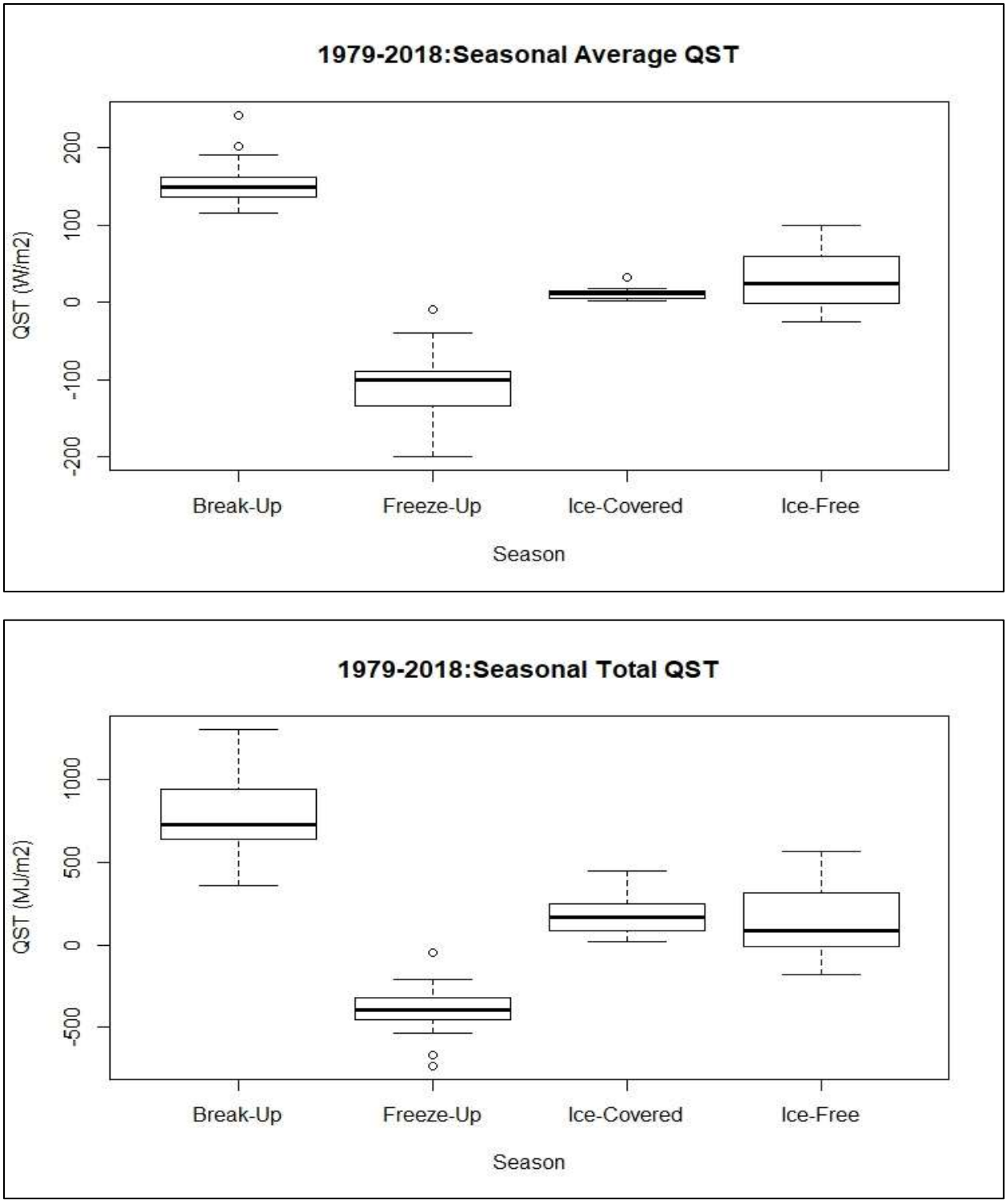

Figure 4.18: Variation in a) average and b) total Q_{ST} for each ice season from 1979 to 2018.

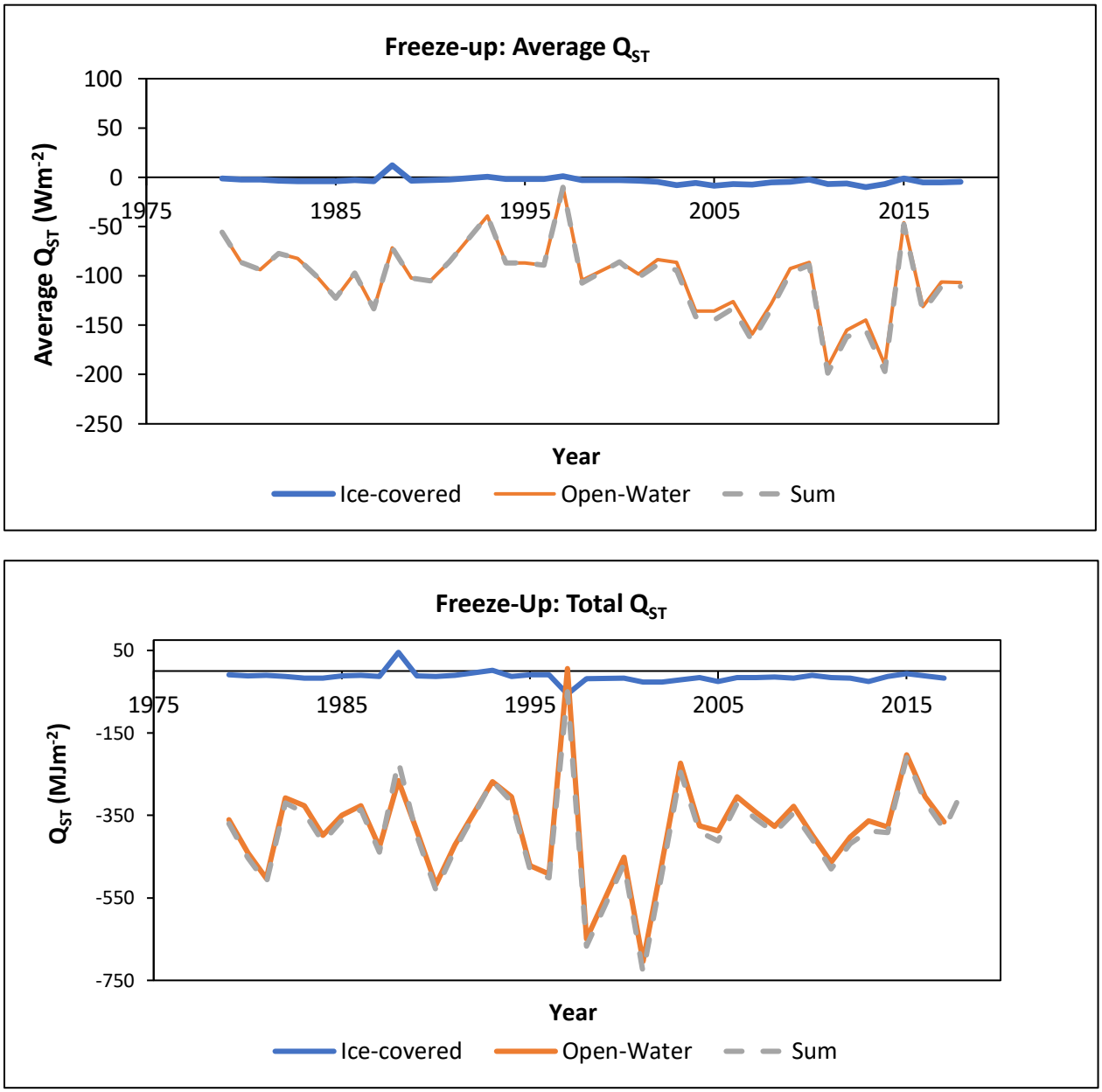

Figure 4.19: Variation in a) average and b) total Q_{ST} for each open-water and ice-covered proportion of HB during FU season from 1979-2018.

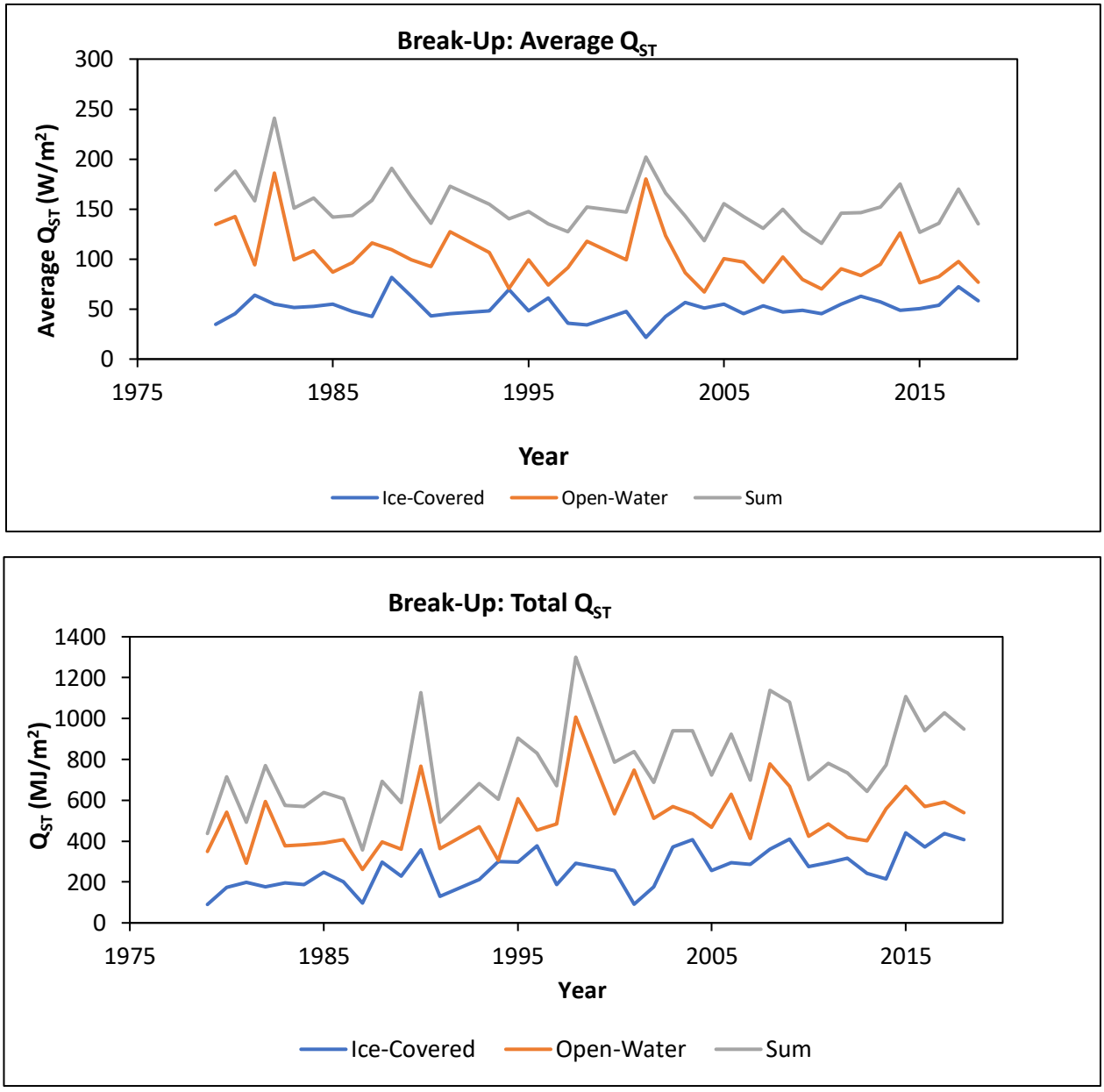

Figure 4.20: Variations in a) average and b) total Q_{ST} for each open-water and ice-covered proportion of HB during BU season from 1979-2018.

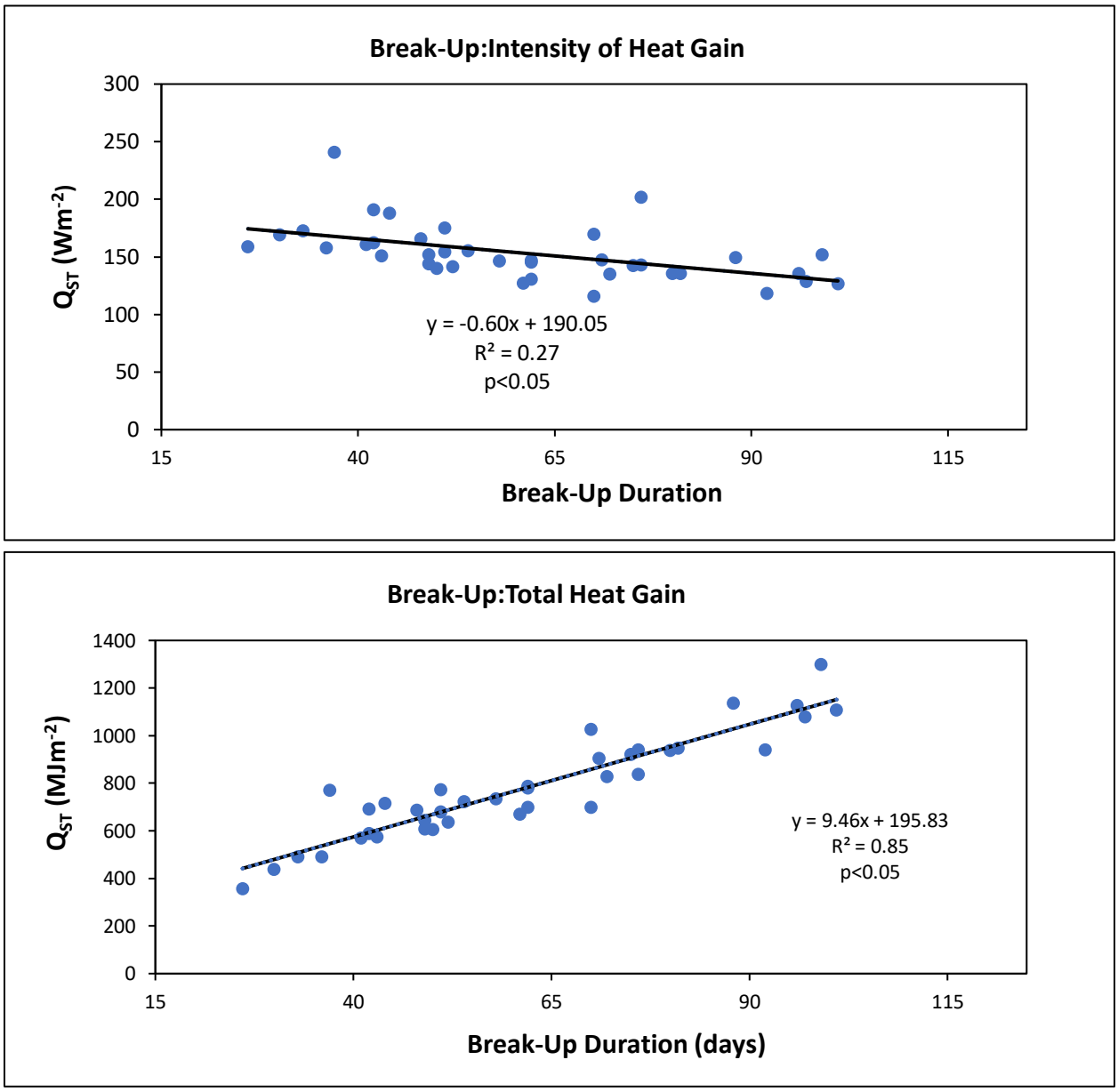

Figure 4.21: Relationship between BU season duration of a) the intensity of ocean heat gains and b) total ocean heat gains for the BU seasons for 1979 to 2018.

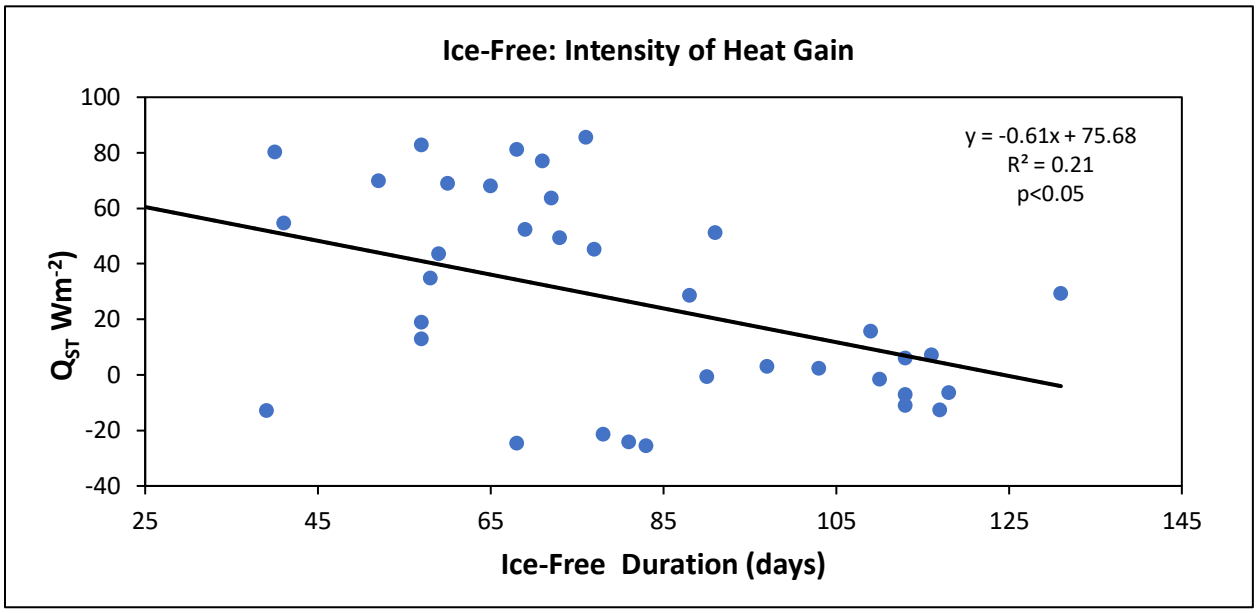

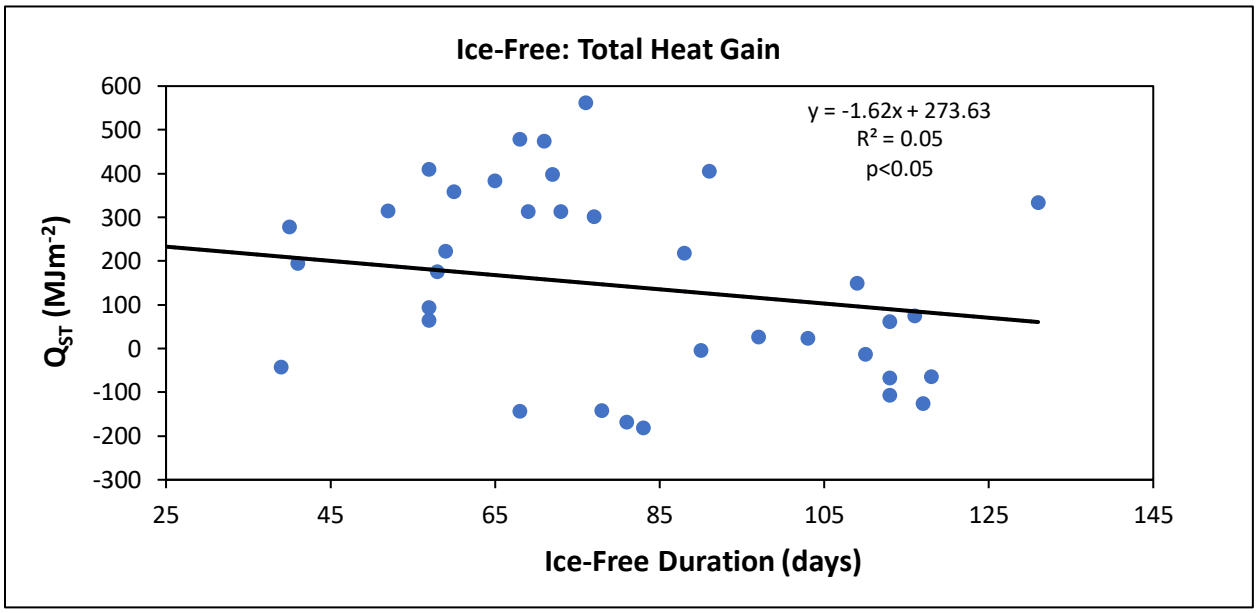

Figure 4.22: a) Intensity of heat gain and b) total energy gained throughout the IF season from 1979-2018.

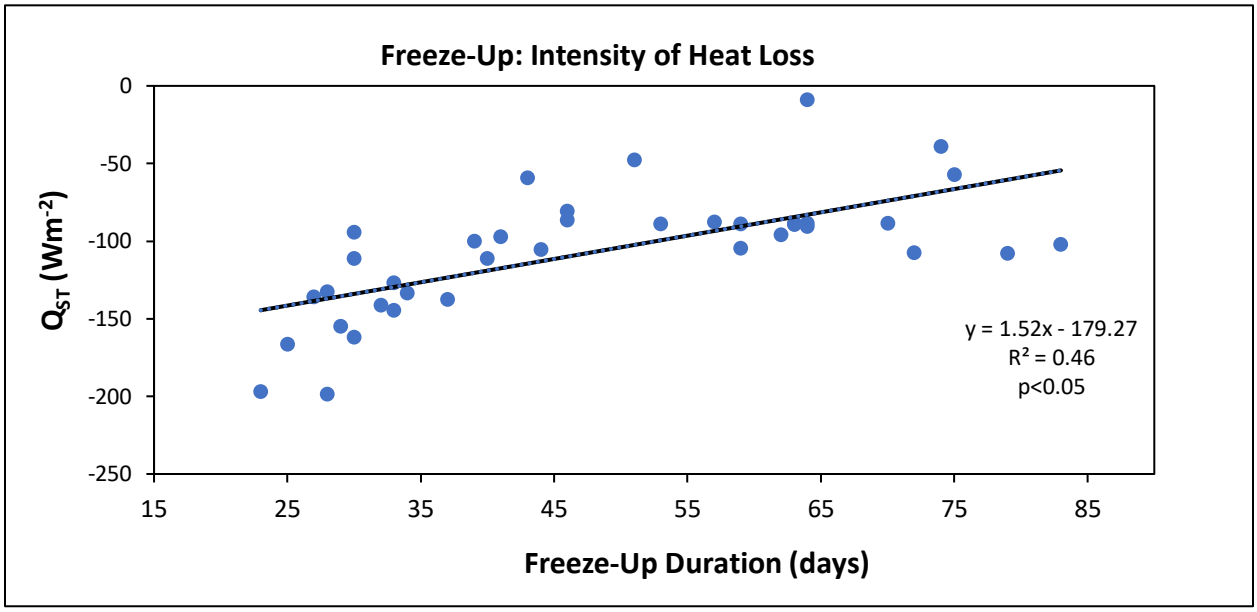

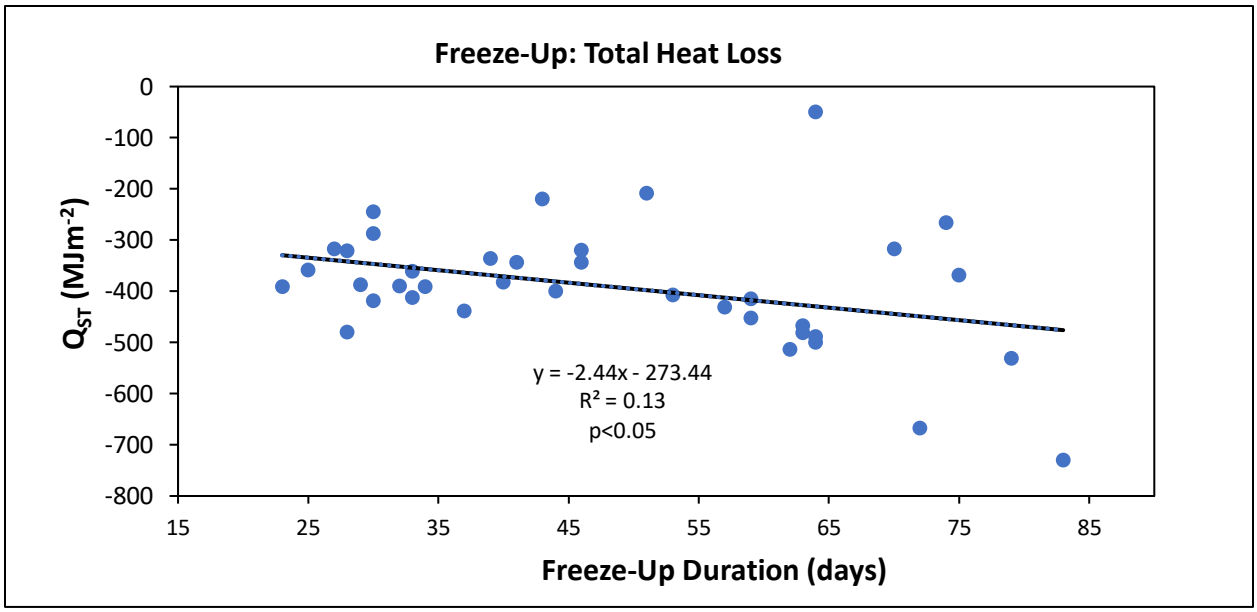

Figure 4.23: a) Intensity of heat loss and b) total energy loss throughout freeze-up season from 1979-2018.

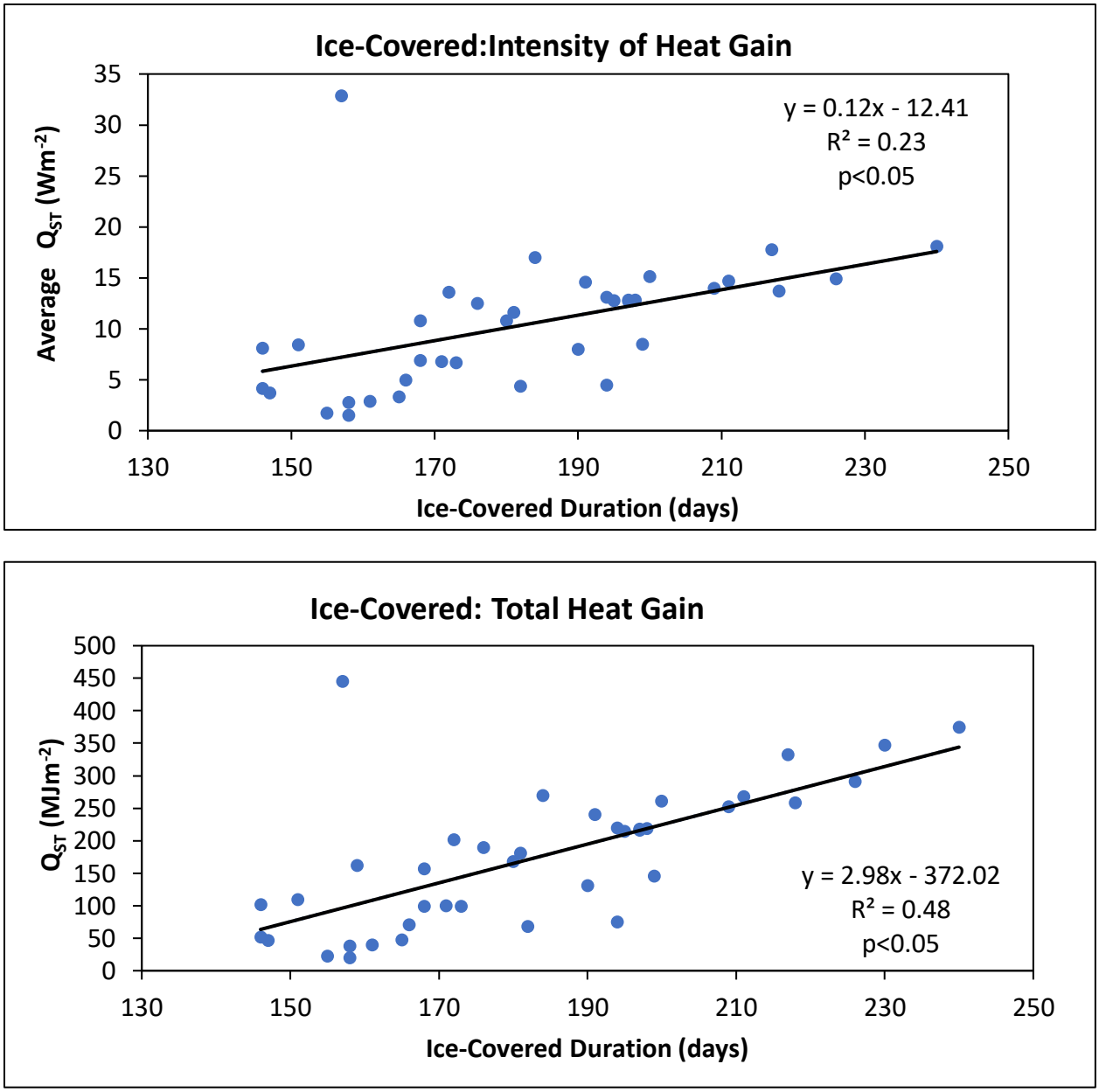

Figure 4.24: a) Intensity of heat gain and b) total energy gained throughout ice-covered season from 1979-2018.

Table 4.4a Total and average Q_{ST} for each ice season from 1979-2018.

Season	Q_{ST} (MJm^{-2})	Coefficient of Variation	Q_{ST} (Wm^{-2})	Coefficient of Variation
Break-up	775	0.27	153	0.16
Ice-Free	148	1.38	29	0.82
Freeze-up	-391	-0.53	-107	-0.22
Ice-Covered	173	1.18	11	2.26
Total	705		86	

Table 4.4b: Apportioning of QST for ice-covered and open-water areas of the Bay during BU and FU seasons from 1979-2018.

Season	Proportion	Average Q_{ST} (MJm^{-2})	Coefficient of Variation	Average Q_{ST} (Wm^{-2})	Coefficient of Variation
Break-Up	Ice-Covered	267	0.36	51	0.21
	Open-Water	508	0.30	102	0.26
	Sum	775	0.27	153	0.16
Freeze-Up	Ice-Covered	-14	-0.93	-4	-0.98
	Open-Water	-377	-0.31	-103	-0.36
	Sum	-391	-0.30	-107	-0.12

4.4 Ice Growth and Ice Thickness During Freeze-Up and Ice Covered Seasons

Ice thickness differs between FU and IC season. Over the past 40 years, maximum mean ice-thickness during the FU season was 5.22cm; while, during the IC season it was 26.36cm. Variation in ice-thickness during FU season is twice as large as during the IC season (Table 4.5). Throughout the FU season, ice thickness fluctuated between 2-8cm but in 1997 ice-thickness was 18.17cm (Figure 4.25a). Moreover, ice thickness increases by 0.03cm/ year but significance was not detected at 95% confidence interval. On the other hand, during the IC season ice-thickness fluctuates between 15-34cm but outliers existed in 1985 (44.34cm) and 1998 (46.56cm) (Figure 4.25b). Over the past 40 years, ice has been decreasing 0.19cm/year, (R^2=0.10), $p<0.05$).

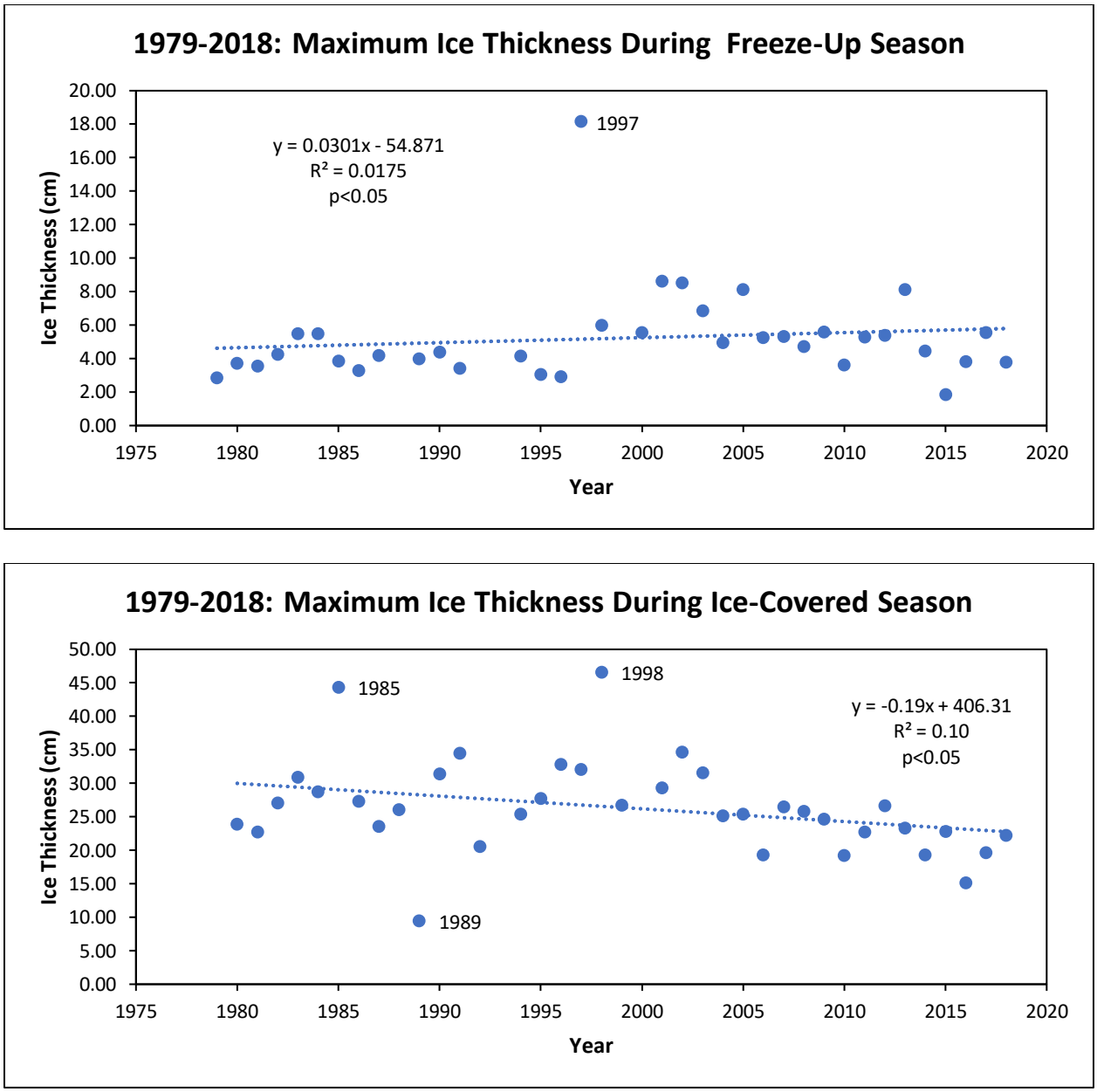

Figure 4.25: Trend in maximum average ice thickness on HB during a) FU and b) IC seasons from 1979 to 2018.

Table 4.5: Maximum average ice-thickness and coefficient of variation during FU and IC seasons.

Season	Maximum Ice Thickness (cm)	Coefficient of Variation
Freeze-up	5.22	0.52
Ice-Covered	26.36	0.26

4.5 Surface Temperature During Break-Up and Freeze-Up Season

Surface temperature (T_0) of HB differs in both the FU and BU season. Ice-covered locations of HB have lower T_0 compared to open-water locations in both seasons.

During the BU season, T_0 remained positive from 1979-2002; afterwards, T_0 was negative with lowest mean temperatures occurring in 2010 (-2.24^{O}C) and 2012 (-2.02^{O}C) (Figure 4.26a). Over the past 40 years, open-water temperatures have been decreasing by -0.19^{O}Cy^{-1} ($p<0.05$). In contrast, T_0 in ice-covered parts of HB has been declining by -0.02^{O}Cy^{-1} ($p<0.05$). During the BU season, ice-covered part of the Bay had maximum mean T_0 in 1982 (-0.83^{O}C), with another peak in 2009 (-2.10^{O}C) and minima occur in 2010 (-4.22^{O}C) (Figure 4.26a). On average, during BU season, T0 for ice-covered areas was -2.71^{O}C; while for open-water areas surface temperature was 0.83^{O}C. T_0 for the entire HB was -1.88^{O}C (Table 4.6). Greatest variability (coefficient of variation =1.88) in T0 existed in open-water parts of the Bay during the BU season (Table 4.6).

During the FU season, T_0 has been decreasing in both open-water and ice-covered parts of the Bay. Maximum (1.69^{O}C) T_0 in open-water parts of Bay occurred in 1993. From 2003-2018, T_0 of open-water has been negative; reaching the lowest mean temperature in 2003 (-2.88^{O}C); onwards; it fluctuated around -2.88^{O}C (Figure 4.26b). On average, T_0 of open-water during the FU season was -1.31^{O}C (Table 4.6) and it has been declining by 0.05^{O}C per year ($p<0.05$; Figure 4.26b). In contrast, T_0 in ice-covered portions of HB has been declining; from 2003 onwards. Minimum T_0 occurred in 2013 (-21.32^{O}C). A maximum occurred in 1993 (-6.71^{O}C) and exhibits a decline with a minimum of -21.32^{O}C occurring in 2013 (Figure 4.2b). On average, T0 of ice-covered parts of Bay is -14.56 ^{O}C and it has been getting colder by -0.02^{O}C per year ($p<0.05$) (Table 4.6). For the entire Bay T_0 during the FU season was -15.86^{O}C and the greatest variability existed in open-water parts of HB (Table 4.6). Overall, the fluctuations in T_0 occur in the same years in both BU and FU seasons.

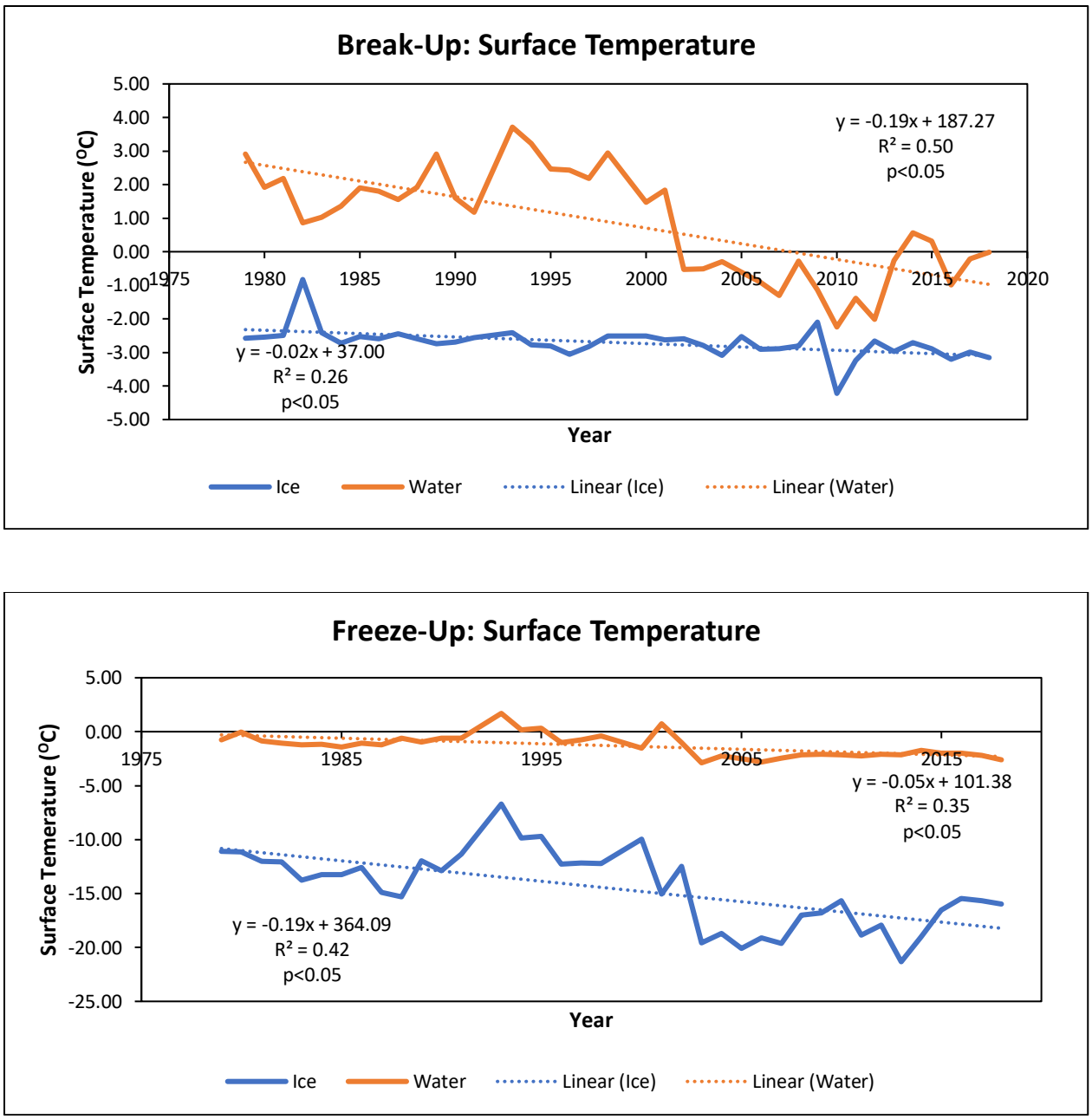

Figure 4.26: Trends in T_0 in both open-water and ice-covered parts of HB during a) BU and b) FU season.

Table 4.6: Average surface temperature in ice-covered and open-water locations on HB during BU and FU seasons.

Season	Proportion	Average T_0 (^{O}C)	Coefficient of Variation
	Ice-Covered	-2.71	-0.17
	Open-Water	0.83	1.88
Break-Up	HB	-1.88	-0.94
	Ice-Covered	-14.56	-0.24
	Open-Water	-1.31	-0.78
Freeze-Up	HB	-15.86	-0.27

Chapter 5: Discussion

5.1 Trends in Ice-Coverage

HB undergoes a complete seasonal cycle in ice coverage, transitioning from fully ice-covered to open-water in ice-free months. Compared to other Canadian Arctic Archipelago to the north of this region, multi-year ice does not persist as it melts entirely. The seasonal cycle of ice-coverage of HB is shown in Figure 4.1 over the last 40 years. The monthly ice-coverage (Figure 4.4) reveals that the region begins to freeze-up in November and ice continues to grow throughout December to March when it reaches the maximum of 99.91%. Ice begins to break-up slightly in April but extensive break-up of ice is triggered in May and the Bay remains completely ice-free August-October; in particular, minimum ice-coverage occurs in September at 1.28% and in August at 3.59%. Annually, ice-coverage in the last 40 years averaged 62.24% (Figure 4.4). This accurately describes previously reported typical monthly ice-conditions across HB (Hochheim & et al., 2010; Danielson, 1971; Gough & Allakhverdova, 1999).

The monthly ice-coverage of HB can be divided into 4 sub-periods (Figure 4.5). First, in comparison to other months, ice-coverage did not change over the study period for January to May. However, among the 5 months, May is the month of greatest change in ice-coverage followed by April because during these months ice break-up is triggered. Second, November and July are good illustrations of the annual growth and retreat of ice. Third, June and December are the months after which ice grows thicker or breaks-up rapidly, respectively. Finally, August-October are the months when ice formation and deformation processes are at a minimum. Over the study period, the magnitude of change in ice-coverage is greatest in July and November; followed by December and June (Figure 4.5a).The four subgroups of ice-coverage showed that growth and melt of sea ice in HB are largely controlled by astronomical cycles. The ice-cover continues to grow until reaching a

peak in March. Melting increases in pace as the spring equinox (March 21st) is crossed allowing Q* to become stronger. After September, ice-coverage begins to increase as the fall equinox is crossed and Q* becomes weaker as days progress towards winter equinox. Ice-coverage often does not reach 100% due to the persistence of polynyas along northwestern HB that are produced by warm upwelling water throughout ice-covered season; whereas in May, leads form (Stewart & et al., 2010) that accelerate ice break-up.

In the last 40 years, annual sea ice-coverage had positive serial correlation. This implies that ice-coverage in one year depends on those of the previous year. Length of IF season, freeze-up timing, albedo and high heat capacity of water influences energy absorbed by the Bay. This influences the formation of ice and its properties in the following seasons. The time trend shows that in the last 40 years, annual sea ice coverage has been declining by 2.2% per decade (Figure 4.3). The declining trend in sea ice-coverage is consistent with similar studies that used passive microwave (Parkinson & et al., 2008) based datasets or CIS ice chart (Tivy & et al., 2011). The annual forty years timeseries (Figure 4.3) can be split into two: 1979-1995 (positive trends), 1996-2018 (negative trend). Cavalieri and Parkinson (2012) examined both monthly, and standard climatology seasonal SIE from 1979-2010 using satellite microwave radiometers. Positive trend from 1979-1996 followed by negative trends from 1996-2010 were identified. Researchers have identified that starting mid-1990s, HB has been warming (Gagnon and Gough, 2005; Laidler et al., 2009). Barber & Hochheim (2010) described the fall period from 1980-1995 as "cool period" and 1996-2005 "warm period" as a result of rising T_A.

Annual maximum ice-coverage (Figure 4.3) was observed in 1992; as a result of, 1991 eruption of Mt. Pinatubo in the Philippines that led to significant cooling of the global climate during 1991 and 1992 (Gagnon and Gough, 2005). In contrast, 2010 was the year of minimum ice-coverage

(Figure 4.3) because North Atlantic Oscillation (NAO) in 2009 was in extreme negative mode. Based on pressure observations at Gibraltar and in southwest Iceland; winter 2009/2010 value of NAO index was: -2.4. This is more negative compare to previous four most negative index winters (1995/96, 1962/63, 1968/69, and 1916/17) which all had NAO indices closed to -1.7 (Osborne, 2011). This led to winter of 2009/10 to be the warmest across the globe. The negative pattern persisted throughout summer and fall; and then intensified even further by December, setting stage for warmer winter in 2010. During the negative season, the southward moving Arctic air masses are less cold. According to Qian & et al. (2008), negative NAO years result in HB sea-ice anomalies to be negative (20% less than the mean). The remaining year remained exceptionally warm (+6.7^{O}C) (Barber & Hochheim, 2014) which reduced sea ice in the preceding years.

The trends and pattern in monthly ice-coverage shows that albedo can be used a proxy to understand changes in ice-coverage across HB. The changes in albedo reflect combination of gradual evolution of ice during the last 40 years. Most importantly, each monthly, seasonal transition and abrupt shifts in ice resulting from synoptic weather events can be identified when daily albedo values are examined. Therefore, it can identify the progression of each ice season: BU, IF, FU and IC. Moreover, changes in albedo values can indicate when large portions of HB are a mixture of ice and water. This helps address the research limitations- apportioning of energy losses from open and ice-covered parts of HB. However, a major drawback is that NARR assigns an albedo using passive microwave radiation. This waveband has low energy levels; hence radiation must be collected over a larger area; in doing so, details of sea ice such as leads and small floating pans of sea ice during FU and BU cannot be detected. Albedo can indicate whether HB is mainly covered by ice or water. Microwave emission is connected to physical properties- atomic composition and crystalline

structure. Since, NARR codes presence of ice as 65% albedo and water by 6% albedo, the thickness of ice cannot be determined by using albedo as a proxy; an alternative parameter is required.

5.2 Shifting Ice Seasons and Thermodynamic Drivers

Ice seasons of HB have changed in the last forty years. The underlying cause of change is related to T_0 and the energy budget of HB. To understand, how energy flows in HB it is important to first understand the daily changes in the energy budget (Figure 4.13).

Temporal and annual variation in the energy budget follows the same pattern outlined in Oke (2002). Q* is the major driver of the energy budget. Q* becomes positive Day 80 (March 21st) as it passes the spring equinox, and reaches maximum (239.85Wm^{-2}) on day 189 (July 7th) shortly after the summer solstice. Clearer skies, in response to a stable atmosphere over HB, are the primary cause of larger K↓ and Q* in July. The small albedo of water implies that more solar radiation is absorbed by the ocean. Q_{ST} largely follows the pattern of Q* throughout summer months until September. Q_H and Q_E remain negative as these are suppressed by inversion temperature gradients over the Bay. As the fall equinox approaches, Q* starts to decline but remains positive; Q_H and Q_E pick-up, evaporation takes place in the fall months utilizing the stored energy from the summer. This initiates ice formation and the Bay becomes ice-covered towards the end of the year. However, at the beginning of the year and at the end of the year Q_H contributes to heating-up the water; while, Q_E indicates evaporation. This opposition of convective fluxes exists due to changes in gradient; warm air above the freezing point is advected into the cooler region; in doing so, a temperature inversion develops. Vapour pressure however, remains lower than saturation vapour pressure at the freezing point. These lapse humidity gradients drive a positive latent heat flux while Q_H is reversed.

5.2.1 Break-Up Season

I. general Dates and Duration

Variation exist in the first day of break-up which differs greatly from year to year and shows a shift over time. On average in the last 40 years, ice begins to break-up on DOY 158 (June 7th) (Table 4.1). This agrees with the typical timing of ice retreat- late May to early June (Gough et al., 1999; Stewart et al., 2010). The duration of BU season is on average 61.26 days (Table 4.2). It is longer than both FU and IC seasons.

Ice has been breaking up earlier by 1.07 days per year (Figure 4.7a) with positive autocorrelation. This means that break-up dates in one year are dependent on the previous year, possibly due to heat storage of water. Similarly, Gagnon and Gough (2005b) examined break-up dates across 36 locations of HB. It was found that ice has been breaking-up earlier by several days in the Bay and positive autocorrelation existed in the break-up dates of western HB. Barber & Hochheim (2014) found that ice has been breaking earlier by several weeks. The shift in break-up dates from several days to weeks exist as most studies looked at spatial variation (east vs. west and south vs. north) in break-up dates ; rather than identifying dates for the entire Bay. Nonetheless, Kowall (2017) found that ice is breaking up earlier by 0.49 days per year from 1979-2011. The difference from this study occurs as their timeseries did not extend to 2018; which excluded the warm years of El Niño and extreme negative phase of NAO - 2015/2016. This results in greater warming of water; which, plays a role in ice-formation and thickness; in turn, strengthening positive albedo feedback. The main cause of earlier BU season was thin ice formation during IC season (Figure 4.25b). Thinner ice can break-up earlier as it requires less energy to break-up compared to a thicker ice pack. Thin ice; in combination, with variability in wind and currents (Etkin, 1991), or freshwater inputs (Prinsenberg, 1988) may be factors producing the great variability in break-up dates shown in Table 4.1.

It was expected that BU seasons would become shorter as ice BU is occurring earlier. However, BU season is becoming longer by 1.17days per year (Figure 4.9b). Longer BU seasons can be explained by ice break-up occurring earlier in both Foxe Basin (FB) and Hudson Bay by 1.5 weeks earlier from 1996-2005 (Barber and Hochheim, 2014). FB had small remnants of second year ice but in the recent years it becomes completely ice-free. This exists because late in the BU season, ice from HS is transported west into southern FB by currents along the northern coast of HS; late-season residual ice is then transported into northern HB (Prinsenberg, 1986a, 1986b). This has likely contributed to BU season being longer; despite, starting earlier.

II. Energy Flows

Q* is the major energy component during BU season (Figure 4.14d) as the day-light hours begin to increase. Q* contributes to the formation of melt ponds that create larger albedo drop and substantial Q_E and Q_H flux to be absorbed by the ice pack. This results in the ice to break rapidly once, the melt ponds form on top. This results in exponential growth of open-water area across the Bay (Figure 4.10a). As the ice breaks, absorbed energy contributes to melting ice and heating up water. During this period, open water gains more heat compared to ice covered portions of the Bay (Figure 4.15a). During, the BU season on average HB gained the most energy at highest intensity (Table 4.4a) as it occurred around Summer Solstice. These are the times when Q* is large positive hence, more energy is available for heating-up the water and dissipating the ice. This resulted in cumulative Q_{ST} increasing throughout the BU season (Figure 4.15a).

In the last 40 years, total energy gained by the Bay during BU season is increasing by 10.41MJm^{-2} per year (Figure 4.17a) with a decrease in the intensity of -0.73Wm^{-2} per year (Figure 4.16a). These trends exist because BU season is starting to begin closer to Spring Equinox and lasts until the Summer Solstice. Thereby, it extends into months in which Q* is smaller positive. The

intensity shows a decline as the sun is lower in the sky now at the beginning of BU season, compared to the past.

III. Surface Temperature

The continuous absorption of Q* in BU season affects sea surface temperature. Heat energy is stored within the mixed layer of water column but T_0 controls the energy across the sea - atmosphere interface. During BU season, T_0 averaged -1.88^{O}C, which was warmer than FU season (Table 4.6). This can be explained by radiative energy inputs that were contributing to heating-up water; allowing open-water temperature to average 0.83^{O}C. Also, presence of melt ponds on portions of the ice, resulted in accelerated melting of sea ice from lowered albedo, raising temperatures of ice-covered parts of HB to an average of -2.71^{O}C (Table 4.6). During BU, T_0 has been decreasing in open-water by 0.19^{O}C per year.; while, in ice-covered parts it has been decreasing by 0.01^{O}C per year (Figure 4.26b). It was expected that T_0 would increase in the past 40 years; but the negative trend is strongly influenced from drop in T_0 from 2002-2018. During this period, there were many strong El Niño and negative NAO years. A probable cause of thin ice; which releases less freshwater at the surface compared to a thicker ice pack during BU season. This implies that the salinity of HB is being less affected by sea ice melt patterns but controlled more by river inputs. The mixing of river inflows with HB does not occur simultaneously; it lags (St-Laurent et al., 2012) freshwater from rivers which remains along the coast; while, freshwater from ice melt is distributed. Therefore, higher salt fluxes in BU season result in sea water to remain liquid despite lowest T_0 reaching -2.24^{O}C in 2010 and -2.02^{O}C in 2012 (Figure 4.26a). It can be surmised that the drop in average open-water temperature from 2002-2018 is caused by an increase in salinity during BU season.

IV. Earliest Break-Up of 2010 and Late Break-Up of 1987

Early break-up in 2010 can be explained by the strong negative NAO phase during 2009/2010 (Osborne,2011). During the negative phase of NAO the jet stream moved slowly

southwards; in doing so, warm air and less snowfall occurred during IC season. NAO exerts its strongest influence on T_0 and air temperature (Mysak et al., 1996). This slows down Q_H losses from HB; in turn, T_0 declines more slowly leading to slower growth of ice. Therefore, in 2010 IC season began very late (DOY 12, January 12th); which reduced growth time of ice which produced thin ice that broke early. In 1987, ice break-up occurred late because 1986 was a strong positive NAO year that led to early formation of ice (Caya et al., 2011). The overlying cold temperatures and strong convective losses to the atmosphere, led to thick ice formation in 1986. Therefore, more energy was needed to trigger BU season.

5.2.2 Ice-Free Season

I. General Dates and Duration

On average over the past 40 years, IF season begins on DOY 219 (August 7th) (Table 4.1). This corresponds to the typical timing of IF season in HB in mid August (Mysak et al., 1996). The duration of IF season on average is 73.30 days (Table 4.2). In the past 40 years, IF season showed a shift of 0.03days per year with no significant trend. This existed as BU season did not show a significant trend. However, the duration of IF season is becoming longer by 1.33 days per year as the IF season is being extended into November; while starting on approximately the same day. This is consistent with the Kowal et al. (2017) findings that the IF season is being extended by 0.91 day/year for the period 1979-2011. The IF season could potentially be lengthened by a later freeze-up date, an earlier breakup date, or both (Gagnon and Gough, 2005a).

II. Energy Flows

The energy budget at the beginning of IF season shows gains of energy from incoming shortwave radiation. This leads Q* to be the dominant term of the energy budget (Figure 4.14b). The absence of ice permits energy to contribute towards heating up the water. Since, water has a low albedo but high heat capacity with a weak thermal response, it was expected that it would absorb more radiant energy however, it is the season with lowest energy gain (Table 4.4a). This occurs because although IF season begins around the same time each year, its length is becoming longer and it is shifting later into the year. IF season crosses the fall solstice when net radiation starts to become increasingly negative. However, freeze-up does not occur until energy gained during BU and the first part of the IF season is lost and surface temperature reaches the freezing point. Throughout IF season, Q_H and Q_E remain negative or close to zero because of temperature gradients;

cold water with overlying warm air. However, towards the end of the IF season Q_H and Q_E transfer to the atmosphere begins to drive Q_{ST} losses as Q* becomes smaller (Figure 4.14b). This led cumulative energy during IF to decline towards the end of the season (Figure 4.15b). Energy gains at the beginning and losses at the end of IF resulted in large variability in Q_{ST} (Table 4.4a) over the entire season. However, the intensity of Q_{ST} losses during IF was higher than during IC season because for most of IC season Q* is either negative or negligible, particularly around the winter solstice. Comparably, during IF season long day light hours and higher sun angles (smaller solar zenith angles) result in the intensity of energy to be higher.

A one day extension of the IF season results in total gained energy of the Bay to decrease by 1.62 MJm^{-2} (Figure 4.22b) significantly. In contrast, intensity decreases by -0.61 Wm-2 (Figure 4.22a). This existed as the early break-up and late freeze-up has contributed to IF season to be extended further into the year. The loss of Q_{ST} by Q_H and Q_E was supressed at the beginning of IF season due to inversion of temperature gradients. However, near the end of IF season stored heat gives rise to steep vertical temperature gradients; which enhances Q_E and Q_H fuelling heat storage losses; thereby, reducing intensity of heat gain. Nonetheles, duration accounts for only 21% of the variability in the intensity of gained energy. Bello and Higuchi (2019) noted that in typical ice-free months (July and August), insolation has been reduced over the past two decades as a result of increased cloud cover. This means Bay receives less radiant energy during the main months of the IF season; hence, the intensity of gained energy also reduces.

III. Absence of Ice-Free Season in 1992 and 1999 and Shortest IF season in 1993

HB was not ice-free during 1992, and 1999; while the IF season in 1993 only lasted for 5 days. The eruption of Mt. Pinatubo in the Philippines resulted in a significant cooling of the global climate during 1991 and 1992. Two years of cool temperatures led water of HB to be colder than

normal likely resulting in thicker ice to form. The 2 cold years were followed by positive NAO year-1993 (Caya & et al., 2011) which is related to cold conditions in winter. It is also possible that remnants of ice could be floating in the Bay but it covered small extent of the 32km grid location that the passive microwave could not detect. Lastly, 1999 was followed by very warm El Niño years (1997-1998) as well as negative NAO years, which began in 1995 (Caya et al., 2011). It was expected that 1999 IF would be completely ice-free but it was not. Hence, 1999 was a very unusual year for which an explanation is elusive.

5.2.3 Freeze-Up Season

I. General Dates and Duration

Freeze-Up characteristically begins on DOY 296 (October 23rd) (Table 4.1). This agrees with the typical timing of freeze-up which is late-October (Danielson, 1971). Positive autocorrelation existed in freeze-up dates. Gagnon and Gough (2005b) found that positive autocorrelation existed in freeze-up dates in the center of HB. Duration of FU season is the shortest – 41.1 days (Table 4.2). This can be explained by the energy flows that are to be discussed later in the chapter.

The most evident cause of later freeze-up dates is caused by extended IF season; as a result of early BU season. Over the last 40 years, FU starts late by 1.29 days per year (Figure 4.7c). The onset of FU has been fluctuating with slightly later freeze-up dates from 1979-1988, earlier onset of freeze-up from 1989-2002 and 2003-2018 showing steep delays in freeze-up (Figure 4.7c). The separation of time-series; in terms, of cool and warm years is likely to effect freeze-up dates. It must be pointed out that shifts in cool and warmth periods coincided with shifting NAO phases. Large changes existed in the NAO phases during 1988-1989, 1995-1996, and 2001-2002; during these years strong positive NAO years were followed by strong negative NAO years (Pingree, 2005). From 2003-2018, extreme warm years occurred in 2009/2010, 2015/2016 (Paek et al., 2017). The

transition towards even later freeze-up dates from 2003-2018 (Figure 4.7c) could be considered the tipping point after which Freeze-Up dates begin to enter a new era of later Freeze-Up occurring in December.

II. Energy Flows

Q* was not the dominant term during FU season, instead loss of turbulent energy fueled Q_{ST}. Throughout the IF and BU seasons, energy that was gained by the ocean earlier must be lost to lower temperatures to the freezing point to trigger ice formation. The currents within HB are dominantly wind-driven and cyclonic at all depths, reaching a maximum in October-November when the winds are strongest (Pinsenberg, 1986b; Gachon & et al., 2004). In addition, faster winds allow turbulent diffusion in the ocean mixed layer; thereby, maintaining vapour pressure gradients between water and air. Also, faster winds result in a rougher surface. This allows Q_H and Q_E losses to occur more effectively compared to calm conditions. Convective cooling takes place during the FU season which allows ice to form. The depletion of ocean energy by turbulent fluxes and declining Q* leads to Q_{ST} showing the greatest energy losses among the four other seasons. As parts of the Bay freeze creating a barrier for energy losses open-water continues to lose energy throughout the season and eventually reach freezing temperatures. As energy is lost primarily from open water, exponential growth in ice coverage occurs (Figure 4.10c).

Freeze-Up is starting later and becoming shorter. This exists because the Bay is losing approximately the same amount of energy in transitioning from no ice cover to complete ice cover but is losing energy more intensely (Figure 4.16 c and Figure 4.17c). This is made possible as the FU season is moving closer to the winter solstice; when air temperatures drop, radiant energy is near minimum and winds are strong. This seasonal shift to more severe conditions allows the same amount of energy to be lost to generate ice-cover but at a higher intensity; hence, the Bay freezes up

faster. Some parts of the Bay becomes ice-covered resulting in a barrier for the energy to escape; while, open-water parts of HB continue to lose energy.

III. Surface Temperature

During FU season, T_0 was much colder than BU season. Freeze-Up typically consists of late October to November. These are the months when T_A becomes colder and the warm water of the Bay loses heat rapidly; resulting in T_0 to drop to -15.86^{O}C (Table 4.6). During FU season, the average temperature of ice-covered parts of Bay (-14.56 ^{O}C) was lower than open-water (-1.31^{O}C) parts (Table 4.6) as ice has higher resistance to heat transfer than turbulent water. This maintains T_0 at or above the freezing point over sea water. From 2002-2018, T_0 in open water is becoming negative (Figure 4.26b).

Sea water typically freezes at -1.8^{O}C but freezing point fluctuates depending on salt concentration and heat content. Salinity at the surface is controlled by river inputs, and brine exclusion or melt water during ice formation and , respectively melt. HB receives large freshwater river inputs during BU season, but on a time scale less than a year, sea ice melt and growth has a greater impact on the freshwater budget compared to river discharge (Prinsenberg, 1988). Freshwater sourced from river discharge is found along the coast; while, freshwater from sea ice melt is distributed more equally around the bay (Granskog & et al., 2007; 2011). During IF season, freshwater is imported into the interior, and is released during fall due to enhanced strong cyclonic winds (St-Laurent et al., 2012). Rapid losses of heat to the atmosphere and freshwater flowing out into HS results in solubility of salt to decline; and reduces its freezing point below -1.8^{O}C. Salt fluxes towards the end of FU season and throughout IC season are controlled by brine rejection when the sea ice growing is rapidly (Saucier & et al., 2004). The surface cooling weakens vertical

stratification and permits very slow vertical mixing (Prinsenberg, 1988). Spatial heterogeneity exists in salt concentrations, which leads to greater variability in the T_O of open water (Table 4.

5.2.4 Ice-Covered Season

I. General Dates and Duration

The IC season begins on DOY 345 (December 10th) on average (Table 4.1). This corresponds to the typical timing of HB becoming completely ice-covered by December (Mysak et al., 1996). Duration of IC season is the longest at 178.69 days (Table 4.2). A shift towards a later onset of ice-covered season was detected of 0.61 days per year (Figure 4.7d), with a shorter duration of 1.77 days per year (Figure 4.9d). These results cannot be compared with other studies as the IC season has not been addressed. Therefore, it is concluded that earlier break-up, later freeze-up has resulted in the delay in the IC season and shortened its duration. This is consistent with a reduction in maximum ice thickness because late sea ice formation means it has less time to grow thick, making it easier to break apart and melt during the BU season. This sets the positive ice albedo feedback into motion..

II. Energy Flows

The energy budget at the beginning of IC season is largely driven by losses of turbulent energy to the atmosphere ,while Q* is negative due to minimal day-light hours (4.14d). However, as the spring equinox passes Q* begins to go positive e as well as Q_{ST}. This results in Bay gaining energy by the end of the IC season. During this period, the loss of Q_H and Q_E were small and hence, had no, to very little, impact on Q_{ST}. This resulted in cumulative Q_{ST} to increase steeply at the end of IC season (Figure 4.15d) which provides the energy to trigger the break-up of ice. The net gain of ocean energy over the IC season, melts ice formed during the FU season as well as ice formed the early part of the IC season.

On average, over the past 40 years HB has been gaining energy during the IC season; although, it was expected that it would be the season with the most energy loss; in both intensity and total energy. However, it was found that the Bay gains 173 MJm^{-2} during the IC season which is larger than the net energy gains during the IF season (148 MJm^{-2}) (Table 4.4a). This exists as the IC season is sensitive to the astronomical cycle. The large energy gains during the second part of the season coincides with the passing of the spring equinox. This means that during the first part of the IC season, ocean energy transfer is negative compared to the positive gains in the second part of IC, resulting in variability to be high. However, the intensity of energy gains during Ice-Covered season was lower due to the slow energy loss at the beginning of ice-covered season, although variability in the intensity of energy gains during winter was very high. Overall, both the intensity ($0.12Wm^{-2}$ per year, R^2= 0.23) and total energy ($2.98MJm^{-2}$per year; R^2=0.48) have increased as the changes in the Ice-Covered season are sensitive to astronomical cycles.

5.3 Climate Memory: Break-Up and Freeze-Up Season

Both FU and BU season have been studied more widely as these are the seasons when HB begins to gain energy and lose energy. This is important as these seasons contribute to "climate memory" wherein the timing of ice at one point in the cryogenic cycle influences the amount of heat stored in the surface waters; in turn, affecting the timing of the subsequent cycle (Gough and Houser, 2005a; Serreze and Barry, 2011; Stroeve et al., 2016). It was found that one day late break-up results in FU season to be delayed. One day late break-up results in freeze-up day to be delayed by 1 day (R^2= 0.48). In addition, it was found that the first day of FU season affects BU season of the following year. One day late freeze-up corresponds to 0.42 days of earlier break-up (R^2=0.39). The R^2 between freeze-up date and break-up date was much higher than duration (R^2=0.02,p>0.05) of both season;

whereas, dates having stronger R^2 indicate that there's climate memory and that astronomical cycles which affect Q_{ST} are playing a role. Moreover, BU season affects the start of FU season (R^2=0.48); more so than FU season affecting the following Break-Up season (R^2=0.39). This indicates that climate memory from breakup (via heat absorbed through the surface layer) has a greater role in the freeze-up date of HB. This exists as heat capacity of water is high, late break-up results in less energy and time to heat water therefore initiating early ice retreat. Meanwhile, that the role of climate memory from freeze-up is less important factor in the following Break-Up season of ice in HB. This might result from spatial heterogeneity during BU season from leads and river inputs (Danielson, 1971).

5.4 The Underlying Mechanism Influenced by Both Freeze-Up and Break-Up Season

Both BU and FU season are critical because in one energy is gained; while, in the other energy is lost. In mid-1990s, natural modes of variability NAO and El Niño resulted in warmer conditions. The natural perturbation resulted in the rising air temperatures by 3^{O}C in mid-1990s (Chambellant & et al., 2012). This produced warmer conditions which resulted in sea ice to melt faster. However, ice transport from FB resulted in duration of BU season to be extended to the summer solstice. This allowed HB to uptake more energy; whereby, a one day extension of BU season resulted in total gained energy of the Bay to increase by 9.46 MJm^{-2} (Figure 4.21b); while, intensity decreased by -0.60 Wm^{-2} (Figure 4.21a). This exists because at the beginning of BU season less energy is now being absorbed by the Bay. The large energy uptake in BU season results in the IF season to be extended later into the year; thereby, triggering later freeze-up.

Each year, the same amount of energy is lost during FU season; despite starting later. This means an energy threshold exists that triggers FU season which must correspond to the freezing-

point *temperature* threshold. However, with a one day extension in FU season total energy loss decreased by 2.44MJm^{-2} (Figure 4.23b) yet intensity increased by 1.52Wm^{-2} (Figure 4.23a). This occurs because a long FU season typically happens earlier around the Fall equinox when Q* is greater, compared to when the FU season occurs faster but closer to the winter solstice. A primary causes of later freeze-up is that energy absorbed during BU and IF season must be lost through Q_H and Q_E. This results in cloud to trap energy that produces even warmer conditions; which, further slowed down formation of ice. However, once ice-covered areas appear, the loss of energy slows down creating cooler conditions and allowing rapid formation of ice. However, the growth time of ice shortens that contributes to thinner ice in the IC season.

5.5. Ice Thickness

There are a few observational studies on sea ice thickness in the HB that are restricted to drill-hole measurements on land-fast first-year ice around the coast prior to 2003 (Landy et al., 2017). The thickness of the ice cover is known from qualitative estimates from satellite images during the peak of winter (St-Laurent & et al., 2011). Ice thickness during each season is difficult to examine as measurements are difficult to obtain in winter months (Gough & et al., 2004b).

Thermodynamic ice thickness, as estimated in this study, does not take into consideration dynamic factors responsible for ice growth or thinning. Despite the fact, the derived magnitudes of ice thickness are highly suspect, the trends in ice thickness may still have relevance. Ice thickness during FU season reached a maximum of 5.22cm (Table 4.5). During the months of the FU season, T_0 has been rising (Bello & Higuchi, 2019); as well as rise in T_A has been observed (Barber & Hochheim, 2010). For every 1^{O}C increase in T_A SIE declines in late November (Hochheim and Barber, 2010). The results from this study show that ice is becoming thicker by 0.03cm per year

during FU season (Figure 4.25) . A common cause of increase can be that energy is being lost from the water more intensely, despite the FU season becoming shorter. Maximum ice thickness during FU season occurred in 1997 (18.17cm;Figure 4.25a) as it was a very strong El Niño year (Paek et al., 2017). It was expected that freeze-up would start very late because of warmer T_A. However, this was not the case; since, freeze-up occurred on day 278 (October 4th) which is earlier than the average day 296 (November 23rd) (Table 4.1) but its duration was longer 64 days (Figure 4.7d; Figure 4.9a). This means warm water temperatures caused the Bay to lose more energy compared to other years producing thick Ice at the end of the FU season in 1997. The ice continued to grow during the IC season.

Ice is becoming thinner during IC season by 0.19cm/year (Figure 4.25b) . Sea ice thickness can be linked to freeze-up and break-up dates because these determine the growth time of ice and the length of time snow can accumulate on ice (Gagnon and Gough, 2006). FU season begins late; while, early start of BU season has contributed to the growth time of ice to be reduced. The trends in freeze-up and breakup dates are mostly driven by changes in atmospheric temperatures and wind strength (Hochheim & Barber, 2014). This has led to the perception that ice is becoming thinner due to rising T_A. Gough & et al. (2004) showed that sea ice thickness is weakly related to T_A. Therefore, loss of sea ice itself is the cause of strengthened positive albedo feedback. Since, early breakup and long IF season contribute to greater energy uptake that slows ice formation; and reduces growth time. This permits even greater energy uptake in the following BU season and reduce ice thickness which sets the stage for the Bay to absorb more energy and form less ice.

Ice thickness was the highest in 1985 (44.34cm) (Figure 4.25b) due to long IC and early FU season. Prinsenberg (1988) used data from Arctic Pilot Project in 1981 in which, research was done on proposed year-round shipping through the Northwest Passage. It was found that on average

maximum ice thickness of HB is 160cm. In HB, tidal mixing generated at ice-water interface and salt rejection from the growing ice-cover deepens the pycnocline depth to 95 m (Prinsenberg, 1986). In a more recent study, it was found that ice thickness varies from west (1.17m) to east (1.27m) HB. Ice is thicker in eastern HB due to prevailing westerly winds that transport ice to eastern HB (Gough, W. A., & Allakhverdova, T, 1999).

Gough & et al. (2004) examined the effect of T_A and snow depth on ice thickness by taking measurements and using CIS charts at 9 locations in the HB region. It was found that snow depth accumulated on top of ice, largely determines sea ice thickness. Since, insulating properties of the snow pack and the sea ice influence T_A once ice has fully formed. Deeper snow-depth resulted in more insulation from below freezing temperatures thereby producing thinner ice (Gough & et al., 2004). In addition, heat loss at the ice surface is dependent on thermal conductivity (Gough, W. A., & Allakhverdova, T, 1999). This is a very important parameter to consider; especially, in the IC season to fully understand ice growth. Ice Ridges were not considered in this study which resulted in maximum ice thickness (26.6cm) (Table 4.5) to differ greatly from the literature; and 1998 to be the year with maximum ice thickness despite being a El Niño year (Paek & et al., 2017). Moreover, the exclusion of sea-ice dynamics that contributes to ice drift and compression leading to thicker ice was not incorporated in the energetics equation. The complex interactions between timing of break-up and freeze-up, thermal conductivity, snow depth and dynamic forces (winds and currents) influences sea ice thickness and helps explain why sea ice thickness in the last 40 years is much smaller than what has been reported in the literature. A limit to using reanalyses models to study ice thickness is that passive microwave is poor at detecting grease ice and nilas; hence, it is difficult to determine actual ice thickness during FU season. Moreover, the growth of sea ice during IC season is influenced by vertical diffusivity of sea water which is a complex mechanism. Therefore, most

studies rely on depth measurements made at various sites across the Bay; very few papers exist on sea ice thickness.

Chapter 6: Conclusion

This study examined changes in sea ice seasons in HB from 1979-2018 Results of this study support that sea ice coverage has been declining across the Bay. Sea ice seasons have been shifting- early break-up and late freeze-up have resulted in long IF and short IC season. The timing of IC season has shifted to later date with shorter duration that has reduced the growth time of ice; hence, producing thinner ice. This is leading to early BU season. The timing of IF season has not shifted possibly because ice transport from FB allows the Bay to become ice-free around the same time each year; despite, the early break-up. This has led to longer BU season; despite starting early. The IF season is shifting towards later in the year due to the energy uptakes during BU season. The timing of break-up influences freeze-up more strongly due to 'climate memory' which highlights the importance of energetics.

HB gained energy in BU season; and lost energy in FU season. A surprising finding was that the IF season had the lowest gain of energy; in fact, IC season is gaining even more energy than the IF season over the study period. The underlying cause of this is that both IC and IF season are sensitive to astronomical cycles. Most importantly, it was found that Bay loses the same amount of energy each year during freeze-up season; in other words, an energetic threshold exists that triggers freeze-up. Lastly, during BU season more energy is being gained but at a lower intensity. This can be explained by energy absorption by the ice-pack, breaking the ice-pack; then heating-up the water. It must be noted that there have been some very large perturbations which have led to shifting sea ice-seasons. The initial perturbation to loss of sea ice and strengthened positive albedo feedback is a result of greenhouse forcing. However, the data shows that losses and gains of energy are mainly controlled by astronomical factors.

Surface temperature was computed using a surface emissivity (ε) of 0.97. It was found that open-water surface temperatures between 2002 and 2018 were decreasing below the freezing point of typical sea-water (-1.8 ^{0}C) and increasing salinity is a possible reason during BU and FU season. Lastly, the thermodynamic-equivalent in the growth of pure ice was calculated from the subsurface heat flux for the FU and IC seasons. Over the last 40 years, ice thickness increased during FU season while it decreased in the IC season. The computed ice thickness differed from the literature because factors such as ice dynamics and snow depth were not considered.

There are some limitation that existed in this study. First, Q_{ST} term is very sensitive to Q*. As Q* increases Q_{ST} increases but in fall Q_H and Q_E become dominant components. This causes energy budget to align with the ice-season reflected by the albedo of the surface. Secondly, the method used to compute ice thickness can indicate trend in ice thickness but to understand it fully thermal conductivity of ice must be incorporated into the equation. Third, BU and FU season are dominant; thereby, variables such as cloud coverage, windspeed, currents and air temperature should be analyzed to identify a more detailed mechanism. Lastly, the study gives an overview of ice season across the entire Bay, a more detailed study that looks at changes in east vs. west, north vs. south should be conducted. This will aid in understanding the shifting ice-seasons and use this information in climate models.

Bibliography

Andrews, J., Babb, D., & Barber, D. (2018). Climate change and sea ice: shipping in Hudson Bay, Hudson Strait, and Foxe Basin (1980–2016). Elem Sci Anth, 6(1).

Aporta, C. (2010). The sea, the land, the coast, and the winds: understanding Inuit sea ice use in context. In SIKU: Knowing Our Ice (pp. 163-180). Springer, Dordrecht.

Bello, R., & Higuchi, K. (2019). Changing surface radiation and energy budgets of the Hudson Bay Complex using the North American regional reanalysis (NARR) model. Arctic Science, 5(4): 218-239.

Cavalieri, D. J., & Parkinson, C. L. (2012). Arctic sea ice variability and trends, 1979-2010. The Cryosphere, 6(4): 881.

Chambellant, M., Lunn, N. J., & Ferguson, S. H. (2012). Temporal variation in distribution and density of ice-obligated seals in western Hudson Bay, Canada. Polar Biology, 35(7): 1105-1117.

Chan, H. M., Fediuk, K., Hamilton, S., Rostas, L., Caughey, A., Kuhnlein, H., ... & Loring, E. (2006). Food security in Nunavut, Canada: barriers and recommendations. International journal of circumpolar health, 65(5): 416-431.

Curry, J., Schramm, J., & Ebert, E. (1995). Sea Ice–Albedo Climate Feedback Mechanism. Journal of Climate, 8(2): 240-247.

Danielson Jr, E. W. (1971). Hudson Bay ice conditions. Arctic: 90-107.

Déry, S. J., Hernández-Henríquez, M. A., Mlynowski, T. J., & Straneo, F. (2011). Interannual variability and interdecadal trends in Hudson Bay streamflow. Journal of Marine Systems, 88(3): 341-351.

Ehn, J. K., Granskog, M. A., Papakyriakou, T., Galley, R., & Barber, D. G. (2006). Surface albedo observations of Hudson Bay (Canada) landfast sea ice during the spring melt. Annals of Glaciology, 44: 23-29.

Etkin, D. A., & Ramseier, R. O. (1993). A comparison of conventional and passive microwave sea-ice datasets for Hudson Bay. Atmosphere-Ocean, 31(3): 359-378.

Gagnon, A. S., & Gough, W. A. (2005a). Climate change scenarios for the Hudson Bay region: an intermodel comparison. Climatic Change, 69(2-3): 269-297.

Gagnon, A. S., & Gough, W. A. (2005b). Trends in the dates of ice freeze-up and breakup over Hudson Bay, Canada. Arctic: 370-382.

Gagnon, A.S. and Gough, W.A. (2006). East–west asymmetry in long-term trends of landfast ice thickness in the Hudson Bay region, Canada. Climate Res 32(3): 177–186.

Galbraith, P. S., & Larouche, P. (2011). Reprint of "Sea-surface temperature in Hudson Bay and Hudson Strait in relation to air temperature and ice cover breakup, 1985–2009". Journal of Marine Systems, 88(3): 463-475.

Gaston, A. J., Smith, P. A., & Provencher, J. F. (2012). Discontinuous change in ice cover in Hudson Bay in the 1990s and some consequences for marine birds and their prey. ICES Journal of Marine Science, 69(7): 1218-1225.

Gough, W. A. (2001). Model tuning and its impact on modelled climate change response: Hudson Bay sea ice, a case study. Canadian Geographer/Le Géographe canadien, 45(2): 300-305.

Gough, W. A., & Allakhverdova, T. (1999). Limitations of using a coarse resolution model to assess the impact of climate change on sea ice in Hudson Bay. Canadian Geographer/Le Géographe canadien, 43(4): 415-422.

Gough, W. A., & Houser, C. (2005a). Climate memory and long-range forecasting of sea ice conditions in Hudson Strait. Polar Geography, 29(1): 17-26.

Gough, W. A., Gagnon, A. S., & Lau, H. P. (2004). Interannual variability of Hudson Bay ice thickness. Polar Geography, 28(3): 222-238.

Gough, W. A., Robinson, C., & Hosseinian, R. (2005b). The influence of James Bay River discharge on Churchill, Manitoba Sea Level. Polar Geography, 29(3): 213–223.

Granskog, M. A., Kuzyk, Z. Z. A., Azetsu-Scott, K., & Macdonald, R. W. (2011). Distributions of runoff, sea-ice melt and brine using δ 18 O and salinity data—A new view on freshwater cycling in Hudson Bay. Journal of Marine Systems, 88: 362–374.

Granskog, M. A., Macdonald, R. W., Mundy, C. J., & Barber, D. G. (2007). Distribution, characteristics and potential impacts of chromophoric dissolved organic matter (CDOM) in Hudson Strait and Hudson Bay, Canada. Continental Shelf Research, 27(15): 2032-2050.

Hochheim K., Barber D.G., Lukovich J.V. (2010) Changing Sea Ice Conditions in Hudson Bay, 1980–2005. In: Ferguson S.H., Loseto L.L., Mallory M.L. (eds) A Little Less Arctic. Springer, Dordrecht

Hochheim, K. P., & Barber, D. G. (2014). An update on the ice climatology of the Hudson Bay system. Arctic, Antarctic, and Alpine Research, 46(1): 66-83.

Hochheim, K. P., Lukovich, J. V., & Barber, D. G. (2011). Atmospheric forcing of sea ice in Hudson Bay during the spring period, 1980–2005. Journal of Marine Systems, 88(3): 476-487.

Ingram, R. G., & Larouche, P. (1987). Variability of an under-ice river plume in Hudson Bay. Journal of Geophysical Research: Oceans, 92(C9): 9541-9547.

Johannessen, O. M., Miles, M., & Bjørgo, E. (1995). The Arctic's shrinking sea ice. Nature, 376(6536): 126-127.

Johannessen, O. M., Shalina, E. V., & Miles, M. W. (1999). Satellite evidence for an Arctic sea ice cover in transformation. Science, 286(5446):1937-1939.

Joly, S., Senneville, S., Caya, D., & Saucier, F. J. (2011). Sensitivity of Hudson Bay sea ice and ocean climate to atmospheric temperature forcing. Climate Dynamics, 36(9-10), 1835-1849.

Kennedy, A. D., Dong, X., Xi, B., Xie, S., Zhang, Y., & Chen, J. (2011). A comparison of MERRA and NARR reanalyses with the DOE ARM SGP data. Journal of Climate, 24(17): 4541-4557.

Kowal, S., Gough, W. A., & Butler, K. (2017). Temporal evolution of Hudson Bay sea ice (1971–2011). Theoretical and Applied Climatology, 127(3-4): 753-760.

Laidler, G. J., Ford, J. D., Gough, W. A., Ikummaq, T., Gagnon, A. S., Kowal, S., ... & Irngaut, C. (2009). Travelling and hunting in a changing Arctic: assessing Inuit vulnerability to sea ice change in Igloolik, Nunavut. Climatic change, 94(3-4): 363-397.

Landy, J. C., Ehn, J. K., Babb, D. G., Thériault, N., & Barber, D. G. (2017). Sea ice thickness in the Eastern Canadian Arctic: Hudson Bay Complex & Baffin Bay. Remote Sensing of Environment, 200:281-294.

Maslanik, J. A., Serreze, M. C., & Barry, R. G. (1996). Recent decreases in Arctic summer ice cover and linkages to atmospheric circulation anomalies. Geophysical Research Letters, 23(13): 1677-1680.

Meier, W. N., Stroeve, J., & Fetterer, F. (2007). Whither Arctic sea ice? A clear signal of decline regionally, seasonally and extending beyond the satellite record. Annals of Glaciology, 46: 428-434.

Mysak, L. A., Ingram, R. G., Wang, J., & Van Der Baaren, A. (1996). The anomalous sea-ice extent in Hudson Bay, Baffin Bay and the Labrador Sea during three simultaneous NAO and ENSO episodes. Atmosphere-Ocean, 34(2), 313-343.

National Snow an Ice Data Center (NSIDC) (2019) Arctic Sea Ice News and Analysis Retrieved from: http://nsidc.org/arcticseaicenews/faq/

Ogi, M., Barber, D. G., & Rysgaard, S. (2016). The relationship between summer sea ice extent in Hudson Bay and the Arctic Ocean via the atmospheric circulation. Atmospheric Science Letters, 17(11): 603-609.

Oke, T. R. (2002). Boundary layer climates. Routledge.

Osborn, T. J. (2011). Winter 2009/2010 temperatures and a record-breaking North Atlantic Oscillation index. Weather, 66(1): 19-21.

Paek, H., Yu, J. Y., & Qian, C. (2017). Why were the 2015/2016 and 1997/1998 extreme El Niños different?. Geophysical Research Letters, 44(4): 1848-1856.

Parkinson, C. L., & Cavalieri, D. J. (2008). Arctic sea ice variability and trends, 1979–2006. Journal of Geophysical Research: Oceans, 113(C7).

Parkinson, C. L., Cavalieri, D. J., Gloersen, P., Zwally, H. J., & Comiso, J. C. (1999). Arctic sea ice extents, areas, and trends, 1978–1996. Journal of Geophysical Research: Oceans, 104(C9): 20837-20856.

Perovich, D.K., T.C. Grenfell, B. Light and P.V. Hobbs.(2002). Seasonal evolution of the albedo of multiyear Arctic sea ice. J. Geophys. Res., 107(C10): 8044.

Pingree, R. (2005). North Atlantic and North Sea climate change: curl up, shut down, NAO and ocean colour. Journal of the Marine Biological Association of the United Kingdom, 85(6):1301-1315.

Prinsenberg, S. J. (1988). Ice-cover and ice-ridge contributions to the freshwater contents of Hudson Bay and Foxe Basin. Arctic: 6-11.

Prinsenberg, S. J., (1986a). The circulation pattern and current structure of Hudson Bay. In Martini, E. P. (ed.), Canadian Inland Seas. Oceanography Series 44. New York: Elsevier, 187–203.

Prinsenberg, S. J., (1986b): On the physical oceanography of Foxe Basin. In Martini, E. P. (ed.), Canadian Inland Seas, Oceanography Series 44. New York: Elsevier, 217–236.

Qian, M., Jones, C., Laprise, R., & Caya, D. (2008). The Influences of NAO and the Hudson Bay sea-ice on the climate of eastern Canada. Climate dynamics, 31(2-3): 169-182.

Qu, B., Gabric, A. J., Zhu, J. N., Lin, D. R., Qian, F., & Zhao, M. (2012). Correlation between sea surface temperature and wind speed in Greenland Sea and their relationships with NAO variability. Water Science and Engineering, 5(3):304-315.

Ridenour, N. A., Hu, X., Jafarikhasragh, S., Landy, J. C., Lukovich, J. V., Stadnyk, T. A., ... & Barber, D. G. (2019a). Sensitivity of freshwater dynamics to ocean model resolution and river discharge forcing in the Hudson Bay Complex. Journal of Marine Systems, 196: 48-64.

Ridenour, N. A., Hu, X., Sydor, K., Myers, P. G., & Barber, D. G. (2019b). Revisiting the Circulation of Hudson Bay: Evidence for a Seasonal Pattern. Geophysical Research Letters, 46(7): 3891-3899.

Rühland, K. M., Paterson, A. M., Keller, W., Michelutti, N., & Smol, J. P. (2013). Global warming triggers the loss of a key Arctic refugium. Proceedings of the Royal Society B: Biological Sciences, 280(1772): 20131887.

Saucier, F. J., Senneville, S., Prinsenberg, S., Roy, F., Smith, G., Gachon, P., ... & Laprise, R. (2004). Modelling the sea ice-ocean seasonal cycle in Hudson Bay, Foxe Basin and Hudson Strait, Canada. Climate Dynamics, 23(3-4), 303-326.

Screen, J. A., Simmonds, I., & Keay, K. (2011). Dramatic interannual changes of perennial Arctic sea ice linked to abnormal summer storm activity. Journal of Geophysical Research: Atmospheres, 116(D15).

Screen, J. A., Simmonds, I., Deser, C., & Tomas, R. (2013). The atmospheric response to three decades of observed Arctic sea ice loss. Journal of Climate, 26(4): 1230-1248.

Serreze, M. C., & Barry, R. G. (2014). The Arctic climate system. Cambridge University Press.

Stewart, D. B., & Lockhart, W. L. (2005). An Overview of the Hudson Bay Marine Ecosystem (Canadian technical report of fisheries and aquatic sciences no. 2586). Available at Government of Canada, Department of Fisheries and Oceans website: http://science-catalogue. canada. ca/record= 4011364&searchscope, 6.

Stewart, E. J., Tivy, A., Howell, S. E. L., Dawson, J., & Draper, D. (2010). Cruise tourism and sea ice in Canada's Hudson Bay region. Arctic: 57-66.

St-Laurent, P., Straneo, F., & Barber, D. G. (2012). A conceptual model of an Arctic sea. Journal of Geophysical Research: Oceans, 117(C6).

St-Laurent, P., Straneo, F., Dumais, J. F., & Barber, D. G. (2011). What is the fate of the river waters of Hudson Bay?. Journal of Marine Systems, 88(3): 352-361.

Stroeve, J. C., Markus, T., Boisvert, L., Miller, J., & Barrett, A. (2014). Changes in Arctic melt season and implications for sea ice loss. Geophysical Research Letters, 41(4): 1216-1225.

Stroeve, J. C., Maslanik, J., Serreze, M. C., Rigor, I., Meier, W., & Fowler, C. (2011). Sea ice response to an extreme negative phase of the Arctic Oscillation during winter 2009/2010. Geophysical Research Letters, 38(2).

Stroeve, J. C., Serreze, M. C., Holland, M. M., Kay, J. E., Malanik, J., & Barrett, A. P. (2012). The Arctic's rapidly shrinking sea ice cover: a research synthesis. Climatic change, 110(3-4):1005-1027.

Tivy, A., Howell, S. E., Alt, B., McCourt, S., Chagnon, R., Crocker, G., ... & Yackel, J. J. (2011). Trends and variability in summer sea ice cover in the Canadian Arctic based on the Canadian Ice Service Digital Archive, 1960–2008 and 1968–2008. Journal of Geophysical Research: Oceans: 116(C3).

Vinnikov, K. Y., Robock, A., Stouffer, R. J., Walsh, J. E., Parkinson, C. L., Cavalieri, D. J., ... & Zakharov, V. F. (1999). Global warming and Northern Hemisphere sea ice extent. Science, 286(5446): 1934-1937.

Wang, J., Mysak, L. A., & Ingram, R. G. (1994). A three-dimensional numerical simulation of Hudson Bay summer ocean circulation: topographic gyres, separations, and coastal jets. Journal of physical oceanography, 24(12):2496-2514.